



Norwegian University of
Science and Technology

Direct Simulation of Surge Tank Stability

Debora Bardini

Hydropower Development

Submission date: July 2018

Supervisor: Kaspar Vatland Vereide, IBM

Co-supervisor: Stefano Malavasi, Politecnico di Milano
Livia Pitorac, IBM

Norwegian University of Science and Technology
Department of Civil and Environmental Engineering

M.Sc. THESIS IN HYDRAULIC ENGINEERING

Candidate: Ms. Debora Bardini

Title: Direct Simulation of Surge Tank Stability

1. Background

Surge tanks are applied in hydropower plants to reduce the pressure forces during acceleration of the water, and to enable speed and power governing of the turbines. Reduction of the pressure forces reduces the necessary strength of the structural components and thereby the costs. Speed governing enables hydropower plants to contribute to controlling the frequency in the power grid and delivering the correct power production from the power plant. In Norway, all hydropower plants above 10 MW are required to run with speed governing to contribute to controlling the grid frequency. Speed and power governing influences the mass oscillations in the surge tank, and may cause an instability. If the surge tank is too small, the speed and power governing can result in amplification of the mass oscillations and cause dangerous water levels and pressures. Thoma (1910) was the first to describe this phenomenon, and derive an equation to calculate the necessary size of the surge tank. Thoma's equation is based on simplifications and neglect the influence of the pressure shaft, the velocity head of the water, and the variable turbine efficiency during oscillations. Thoma's equation is still the standard method for selection of necessary surge tank area for stability. To enable more accurate design of surge tanks, improved methods are necessary. Modern advances in numerical simulation of hydropower plants may enable an improved method called direct numerical simulation. This method involves one-dimensional (1D) numerical simulation of the entire hydropower plant without the simplifications embedded in the Thoma method. Direct simulation has been used in the past, but mainly as a supplement to the standard Thoma method. It is now time to test whether the direct numerical simulations can be used to replace the Thoma method.

2. Main questions for the thesis

The thesis shall cover, though not necessarily be limited to the main questions listed below.

2.1 Literature and desk study

The candidate shall carry out a literature study of Italian literature on surge tank stability and present a summary in the thesis.

2.2 Main tasks

The candidate must collect available background material such as technical information, reports, former studies, maps and drawings of possible case-studies. Related to this material the following must be carried out:

- 1 Selection of case-studies
- 2 Field trip to relevant sites and collection of available data
- 3 Establish and calibrate 1D numerical model
- 4 Compare direct numerical simulation with the Thoma method
- 5 Conclusions

- 6 Proposals for future work
- 7 Presentation

3 Supervision and data input

Adjunct Associate Professor Kaspar Vereide from NTNU and Tenured Professor Stefano Malavasi from Politecnico di Milano will be the main supervisors and PhD Candidate Livia Pitorac will be co-supervisor. The supervisors shall assist the candidate, and make relevant information available.

Discussion with and input from colleagues and other research or engineering staff at NTNU is recommended. Discussion with Sira-Kvina kraftselskap or other power companies are recommended. Significant inputs from other shall be referenced in a convenient manner.

The main contact person in Sira-Kvina kraftselskap will be: Kaspar Vereide.

The research and engineering work carried out by the candidate relating to this thesis shall remain within an educational context. The candidate and the supervisors are free to introduce assumptions and limitations which may be considered unrealistic or inappropriate in a contract research or a professional/commercial context.

4 Report format and reference statement

The report should be written with a text editing software, and figures, tables, photos etc. should be of good quality. The report should contain an executive summary, a table of content, a list of figures and tables, a list of references and information about other relevant sources. The report should be submitted electronically in B5-format .pdf-file in DAIM, and three paper copies should be handed in to the department at each of the hosting universities.

The executive summary should not exceed 450 words, and should be suitable for electronic reporting. The Master's thesis should be submitted within Monday 2th of July 2018.



Kaspar Vereide
Adjunct Associate Professor
Dept. of Civil and Env. Eng.
NTNU

Stefano Malavasi
Tenured Professor
Dept. of Civil and Env. Eng.
Politecnico di Milano

Abstract

This thesis deals with the issue of surge tank stability in hydropower plants, investigating methods used to design the surge tank area required to guarantee stability.

Currently, Thoma equation (1910) is widely accepted as the standard approach for surge tank dimensioning. However, this approach has proven excessively conservative, often leading to over-dimensioned surge tanks. Recent developments in computational power enable us to consider alternative methods, with the direct simulation, consisting in the numerical simulation of the entire hydropower plant, as one of the most promising.

This study draws a comparison between Thoma equation approach and the direct simulation. A 1D numerical model of Roskrepp power plant (Vest-Agder County, Norway) is developed and calibrated in the LVtrans freeware. Transients originating from different scenarios are analysed.

Simulation results show that the direct simulation method proves superior, with a more accurate dimensioning of the surge tank. However, Thoma equation, albeit less accurate, still proves relevant for the early stages of design, when limited design data are available.

Keywords Hydropower, Stability, Transients, Surge tanks, Direct simulation, 1D numerical model, LVtrans, Thoma method

Sommario

Questa tesi tratta l'argomento della stabilità del pozzo piezometrico negli impianti idroelettrici, con l'intento di analizzare alcuni metodi per selezionare l'area di un pozzo piezometrico necessaria per garantire la stabilità.

Attualmente, l'equazione di Thoma (1910) è il metodo standard nel dimensionamento dei pozzi piezometrici. Tuttavia, esso si è dimostrato eccessivamente conservativo, portando al sovradimensionamento. L'aumento di potenza di calcolo degli ultimi anni permette di valutare metodi alternativi, fra cui la simulazione diretta, che consiste nella simulazione numerica dell'intero impianto, rappresenta uno dei più promettenti.

Questo studio presenta un confronto fra l'equazione di Thoma e la simulazione diretta. Un modello numerico monodimensionale dell'impianto di Roskrepp (Contea di Vest-Agder, Norvegia) è stato costruito e calibrato utilizzando il freeware LVtrans. I transitori generati in diversi scenari sono stati analizzati.

Dai risultati delle simulazioni emerge che la simulazione diretta è un metodo migliore, che permette un dimensionamento più accurato del pozzo piezometrico. Tuttavia, il metodo di Thoma, nonostante la minore accuratezza, è ancora rilevante per le prime fasi della progettazione, quando i dati disponibili sono limitati.

Parole chiave: Energia idroelettrica, Stabilità, Transitori, Pozzi piezometrici, Simulazione diretta, Modello numerico monodimensionale, LVtrans, Metodo di Thoma

Acknowledgments

My gratitude goes to my supervisors, Prof. Kaspar Vereide from NTNU and Prof. Stefano Malavasi from Politecnico di Milano, for their precious guidance and support during the entire thesis work. I also intend to thank my co-supervisor, Livia Pitorac, for her constant availability and help.

Special thanks to prof. Lanzoni and prof. Defina, from the University of Padova, for providing me the proceedings of the conference on hydraulics held in Padova in 1947, not publicly available.

Then, I would like to thank my alma mater, Politecnico di Milano, for giving me the opportunity to participate in a Double Degree programme and come to Norway to complete my studies.

Finally, I am very grateful to my parents, my boyfriend, and my friends. Despite the distance, their love, support, and encouragement were present every day.

Note to the reader

In the context of the thesis, also a conference paper has been written and will be published later on this year. The reader interested in a more synthetic exposition of the study in the thesis is therefore addressed to the following publication:

Pitorac, L., Bardini, D., Vereide, K., Lia, L., (2018), *The effect of brook intakes, downstream surge tanks and reservoir levels on surge tank stability*, Proceedings of the BHR 13th International Conference on Pressure Surges, Bordeaux.

Contents

Abstract	II
Sommario	III
Acknowledgments	IV
Note to the reader	VI
List of figures	X
List of tables	XIII
List of symbols	XIV
1. Introduction	1
1.1 Background.....	1
1.2 Organisation of the study.....	3
2. Theory	5
2.1 Governing equations.....	5
2.1.1 Equation of motion.....	5
2.1.2 Continuity equation	7
2.2 Method of characteristics	11
2.3 Water hammer	13
2.3.1 Impulse-Momentum theorem.....	13
2.3.2 Qualitative description of water hammer	16
2.3.3 Sudden and slow valve closure	18
2.4 Mass oscillations	20
2.4.1 Description of the phenomenon	20
2.4.2 Fundamental equations.....	21
2.4.3 Direct integration.....	24
2.4.4 Rule of thumb.....	26
2.5 Stability	27
2.5.1 The time-constants T_w and T_a	28
2.5.2 Algebraic investigation of the limit of stability.....	28
2.5.3 Thoma method.....	30
3. Literature review: Italian literature on surge tank stability	33
4. Method	36
4.1 Roskrepp power plant.....	36
4.1.1 Upper and lower reservoir.....	38
4.1.2 Brook intake	39
4.1.3 Upstream surge tank.....	40

4.1.4 Turbine	41
4.1.5 Downstream surge tank.....	41
4.1.6 Pipes	42
4.2 LVtrans	44
4.3 Calibration.....	47
4.3.1 Calibration of steady-state operation.....	49
4.3.2 Calibration of transient operation.....	50
4.4 Validation	53
5. Results and discussion.....	56
5.1 Influence on stability	56
5.1.1 Influence of the brook intake.....	56
5.1.2 Influence of the downstream surge tank.....	59
5.2 Possibility of abolishing the upstream surge tank	61
5.2.1 Real value for $D_{\text{brook intake}}$	61
5.2.2 Calibrated value for $D_{\text{brook intake}}$	62
5.3 Stability analysis.....	63
5.3.1 Thoma method.....	64
5.3.2 Direct simulation	65
5.3.3 Comparison	70
5.3.4 Minimum diameter required for stability, case with reduced $D_{\text{brook intake}}$	71
6. Conclusions and suggestions for future work	75
6.1 Conclusions	75
6.2 Suggestions for future work	75
A. Annex	77
Annex 1: Parameters of the LVtrans model	77
Annex 2: Procedure of the calibration of transient operation.....	86
Annex 3: Comparison between Thoma area and actual size of the upstream surge tank.....	95
Bibliography.....	99

List of figures

Figure 1.1 - Pressure wave travel space in the upstream waterway of a hydropower plant scheme, (a) without surge tank, (b) with surge tank.....	2
Figure 1.2 - Surge tank oscillations.....	3
Figure 2.1 - Free-body diagram for the application of the equation of motion.....	5
Figure 2.2 - Control volume for continuity equation	7
Figure 2.3 - Characteristic lines	13
Figure 2.4 - Simplified scheme of a hydropower plant.....	14
Figure 2.5 - Pipe in the time interval immediately after the valve closure	14
Figure 2.6 - Phases of the water hammer	16
Figure 2.7 - Development of pressure (left-hand side) and velocity (right-hand side) over time.....	17
Figure 2.8 - Pressure waves development over time.....	18
Figure 2.9 - Pressure history when $T_c < \tau$	19
Figure 2.10 - Pressure history when $T_c > \tau$	19
Figure 2.11 - Mass oscillations in a power plant with a surge shaft	20
Figure 2.12 - Notation for the surge tank.....	21
Figure 2.13 - Oscillation of water level in the surge tank following the sudden closure of turbine valve, when tunnel friction is neglected.....	26
Figure 2.14 - Water level variation in the surge tank consequently to a partial closure of the turbine guide vanes, theoretical case (no friction in the tunnel).....	27
Figure 2.15 - Outline of stability analysis	29
Figure 2.16 - Governor characteristics	30
Figure 4.1 - Roskrepp power plant, part 1.....	37
Figure 4.2 - Roskrepp power plant, part 2.....	37
Figure 4.3 - Intake and outlet location	38
Figure 4.4 - Roskrepp power plant, plan view	39
Figure 4.5 - Brook intake of Roskrepp power plant.....	39
Figure 4.6 - Surge tank design - alternative I and II.....	40
Figure 4.7 - Simplified design of the upstream surge tank	41
Figure 4.8 - Downstream surge tank, side view	41
Figure 4.9 - Original cross-section of the headrace tunnel.....	42
Figure 4.10 - Cross section of the headrace tunnel after the asphalt removal.....	43
Figure 4.11 - Headrace tunnel and its cross-sections	43
Figure 4.12 - Draft tube, side view.....	44
Figure 4.13 - Tailrace tunnel and its cross-section.....	44
Figure 4.14 - Program interface, block diagram window.....	45
Figure 4.15 - Program interface, simulation settings window	45
Figure 4.16 - LVtrans model of Roskrepp power plant, part 1	46
Figure 4.17 - LVtrans model of Roskrepp power plant, part 2	46
Figure 4.18 - Power output during the measurements, September 19 th , 2017	48
Figure 4.19 - Water level in the upper reservoir during the measurements	48
Figure 4.20 - Water level in the lower reservoir during the measurements	48
Figure 4.21 - Shutdown: adjusted static head downstream the turbine.....	50
Figure 4.22 - Shutdown: static head in front of the turbine, comparison between measurements and model output.....	52
Figure 4.23 - Shutdown: static head downstream the turbine, comparison between measurements and model output.....	53

Figure 4.24 - Small load change: guide vanes opening, comparison between measurements and model	54
Figure 4.25 - Small load change: static head in front of the turbine, comparison between measurements and model output	54
Figure 5.1 - Influence of the brook intake, scenario A: water level variation in the upstream surge tank	57
Figure 5.2 - Influence of the brook intake, scenario A: water level variation in the downstream surge tank	57
Figure 5.3 - Part of pipe affected by mass oscillations in the existing design, with one brook intake	58
Figure 5.4 - Part of pipe affected by mass oscillations in the design without any brook intake	58
Figure 5.5 - Part of pipe affected by mass oscillations in the design with two brook intakes	58
Figure 5.6 - Influence of the brook intake, scenario B: water level variation in the upstream surge tank	59
Figure 5.7 - Influence of the brook intake, scenario B: water level variation in the downstream surge tank	59
Figure 5.8 - Influence of the downstream surge tank, scenario A: water level variation in the upstream surge tank	60
Figure 5.9 - Influence of the downstream surge tank, scenario B: water level variation in the upstream surge tank	60
Figure 5.10 - Brook intake: diameter and diameter of the equivalent water table surface	61
Figure 5.11 - Abolition of the upstream surge tank, start-up to full load: water level variation in the brook intake ($D_{\text{brook intake}} = 27 \text{ m}$)	62
Figure 5.12 - Abolition of the upstream surge tank, start-up to full load: water level variation in the downstream surge tank ($D_{\text{brook intake}} = 27 \text{ m}$)	62
Figure 5.13 - Abolition of the upstream surge tank, start-up to full load: water level variation in the brook intake ($D_{\text{brook intake}} = 18 \text{ m}$)	63
Figure 5.14 - Abolition of the upstream surge tank, start-up to full load: water level variation in the downstream surge tank ($D_{\text{brook intake}} = 18 \text{ m}$)	63
Figure 5.15 - Sensitivity analysis: sensitivity of A_{Thoma} to the variation of Manning number	65
Figure 5.16 - scenario a: water level variation in the brook intake, comparison of different $D_{\text{brook intake}}$	66
Figure 5.17 - scenario a: water level variation in the downstream surge tank, comparison of different $D_{\text{brook intake}}$	66
Figure 5.18 - scenario b: water level variation in the brook intake, comparison of different $D_{\text{brook intake}}$	67
Figure 5.19 - scenario b: water level variation in the downstream surge tank, comparison of different $D_{\text{brook intake}}$	67
Figure 5.20 - scenario c: water level variation in the upstream surge tank, comparison of different $D_{\text{upstream surge shaft}}$	68
Figure 5.21 - scenario c: water level variation in the downstream surge tank, comparison of different $D_{\text{upstream surge shaft}}$	68
Figure 5.22 - scenario d: water level variation in the upstream surge tank, comparison of different $D_{\text{upstream surge shaft}}$	69
Figure 5.23 - scenario d: water level variation in the brook intake when $D_{\text{brook intake}} = 18 \text{ m}$	69
Figure 5.24 - scenario d: water level variation in the brook intake, comparison of different $D_{\text{brook intake}}$	70
Figure 5.25 - scenario a: water level variation in the upstream surge tank, comparison of different $D_{\text{upstream surge shaft}}$	71
Figure 5.26 - scenario a: water level variation in the downstream surge tank, comparison of different $D_{\text{upstream surge shaft}}$	72
Figure 5.27 - scenario b: water level variation in the upstream surge tank, comparison of different $D_{\text{upstream surge shaft}}$	72
Figure 5.28 - scenario b: water level variation in the downstream surge tank, comparison of different $D_{\text{upstream surge shaft}}$	73

Figure 5.29 - scenario d: water level variation in the upstream surge tank, comparison of different	
Dupstream surge shaft	73
Figure A.1 - Turbine opening during the shutdown.....	86
Figure A.2 - Measured static head in front of the turbine	87
Figure A.3 - Static head in front of the turbine: measurements and simulations for different brook intake diameters	87
Figure A.4 - Static head in front of the turbine: measurements and model calibrated for the brook intake diameter.....	88
Figure A.5 - Static head in front of the turbine: measurements and simulations for different loss coefficients C_{vp} for the brook intake	88
Figure A.6 - Static head in front of the turbine: measurements and model calibrated for the loss coefficient C_{vp} for the brook intake.....	89
Figure A.7 - Static head in front of the turbine: measurements and simulations for different loss coefficients C_{vm} for the brook intake	89
Figure A.8 - Static head in front of the turbine: measurements and model calibrated for the loss coefficient C_{vp} for the brook intake.....	90
Figure A.9 - Static head in front of the turbine: measurements and simulations for different areas of the vertical shaft of the upstream surge tank.....	90
Figure A.10 - Static head in front of the turbine: measurements and model calibrated for the area of the vertical shaft of the upstream surge tank.....	91
Figure A.11 - Static head in front of the turbine: measurements and simulations for different loss coefficients C_{vp} for the upstream surge tank	91
Figure A.12 - Static head in front of the turbine: measurements and model calibrated for the loss coefficient C_{vp} for the upstream surge tank	92
Figure A.13 - Adjusted hydraulic head downstream the turbine	92
Figure A.14 - Static head downstream the turbine: measurements and simulations for different diameters of the downstream surge tank.....	93
Figure A.15 - Static head downstream the turbine: measurements and model calibrated for the diameter of the downstream surge tank.....	93
Figure A.16 - Static head in downstream the turbine: measurements and simulations for different loss coefficients C_{vp} and C_{vm} for the downstream, surge tank	94
Figure A.17 - Static head downstream the turbine: measurements and model calibrated for the loss coefficients C_{vp} and C_{vm} for the downstream surge tank	94
Figure A.18 - scenario a: water level variation in the upstream surge tank, comparison between Thoma area and actual size of the upstream surge tank	95
Figure A.19 - scenario a: water level variation in the downstream surge tank, comparison between Thoma area and actual size of the upstream surge tank	95
Figure A.20 - scenario b: water level variation in the upstream surge tank, comparison between Thoma area and actual size of the upstream surge tank	96
Figure A.21 - scenario b: water level variation in the downstream surge tank, comparison between Thoma area and actual size of the upstream surge tank	96
Figure A.22 - scenario c: water level variation in the upstream surge tank, comparison between Thoma area and actual size of the upstream surge tank	97
Figure A.23 - scenario c: water level variation in the downstream surge tank, comparison between Thoma area and actual size of the upstream surge tank	97
Figure A.24 - scenario d: water level variation in the upstream surge tank, comparison between Thoma area and actual size of the upstream surge tank	98

List of tables

Table 4-1 - Technical data of Roskrepp power plant	36
Table 4-2 - Characteristics of the reservoirs	38
Table 4-3 - Characteristics of the brook intake	39
Table 4-4 - Upstream surge tank, cross-section areas	40
Table 4-5 - Characteristics of the turbine.....	41
Table 4-6 - Characteristics of the downstream surge tank	42
Table 4-7 - Characteristics of the headrace tunnel cross-sections.....	43
Table 4-8 - Components of the model.....	47
Table 4-9 - Measured power output and pressure in front of the turbine.....	49
Table 4-10 - Calibration of steady-state operation: comparison between measurements and calibrated model.....	50
Table 4-11 - Parameters to be calibrated upstream the turbine	51
Table 4-12 - Calibrated set of parameters upstream the turbine	51
Table 4-13 - Parameters to be calibrated downstream the turbine	52
Table 4-14 - Calibrated set of parameters downstream the turbine	53
Table 4-15 - Validation: comparison between measurements and validated model	55
Table 5-1 - Computation of weighted averages of area and Manning number for the headrace tunnel ...	64
Table 5-2 - Thoma area and correspondent diameter for Roskrepp power plant.....	65
Table 5-3 - Comparison between Thoma method and direct simulation	70
Table 5-4 – Minimum area required for stability for each scenario.....	74

List of symbols

Symbol	Description	Unit
A	Tunnel area	[m ²]
A_s	Surge tank area	[m ²]
A_{Thoma}	Thoma area	[m ²]
a	Celerity	[m/s]
acc	Acceleration	[m/s ²]
D	Pipe diameter	[m]
g	Gravitational acceleration	[m/s ²]
H	Hydraulic head	[mWC]
H_{net}	Net head	[mWC]
J	Moment of inertia	[kg·m ²]
K_{st}	Strickler coefficient	[m ^{1/3} /s]
L	Length of the tunnel	[m]
m	Mass	[kg]
M	Manning number	[m ^{1/3} /s]
n	Speed of rotation	[rpm]
p	Pressure	[Pa]
P	Power	[W]
Q	Water discharge	[m ³ /s]
v	Fluid velocity	[m/s]
t	Time	[s]
T_a	Acceleration time of rotating masses	[s]
T_w	Inflow time of masses of water	[s]
γ	Specific weight	[kN/m ³]
η	Efficiency	[-]
ζ	Singular loss coefficient	[-]
ρ	Density	[kg/m ³]

1. Introduction

In a hydropower plant, every time the wicket gates are operated, pressure transients occur. These can result in large pressures affecting the hydraulic system, particularly in the case of fast shutdown from full load.

The amplitude of these transients can be reduced by installing a surge tank, which helps by reflecting incoming pressure waves (Chaudhry, 1987). In addition, a surge tank improves quality of frequency governing (Nielsen, 2015). For these reasons, surge tanks should be included in hydropower plants with long water conduits.

In the last years, we have witnessed an energy transition, from fossil fuels to renewable sources. Climatic policies will strengthen this tendency in the future. The larger use of intermittent sources as wind and solar makes hydropower crucial as a balancer. So, the consequence of this transition on hydropower market will be the need of larger hydropower, subjected to more frequent start-stop operations. The increase of the size of the power plant and the requirement of more frequent start-stop operations make the surge tank design crucial to achieve products able to cope with the new challenges (Vereide, 2016).

1.1 Background

The wicket gates are adjusted in order to regulate the flow to match the production with the demand. The resulting pressure transients occur between the turbine and the closest free water surface - the upper reservoir if a surge tank is not present. The introduction of a surge tank prevents the high-pressure waves from reaching the headrace, as the surge tank reflects back the water hammer.

Hence, the headrace has not to be designed to withstand such high pressures, with a consequent cost-reduction.

Besides, the conduit length affected by water hammer is reduced by the introduction of a surge tank. Therefore, the hydraulic mass involved is reduced, as can be seen in Figure 1.1, and this results in a decrease of the amplitude of the pressure transients.

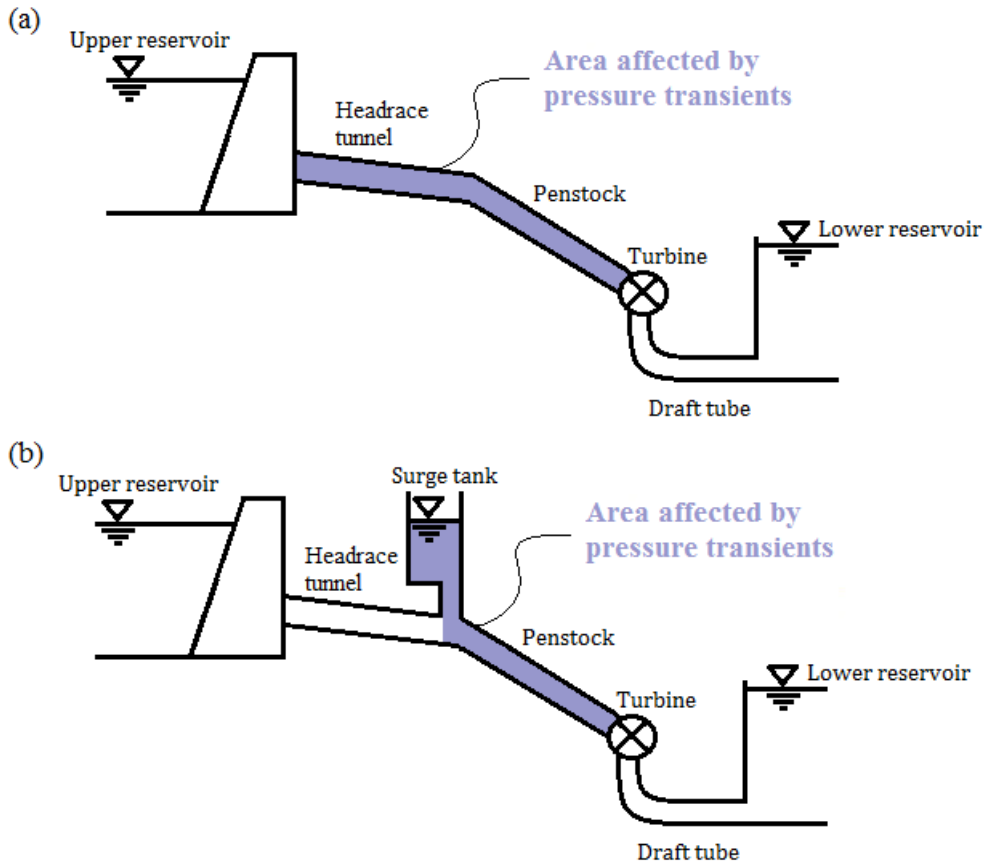


Figure 1.1 - Pressure wave travel space in the upstream waterway of a hydropower plant scheme, (a) without surge tank, (b) with surge tank

Besides, a surge tank improves quality of frequency governing. All over Europe, the demand is to keep the grid frequency at 50 Hz, and the electric components in the household have the specific requirement to be operated at this frequency, with some tolerance (usually ± 0.1 Hz). If this requirement is not satisfied, this will not affect IT equipment, as it is tolerant of minor shifts in frequency, but it may have consequences on any motor device or sensitive device that relies on steady regular cycling of power over time. Frequency variations may cause a motor to run faster or slower, in order to match the frequency of the input power. This will result in its inefficiency and, likely, in its degradation (Seymour and Horsley, 2005).

The stability of the grid frequency is guaranteed by maintaining the speed of rotation constant and equal to the synchronous speed value. In fact, speed of rotation n and frequency are related by the following relationship:

$$n = \frac{60 \text{ s} \cdot \text{frequency}}{\text{number of pole pairs in the generator}} \quad (1.1)$$

Hence, if the speed of rotation is constant, the frequency will be stable.

In a hydropower plant, the turbine transforms the hydraulic power in mechanical power, then transformed by the generator in electrical power and delivered to the grid (Nielsen, 2016). Therefore, in order to maintain the frequency stability, it is crucial to keep the electric power demand in balance with the hydraulic power output, which means to adapt fast the production to match the demand.

A surge tank helps in achieving the frequency stability. In fact, the introduction of a surge tank reduces the water-starting time, i.e. the time needed to mobilize the water, making the response of the power plant faster.

However, by introducing a surge tank, the system is opened to mass oscillations, i.e. the water level oscillation in the surge tank. For instance, when the turbine is required to shut down, the momentum of the water in the tunnel is not destroyed quickly, so the water continues to flow and passes into the surge tank until the flow stops. At this point, the level in the surge tank will be higher than the one in the upper reservoir, so reversed flow will occur, setting up a long-period oscillation between the surge tank and the upper reservoir (Featherstone et al., 2009). This phenomenon is called U-tube oscillation. Figure 1.2 represents a typical time variation of the water level in a surge tank.

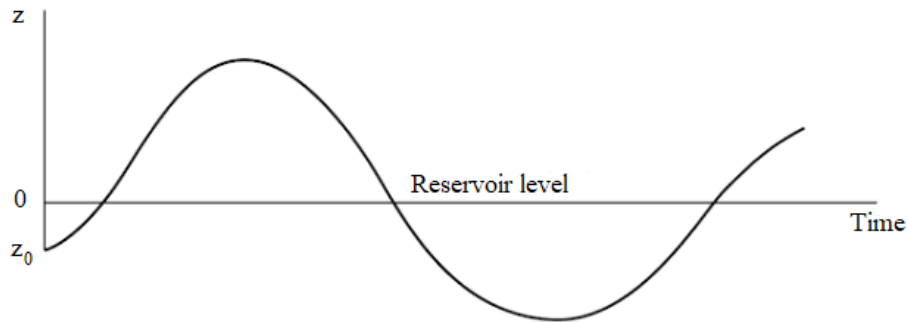


Figure 1.2 - Surge tank oscillations

Surge tank design is crucial in order to deal safely with this phenomenon, preventing overflow in case of upsurge and air entrainment in the tunnel in case of downsurge.

Thoma equation (1910) is the standard method to select the area of a surge tank sufficient to guarantee stability. However, this method is based on simplifications and neglect the influence of the pressure shaft, the velocity head of the water, and the variable turbine efficiency during oscillations.

Improvements in computational power give the chance to adopt more advanced methods, relying on complex numerical simulations. Prominent among them is the direct simulation, consisting in a one-dimensional numerical simulation of the entire hydropower plant, without the simplifications adopted in Thoma equation.

The aim of this thesis is to test whether direct simulation represents a more effective and punctual alternative to Thoma method. In order to answer this question, a one-dimensional numerical model of Roskrepp power plant, owned by Sira-Kvina kraftselskap, is established and calibrated. The model is then used to compare results of direct simulation method with those of Thoma method.

1.2 Organisation of the study

The thesis proposes to analyse the problem presented above with the following organisation:

- In *Chapter 1*, the topic is introduced and the background information is presented.
- In *Chapter 2*, the theoretical background of the thesis is illustrated. The theory behind water hammer and mass oscillation is presented, together with the equations describing these phenomena. The topic of stability is discussed, and the standard stability criterion, Thoma method, is introduced.
- In *Chapter 3*, a literature review that focuses on the Italian contribution is presented.
- In *Chapter 4*, the method is discussed. In the first part of the chapter, the hydropower plant used for the case study, Roskrepp power plant, is described. In the second part, the developed model is introduced, and its calibration and validation are presented.

- In *Chapter 5*, the results are presented and discussed. First, the influence on stability of some elements of the power plant and the possibility to abolish the upstream surge tank are investigated. Then, a comparison between Thoma method and the direct simulation is presented. Finally, the stability analysis for unfavourable conditions is illustrated.
- In *Chapter 6*, the study is concluded. The chapter presents the conclusions, pointing out the reasons that lead to them, and the suggestions for future work.

2. Theory

This chapter presents the theory behind the method, providing the information necessary to understand the modelling. The governing equations and the method of characteristics are described and derived. Then the phenomena of water hammer and mass oscillations are introduced. The last part deals with the stability in hydropower plants.

2.1 Governing equations

Non-stationary flow is a condition that occurs whenever a change takes place. The result is hydraulic transients, such as water hammer and mass oscillations.

Water hammer is a pressure wave with a short period (few seconds) and, when analysing this phenomenon, compressibility cannot be neglected. Mass oscillations are surface waves, and their period is much longer than the one of water hammer. In their study, compressibility can be neglected.

Since the periods are so different, the two phenomena can be solved separately. In fact, water hammer will be dampened out already when the mass oscillations will start to develop (Guttormsen, 2006).

The governing equations behind these two phenomena are the equation of motion and the continuity equation, here described according to Wylie and Streeter (1993).

2.1.1 Equation of motion

This equation is derived from the dynamic equilibrium of an element of fluid between two sections. The coordinate distance between these sections along the axis of the tube is dx (Marchi and Rubatta, 1981).

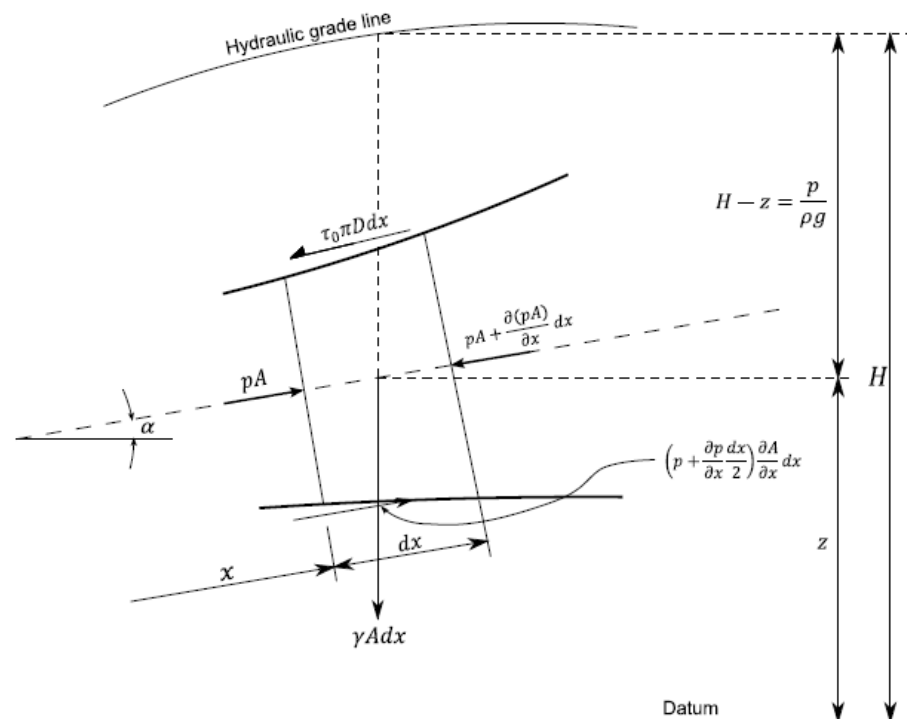


Figure 2.1 - Free-body diagram for the application of the equation of motion

The forces acting on the control volume are:

- thrusts due to normal pressures acting on transverse faces: pA and $pA + \frac{\partial(pA)}{\partial x} dx$;
- gravity axial load: $\gamma A dx \sin\alpha$, where $\sin\alpha = \frac{dz}{dx}$;
- axial pressure load on the periphery: $\left(p + \frac{\partial p}{\partial x} \frac{dx}{2}\right) \frac{\partial A}{\partial x} dx$;
- shear component on the periphery: $\tau_0 \pi D dx$

Newton's second law is: $\sum_i F_i = m \cdot acc$. Since the mass of the control volume is equal to $m = \rho A dx$ and the acceleration can be expressed as the derivative of velocity with respect to time $acc = \frac{dv}{dt} = \dot{v}$, Newton's second law for the control volume can be written as:

$$pA - \left[pA + \frac{\partial(pA)}{\partial x} dx \right] + \left(p + \frac{\partial p}{\partial x} \frac{dx}{2} \right) \frac{\partial A}{\partial x} dx - \tau_0 \pi D dx - \gamma A dx \sin\alpha = \rho A dx \dot{v} \quad (2.1)$$

By dropping out the second order infinitesimals and simplifying, the equation finally becomes:

$$\frac{\partial p}{\partial x} A + \tau_0 \pi D + \gamma A \sin\alpha + \rho A \dot{v} = 0 \quad (2.2)$$

In transient flow calculations, the shear stress is assumed to be equal to the one under steady behaviour, so, by applying the Darcy-Weissbach friction factor f :

$$\tau_0 = \frac{\rho f v |v|}{8} \quad (2.3)$$

where the absolute sign is to guarantee that the shear stress opposes the direction of the velocity.

The acceleration \dot{v} in equation (2.2) is the total derivate of velocity with respect to time, and it can be written as:

$$\dot{v} = v \frac{\partial v}{\partial x} + \frac{\partial v}{\partial t} \quad (2.4)$$

So, by substituting (2.3) and (2.4) in (2.2), it yields:

$$\frac{\partial p}{\partial x} A + \frac{\rho f v |v|}{8} \pi D + \gamma A \sin\alpha + \rho A \left(v \frac{\partial v}{\partial x} + \frac{\partial v}{\partial t} \right) = 0 \quad (2.5)$$

By dividing every term by (ρA) , remembering that $A = \frac{\pi D^2}{4}$, the resulting equation is:

$$\frac{\partial p}{\partial x} \frac{1}{\rho} + \frac{f v |v|}{2 D} + g \sin\alpha + v \frac{\partial v}{\partial x} + \frac{\partial v}{\partial t} = 0 \quad (2.6)$$

When assuming a low Mach number¹, it is possible to neglect the term $v \frac{\partial v}{\partial x}$ (because of this, the following formulas will be valid only for less compressible fluids, at low velocities), so:

$$\frac{\partial p}{\partial x} \frac{1}{\rho} + \frac{f v |v|}{2 D} + g \sin \alpha + \frac{\partial v}{\partial t} = 0 \quad (2.7)$$

p may be replaced by the piezometric head, $p = \rho g (H - z)$, where z is the elevation of the centreline of the pipe at position x . So:

$$\frac{\partial p}{\partial x} = \rho g \left(\frac{\partial H}{\partial x} - \sin \alpha \right) \quad (2.8)$$

By substituting (2.8) in (2.7) and simplifying:

$$g \frac{\partial H}{\partial x} + \frac{\partial v}{\partial t} + \frac{f v |v|}{2 D} = 0 \quad (2.9)$$

2.1.2 Continuity equation

The continuity equation is derived referring to a moving control volume of length dx that, at time t , may be considered as fixed with respect to the pipe, since it moves and stretches at velocity u as the inside surface of the pipe moves and stretches. On the other hand, v is the velocity of the flow in the pipe.

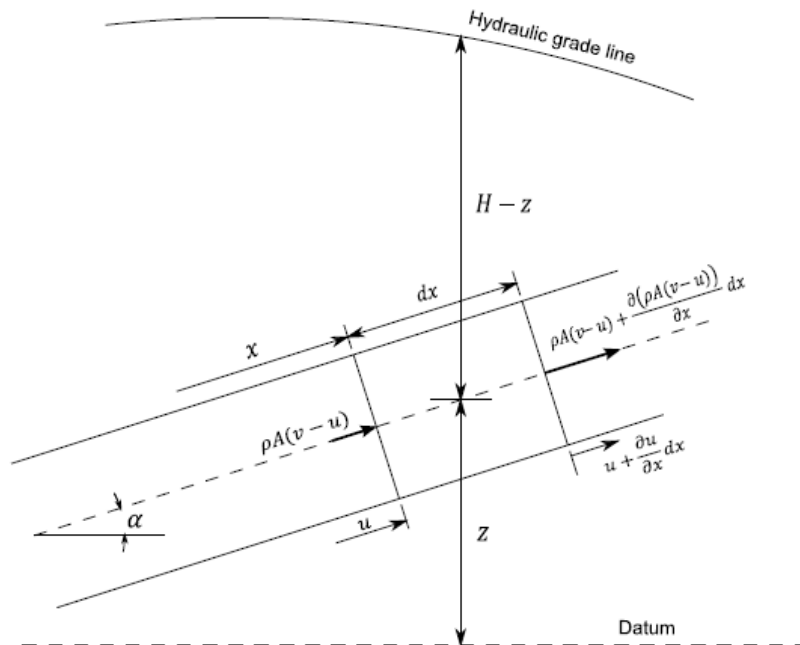


Figure 2.2 - Control volume for continuity equation

To derive the continuity equation, the principle of conservation of mass must be applied to the control volume, by stating that the rate of mass inflow into the control volume is just equal to the time rate of increase of mass within the control volume.

¹Mach number is equal to the speed of the object divided by the speed of sound in the medium

So:

$$-\frac{\partial [\rho A (v - u)]}{\partial x} dx = \frac{d}{dt} (\rho A dx) \quad (2.10)$$

The total derivative with respect to the axial motion of the pipe (which has velocity u) may be written as:

$$\frac{d}{dt} = u \frac{\partial}{\partial x} + \frac{\partial}{\partial t} \quad (2.11)$$

And the time rate increase of the length dx of the control volume is:

$$\frac{d}{dt} dx = \frac{\partial u}{\partial x} dx \quad (2.12)$$

as shown in Figure 2.2.

The right-hand term in (2.10) can be expanded as:

$$\frac{d}{dt} (\rho A dx) = \frac{d}{dt} (dx) \rho A + \frac{d}{dt} (\rho A) dx \quad (2.13)$$

By using (2.12), the first right-hand term in (2.13) can be written as:

$$\frac{d}{dt} (dx) \rho A = \rho A \frac{\partial u}{\partial x} dx \quad (2.14)$$

By using (2.11), the second right-hand term in (2.13) can be written as:

$$\frac{d}{dt} (\rho A) dx = u \frac{\partial (\rho A)}{\partial x} dx + \frac{\partial (\rho A)}{\partial t} dx \quad (2.15)$$

By expanding the left-hand term in (2.10) and using (2.14) and (2.15), the resulting equation is:

$$\begin{aligned} \rho A \frac{\partial v}{\partial x} dx + v \frac{\partial (\rho A)}{\partial x} dx - \rho A \frac{\partial u}{\partial x} dx - u \frac{\partial (\rho A)}{\partial x} dx + \rho A \frac{\partial u}{\partial x} dx + u \frac{\partial (\rho A)}{\partial x} dx \\ + \frac{\partial (\rho A)}{\partial t} dx = 0 \end{aligned} \quad (2.16)$$

By simplifying dx and removing the equal terms:

$$\rho A \frac{\partial v}{\partial x} + v \frac{\partial (\rho A)}{\partial x} + \frac{\partial (\rho A)}{\partial t} = 0 \quad (2.17)$$

$v \frac{\partial (\rho A)}{\partial x}$ and $\frac{\partial (\rho A)}{\partial t}$ can be expanded, so:

$$\rho A \frac{\partial v}{\partial x} + v \frac{\partial \rho}{\partial x} A + v \frac{\partial A}{\partial x} \rho + \frac{\partial \rho}{\partial t} A + \frac{\partial A}{\partial t} \rho = 0 \quad (2.18)$$

By dividing every term by (ρA) , (2.18) becomes

$$\frac{\partial v}{\partial x} + v \frac{\partial \rho}{\partial x} \frac{1}{\rho} + v \frac{\partial A}{\partial x} \frac{1}{A} + \frac{\partial \rho}{\partial t} \frac{1}{\rho} + \frac{\partial A}{\partial t} \frac{1}{A} = 0 \quad (2.19)$$

By rearranging the previous equation, it yields:

$$\frac{\frac{\partial \rho}{\partial t} + v \frac{\partial \rho}{\partial x}}{\rho} + \frac{\frac{\partial A}{\partial t} + v \frac{\partial A}{\partial x}}{A} + \frac{\partial v}{\partial x} = 0 \quad (2.20)$$

Since the total derivative with respect to the motion of a mass particle is:

$$\frac{d}{dt} = v \frac{\partial}{\partial x} + \frac{\partial}{\partial t} \quad (2.21)$$

and since the total derivative can be indicated by a dot over the dependent variable, (2.20) becomes:

$$\frac{\dot{\rho}}{\rho} + \frac{\dot{A}}{A} + \frac{\partial v}{\partial x} = 0 \quad (2.22)$$

(2.22) has general validity. Now, some hypotheses which are common in practical applications of hydraulic engineering are introduced (Mambretti, 2004):

- Newtonian fluid

By introducing the bulk modulus of elasticity of a fluid K , the following relationship is valid for a Newtonian fluid:

$$\frac{\dot{\rho}}{\rho} = \frac{\dot{p}}{K} \quad (2.23)$$

- Prismatic pipe

The pipe has constant dimensions along its length, so the area is a function of the pressure only:

$$\dot{A} = \frac{dA}{dp} \dot{p} \quad (2.24)$$

By substituting (2.23) and (2.24) in (2.22), it yields:

$$\frac{\dot{p}}{K} + \frac{dA}{dp} \frac{\dot{p}}{A} + \frac{\partial v}{\partial x} = 0 \quad (2.25)$$

Rearranging, the resulting equation is:

$$\frac{\partial v}{\partial x} + \frac{\dot{p}}{K} \left(1 + \frac{dA}{dp} \frac{K}{A} \right) = 0 \quad (2.26)$$

Since the wave speed a can be expressed as²:

$$a^2 = \frac{\frac{K}{\rho}}{1 + \frac{K}{A} \frac{\Delta A}{\Delta p}} \quad (2.27)$$

(2.26) can be rewritten as:

$$\rho a^2 \frac{\partial v}{\partial x} + \dot{p} = 0 \quad (2.28)$$

where \dot{p} can be expanded as:

$$\rho a^2 \frac{\partial v}{\partial x} + \frac{\partial p}{\partial t} + v \frac{\partial p}{\partial x} = 0 \quad (2.29)$$

By dropping the transport term, as being small with respect to the others, it yields:

$$\rho a^2 \frac{\partial v}{\partial x} + \frac{\partial p}{\partial t} = 0 \quad (2.30)$$

which is valid for low-Mach number unsteady flows.

Again, p can be replaced by the piezometric head, $p = \rho g (H - z)$, so:

$$\frac{\partial p}{\partial t} = \rho g \frac{\partial H}{\partial t} \quad (2.31)$$

Hence, (2.30) becomes:

$$\rho a^2 \frac{\partial v}{\partial x} + \rho g \frac{\partial H}{\partial t} = 0 \quad (2.32)$$

Finally, by dividing every term by (ρg) :

$$\frac{a^2}{g} \frac{\partial v}{\partial x} + \frac{\partial H}{\partial t} = 0 \quad (2.33)$$

² for the derivation, refer to Wylie and Streeter, 1993, Fluid Transients in Systems - Chapter 1

2.2 Method of characteristics

As shown in the paragraph above, a system of partial differential equations describes water hammer and mass oscillations:

$$\left\{ \begin{array}{l} g \frac{\partial H}{\partial x} + \frac{\partial v}{\partial t} + \frac{f v |v|}{2 D} = 0 \\ \frac{a^2}{g} \frac{\partial v}{\partial x} + \frac{\partial H}{\partial t} = 0 \end{array} \right. \quad (2.9)$$

$$\left\{ \begin{array}{l} \frac{a^2}{g} \frac{\partial v}{\partial x} + \frac{\partial H}{\partial t} = 0 \end{array} \right. \quad (2.33)$$

A general solution for it is not available. Therefore, the partial differential equations may be transformed into particular total differential equations by using the method of characteristics.

The method is here presented according to Wylie and Streeter (1993).

First, the two equations are renamed:

$$L_1 = g \frac{\partial H}{\partial x} + \frac{\partial v}{\partial t} + \frac{f v |v|}{2 D} = 0 \quad (2.34)$$

$$L_2 = \frac{a^2}{g} \frac{\partial v}{\partial x} + \frac{\partial H}{\partial t} = 0 \quad (2.35)$$

Then L_1 and L_2 are combined linearly by means of an unknown multiplier λ :

$$L = L_1 + \lambda L_2 = \lambda \left(\frac{g}{\lambda} \frac{\partial H}{\partial x} + \frac{\partial H}{\partial t} \right) + \left(\lambda \frac{a^2}{g} \frac{\partial v}{\partial x} + \frac{\partial v}{\partial t} \right) + \frac{f v |v|}{2 D} = 0 \quad (2.36)$$

Both of the λ real values will give two equations in term of v and H .

In general, both variables v and H are functions of x and t . If x is permitted to be a function of t , then total derivatives of H and v with respect to time can be expanded to be, respectively:

$$\frac{dH}{dt} = \frac{\partial H}{\partial x} \frac{dx}{dt} + \frac{\partial H}{\partial t} \quad (2.37)$$

$$\frac{dv}{dt} = \frac{\partial v}{\partial x} \frac{dx}{dt} + \frac{\partial v}{\partial t} \quad (2.38)$$

If the λ values are selected in such a way that:

$$\frac{dx}{dt} = \frac{g}{\lambda} = \lambda \frac{a^2}{g} \quad (2.39)$$

(2.36) becomes the following ordinary differential equation:

$$\lambda \frac{dH}{dt} + \frac{dv}{dt} + \frac{f v |v|}{2 D} = 0 \quad (2.40)$$

(2.39) makes possible to find the λ values, which result to be:

$$\lambda = \pm \frac{g}{a} \quad (2.41)$$

By substituting them in (2.39), it yields:

$$\frac{dx}{dt} = \pm a \quad (2.42)$$

which means that the change in position of a wave is related to the change in time by the wave propagation velocity a .

It may be worth to underline that, when the positive value of λ is used in (2.41), it must be used also in (2.40), and vice versa. This leads to two pairs of equations, identified as C^+ and C^- :

$$C^+ \left\{ \begin{array}{l} \frac{g}{a} \frac{dH}{dt} + \frac{dv}{dt} + \frac{f v |v|}{2 D} = 0 \\ \frac{dx}{dt} = +a \end{array} \right. \quad (2.43)$$

$$\frac{dx}{dt} = +a \quad (2.44)$$

$$C^- \left\{ \begin{array}{l} -\frac{g}{a} \frac{dH}{dt} + \frac{dv}{dt} + \frac{f v |v|}{2 D} = 0 \\ \frac{dx}{dt} = -a \end{array} \right. \quad (2.45)$$

$$\frac{dx}{dt} = -a \quad (2.46)$$

a is usually constant for a given plane. So, by plotting (2.44) and (2.46) in the $x-t$ plane, the resulting graph will consist in two straight lines - called *characteristic lines* - along which, respectively, (2.43) and (2.45) are valid.

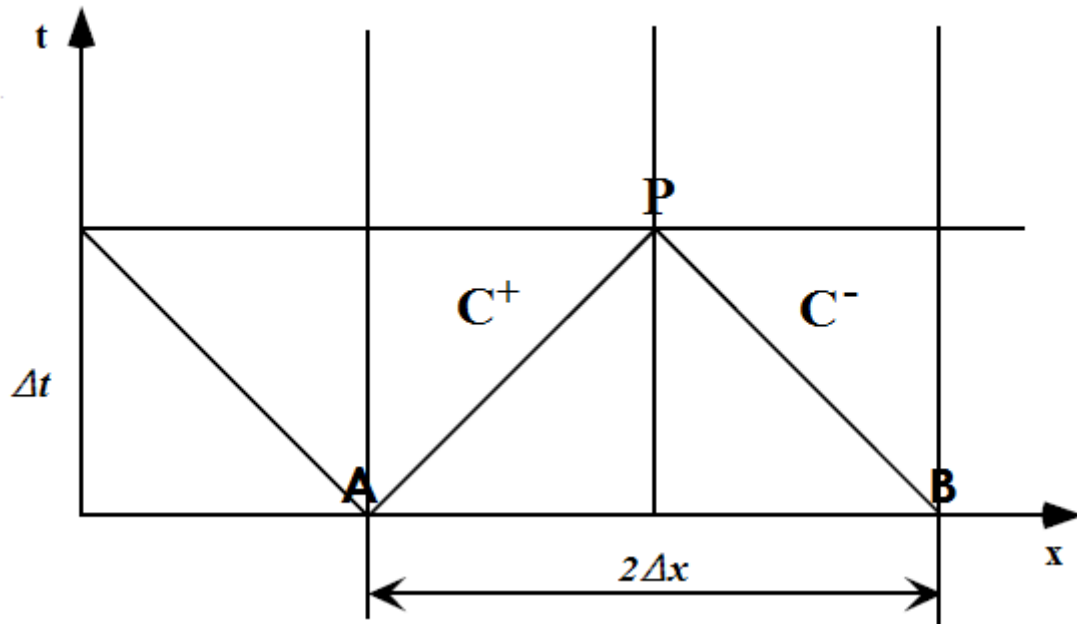


Figure 2.3 - Characteristic lines

(2.43) is satisfied along AP. Hence, if the variables v and H are known in the point A, the equation (2.43) can be integrated along the C^+ line between A and P.

(2.45) is satisfied along BP. Therefore, if the variables v and H are known in the point B, the equation (2.45) can be integrated along the C^- line between B and P.

A simultaneous solution of the two equations (2.43) and (2.45) leads to the values of the unknowns v and H in point P. Remembering that $Q = vA$, it is straightforward to obtain the discharge.

By following an iterative procedure, it is possible to compute the pressure propagation in a pipe. The steps to be iterated are, according to Nielsen (2015):

1. The pipeline is discretized and each segment Δx is equal to $a \cdot \Delta t$. In order to fit in the border conditions, the total length of the pipeline must be $N \cdot \Delta x$, where N is an integer.
2. Q and H for all the internal points of the pipeline at time t_0 are found.
3. Equations (2.43) and (2.45) are integrated and solved with respect to the P-point, i.e. the conditions at time $t_0 + \Delta t$ are found.
4. As the conditions at time $t_0 + \Delta t$ are now known, they can be used to find those at time $t_0 + 2\Delta t$.

The procedure is iterated until Q and A are found for all the pipe.

2.3 Water hammer

The regulation of the turbine discharge produces velocity and pressure variations which travel upstream. This phenomenon is called water hammer, since it yields to rapid increases of pressure that hit the pipe walls (Citirini and Nosedà, 1975). In its description, the water compressibility cannot be neglected, because this would lead to unreliable results.

2.3.1 Impulse-Momentum theorem

The physics behind this phenomenon can be explained by means of the Impulse-Momentum theorem (Mambretti, 2004). Some hypothesis must be introduced, in the interest of simplicity:

- the pipe material is non-deformable ($\frac{\partial A}{\partial t} = 0$);

- the upstream reservoir is very large (therefore, its water level is not influenced by the pipe and stays the same).

The Impulse-Momentum theorem states that, if a body is subjected to an impulse \vec{I} , its momentum will change of a quantity $\vec{\Delta q} = \vec{q}_f - \vec{q}_i$, where \vec{q}_f is the final momentum and \vec{q}_i is the initial one:

$$\vec{I} = \vec{\Delta q}$$

Since the impulse \vec{I} is equal to the product between a force and the time interval during which this force is acting ($\vec{I} = \vec{F}\Delta t$), it can be stated that a force acting on a body causes a variation of the momentum of the body, and vice versa, a variation of the momentum of a body is due to a force acting on it.

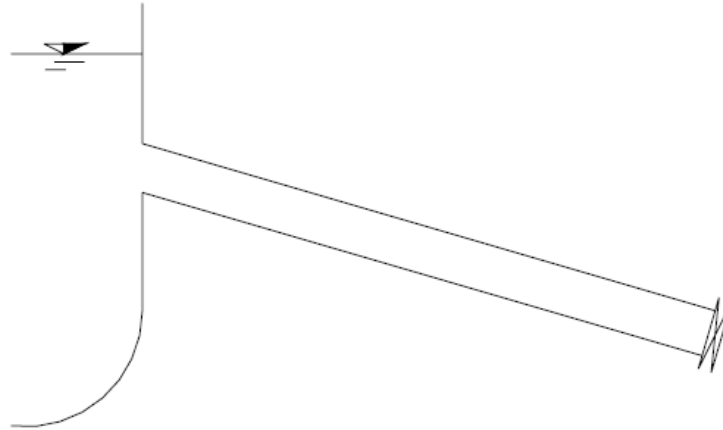


Figure 2.4 - Simplified scheme of a hydropower plant

Referring to the simplified scheme of a plant in Figure 2.4, if the valve downstream is instantly closed, the water in the pipe cannot suddenly stop, because this would cause the momentum to go to zero, which, according to the Impulse-Momentum theorem, would result in an infinite pressure increase in the pipe. Therefore, what actually happens is that, in the infinitesimal time interval dt immediately following the valve closure, an infinitesimal volume of water $A \cdot dx$ stops, whereas the rest of the water in the pipe continues to flow with initial velocity v_0 , as shown in Figure 2.5.

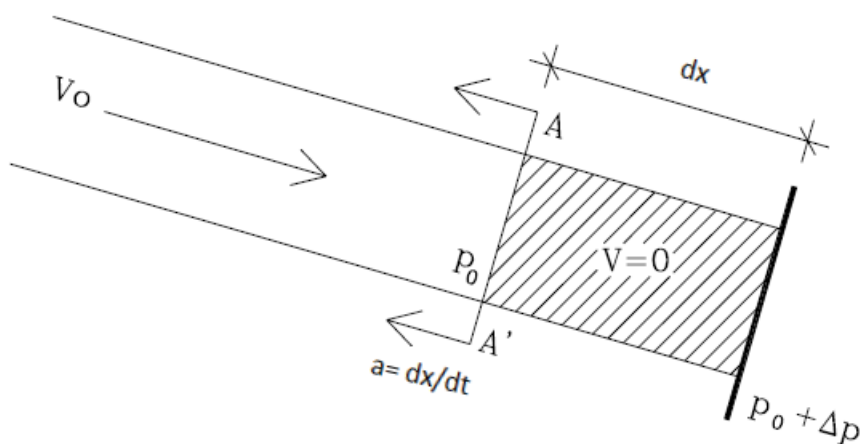


Figure 2.5 - Pipe in the time interval immediately after the valve closure

So, the water contained in the infinitesimal volume $A \cdot dx$ is subjected to a variation in the momentum, since the velocity in there goes to 0. Because of the Impulse-Momentum theorem, this change in the

momentum is balanced by the impulse of a force acting on the water volume: the increase of pressure generated by the valve closure, Δp . This means:

$$\rho A dx v_0 = A \Delta p dt \quad (2.47)$$

which yields to:

$$\Delta p = \rho \frac{dx}{dt} v_0 \quad (2.48)$$

And, since $\frac{dx}{dt}$ is equal to the wave speed a :

$$\Delta p = \rho a v_0 \quad (2.49)$$

It is possible to express (2.49) in terms of height of the water column, Δh (Citrini and Nosedà, 1975):

$$\Delta h = \frac{a}{g} v_0 \quad (2.50)$$

(2.50) represents the so-called Allievi-Joukowski formula.

2.3.2 Qualitative description of water hammer

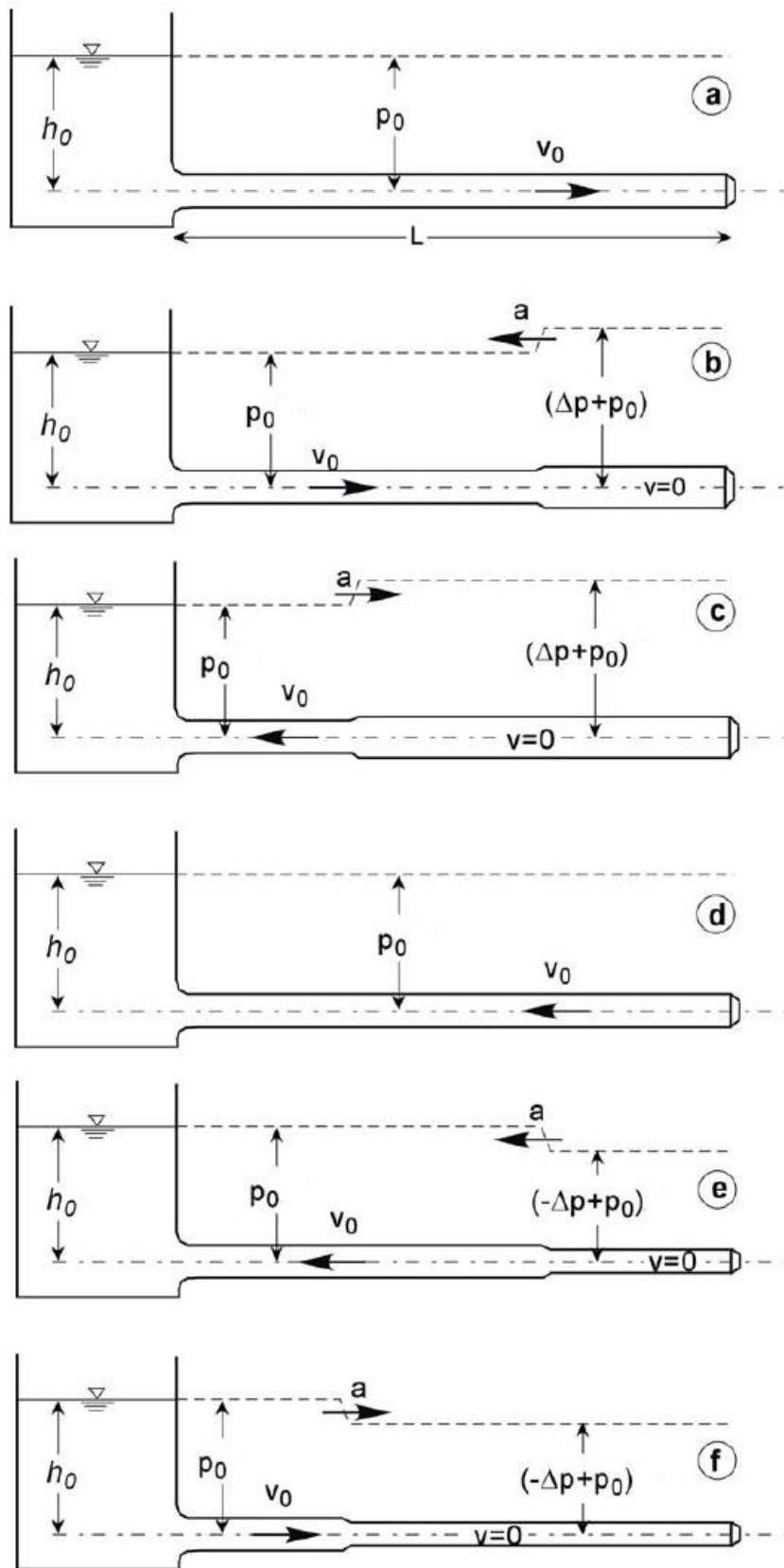


Figure 2.6 - Phases of the water hammer

- The water is flowing from the upper reservoir to the turbine with velocity v_0 .
- The turbine is instantaneously closed. In the part of the pipe close to the turbine, the velocity goes to 0, and this results in an increase of pressure. The pressure wave travels upstream with celerity a . In the rest of the pipe, pressure and velocity are equal to the initial values, respectively, p_0 and v_0 .
- The pressure wave reaches the upper reservoir, where it is reflected. So, it starts to travel downstream, with celerity a . Its passage results in restoring the initial pressure value p_0 , but also causes the water to flow from the turbine to the upper reservoir with velocity v_0 .
- At $t = \frac{2L}{a}$, the pressure wave reaches the turbine. In the whole pipe the pressure is equal to the initial value p_0 , but now the water is flowing in the opposite direction with respect to phase a).
- Since the turbine is closed, a new pressure wave is generated, this time negative, equal and opposite to the first one, because of the opposite velocity direction. The pressure wave travels upstream with celerity a , and generates a negative pressure $-\Delta p_0$.
- When the pressure wave reaches the upper reservoir, it is reflected. The passage of the reflected wave restores the initial pressure and determines the water to flow from the reservoir to the turbine with velocity v_0 .

At $t = \frac{4L}{a}$, the reflected pressure wave reaches the turbine, and the phenomenon restarts from phase a). It continues periodically, until it is dampened out by energy dissipations. The pressure and velocity values at the different phases are shown in Figure 2.7.

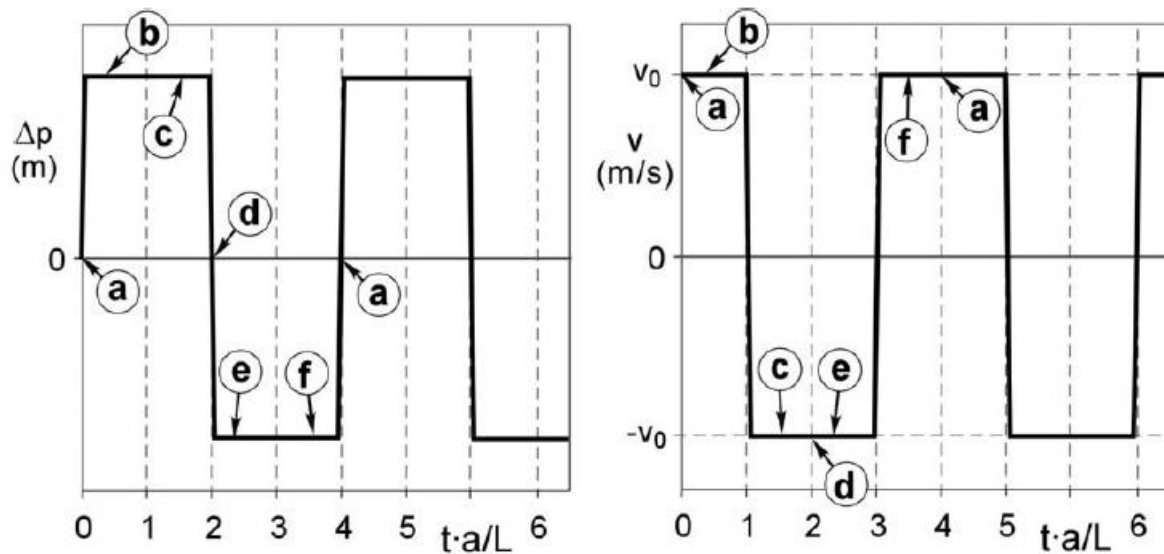


Figure 2.7 - Development of pressure (left-hand side) and velocity (right-hand side) over time

The figure 2.8 shows how the pressure waves develop over time.

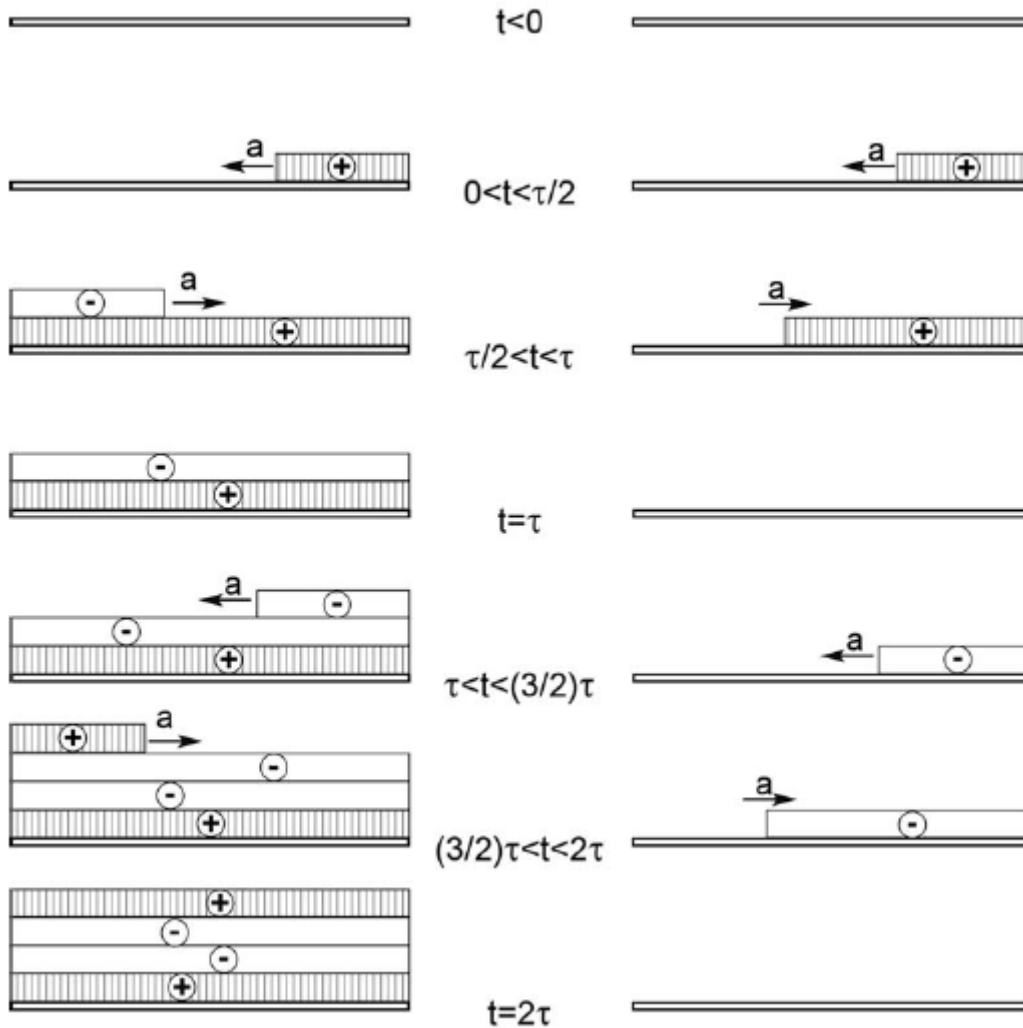


Figure 2.8 - Pressure waves development over time

On the left-hand side, the different waves are represented, whereas on the right-hand side, their summation is depicted, i.e. the actual pressure state in the pipe.

The reflection time $\frac{2L}{a}$ is named τ : this is the time needed for the pressure wave produced by the closure of the turbine to travel upstream and then come back.

2.3.3 Sudden and slow valve closure

The time needed to completely close the valve in front of the turbine is named T_c , closure time.

If $T_c < \tau$, the valve closure is considered as sudden and the maximum pressure rise is given by the Allievi-Joukowski formula, already mentioned in section 2.3.1:

$$\Delta h = \frac{a}{g} \Delta v \quad (2.51)$$

where Δv is the difference between the initial and the final velocity. Since the final velocity is 0, if the initial one is called v_0 , Δv can be replaced by $v_0 - 0 = v_0$.

Figure 2.9 illustrates the pressure development when $T_c < \tau$, where H represents the pressure at the valve and Y its opening degree.

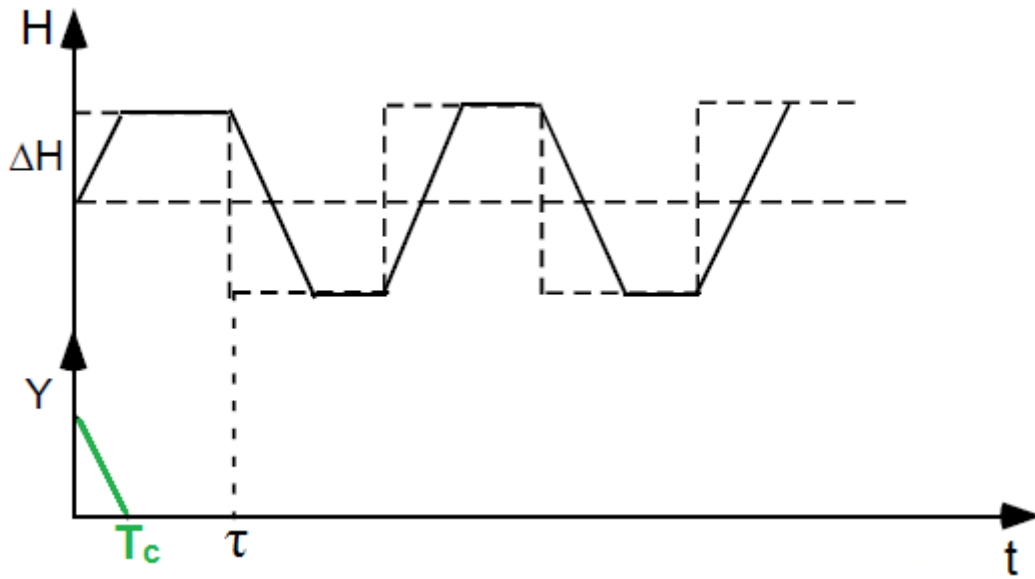


Figure 2.9 - Pressure history when $T_c < \tau$

If $T_c > \tau$, when the reflected pressure wave reaches the valve, this one is not completely closed yet; so, the maximum pressure rise is reduced, according to the formula:

$$\Delta h = \frac{a}{g} \Delta v \frac{\tau}{T_c} \quad (2.52)$$

Figure 2.10 illustrates the pressure development when $T_c > \tau$.

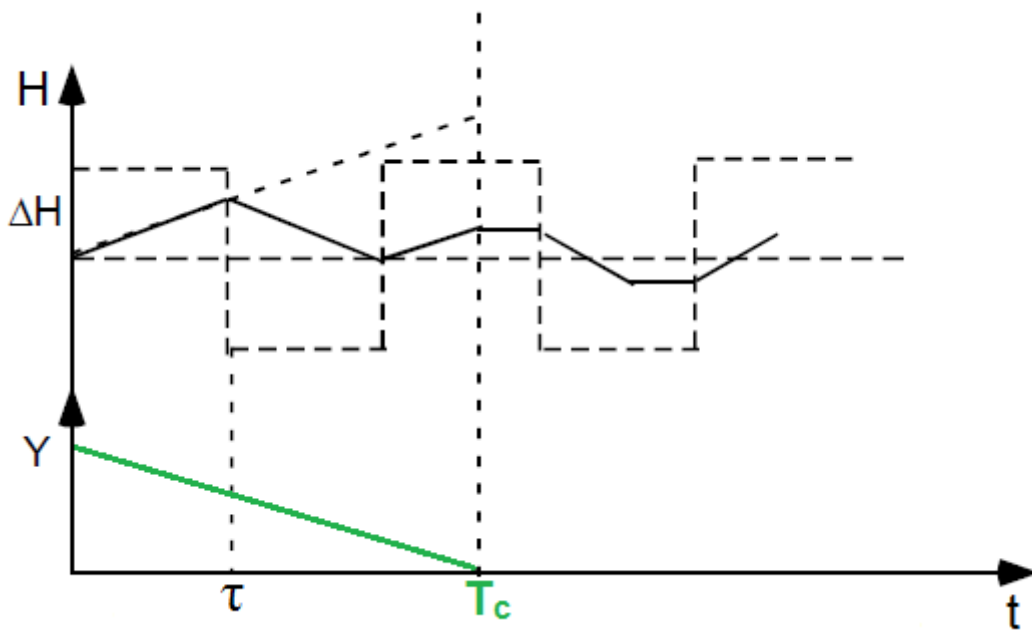


Figure 2.10 - Pressure history when $T_c > \tau$

2.4 Mass oscillations

As stated before, the introduction of a surge tank yields to two free surfaces in the tunnel system, introducing the problem of mass oscillations.

2.4.1 Description of the phenomenon

Referring to Figure 2.11, it is possible to describe the different phases of mass oscillations. The description is here presented for a surge shaft, but the same principle applies to a surge tank or to an air cushion chamber.

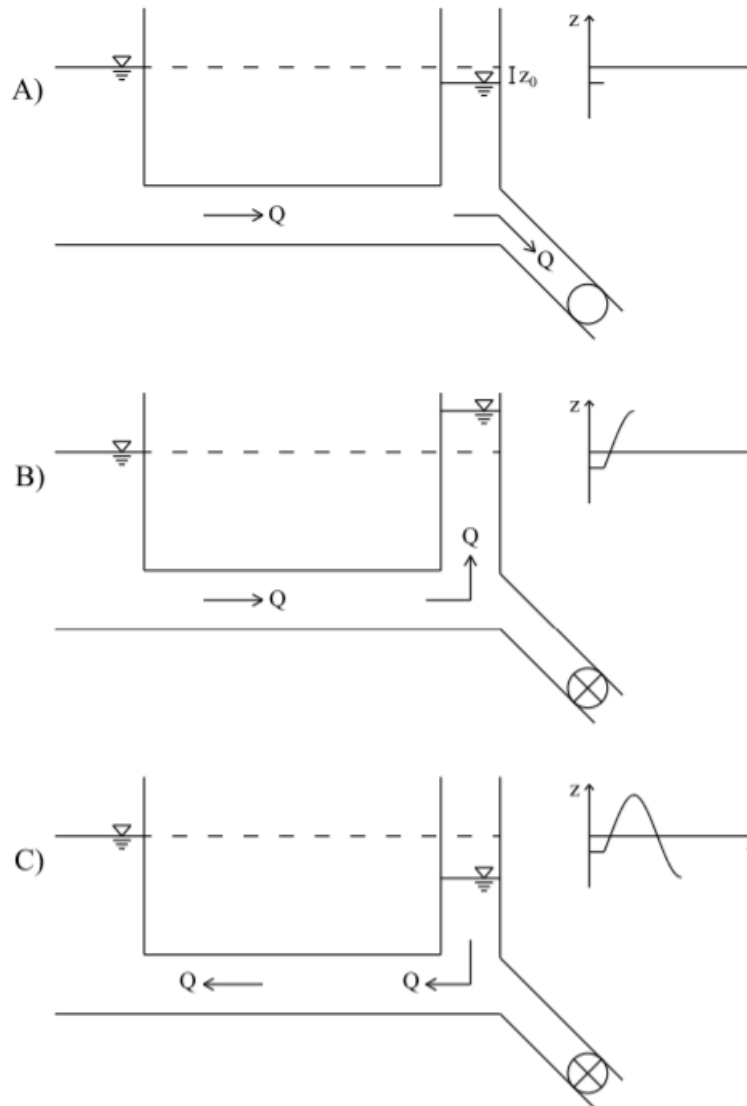


Figure 2.11 - Mass oscillations in a power plant with a surge shaft

- A) When the turbine is open, the surge shaft water level will be equal to the one in the upper reservoir, minus the head loss in the headrace tunnel, due to singular and friction losses.
- B) The turbine is shut down, so the incoming water from the reservoir is no more admitted through it and goes into the surge shaft, resulting in an increase of the water level. When the pressure reaches the value needed to restore the hydraulic equilibrium, the water rise stops. Now, the water level in the surge shaft is higher than the one in the upper reservoir, so the water starts to flow back to the reservoir.

C) The water level in the surge shaft drops, until the hydraulic equilibrium is restored. Now, the water level in the reservoir is higher than the one in the surge shaft, so the water starts to flow back to the surge shaft.

The water continues to flow back and forth until the oscillations are dampened out by friction and local losses.

2.4.2 Fundamental equations

The theory of mass oscillations is based upon three fundamental equations³:

1) Equation of motion

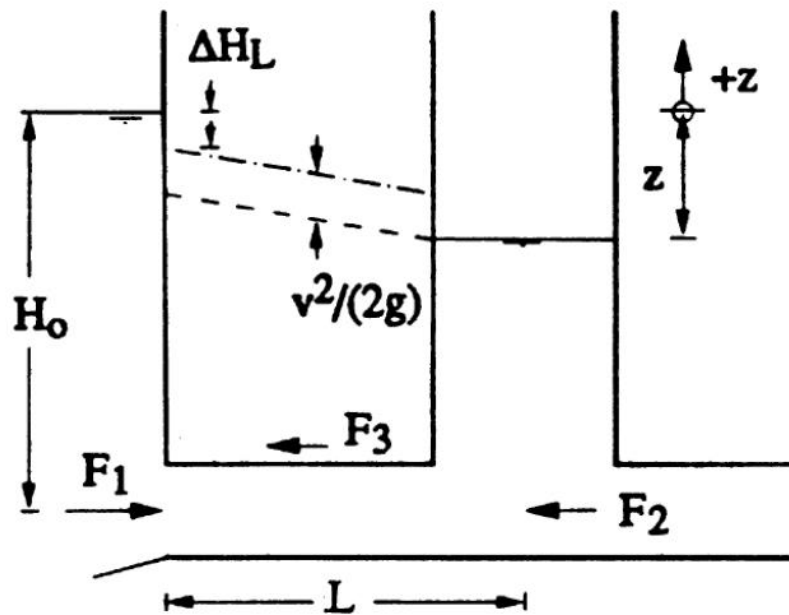


Figure 2.12 - Notation for the surge tank

Figure 2.12 represents the system and the forces at play. Considering a hydrostatic pressure distribution along the conduit, the forces are:

- F_1 , due to the upper reservoir

$$F_1 = \rho g A \left(H_0 - \Delta H_L - \frac{v^2}{2g} \right) \quad (2.53)$$

- F_2 , due to the surge tank

$$F_2 = \rho g A (H_0 + z) \quad (2.54)$$

- F_3 , due to friction

³ The derivation of the equation of motion and continuity equation was discussed in paragraph 2.1

$$F_3 = \rho g A \Delta H_R \quad (2.55)$$

where

A : cross-section area of the waterway

H_0 : water level in the upper reservoir

ΔH_L : singular loss due to the entry in the tunnel and other singularities

v : velocity in the waterway

z : difference between the water level in the surge tank and the water level in the upper reservoir. It is positive when $WL_{surge\ tank} > WL_{reservoir}$, negative when $WL_{surge\ tank} < WL_{reservoir}$

ΔH_R : distributed loss due to friction

Considering the flow direction positive if downstream, the application of Newton's law yields to:

$$m \frac{dv}{dt} = F_1 - F_2 - F_3 \quad (2.56)$$

where the mass m is equal to $(\rho A L)$. So, the above equation becomes:

$$\rho A L \frac{dv}{dt} = -\rho g A \left(z + \Delta H_L + \Delta H_R + \frac{v^2}{2g} \right) \quad (2.57)$$

(2.57) can be rewritten as:

$$\frac{dv}{dt} + \frac{g}{L} \left(z + \Delta H + \frac{v^2}{2g} \right) = 0 \quad (2.58)$$

where the total head loss ΔH is the sum of the singular loss ΔH_L , which is equal to:

$$\Delta H_L = \sum_i \xi_i \frac{v^2}{2g} \quad (2.59)$$

and of the distributed loss ΔH_R , which, according to the Manning-Strickler formula is equal to:

$$\Delta H_R = \frac{v^2 L}{K_{st}^2 R_h^{4/3}} \quad (2.60)$$

where:

K_{st} : Strickler coefficient

R_h : hydraulic radius

So, (2.58) becomes:

$$\frac{dv}{dt} + \frac{g}{L} \left(z + \sum_i \xi_i \frac{v^2}{2g} + \frac{v^2 L}{K_{st}^2 R_h^{4/3}} + \frac{v^2}{2g} \right) = 0 \quad (2.61)$$

By writing this equivalence:

$$\frac{1}{\bar{K}^2} = \frac{1}{K_{st}^2} + \frac{R_h^{4/3}}{2gL} \left(1 + \sum_i \xi_i \right) \quad (2.62)$$

(2.61) can be rewritten as:

$$\frac{dv}{dt} + \frac{g}{L} \left(z + \frac{v^2 L}{\bar{K}^2 R_h^{4/3}} \right) = 0 \quad (2.63)$$

By imposing:

$$\frac{L}{\bar{K}^2 R_h^{4/3}} = F \quad (2.64)$$

where F is defined as head loss coefficient, the equation of motion (2.58) can be written as (Jaeger, 1977):

$$\frac{L}{g} \frac{dv}{dt} + z + F v^2 = 0 \quad (2.65)$$

2) Continuity equation

Referring to Figure 2.12, according to continuity principle, the water flux in the headrace tunnel must be equal to the sum of the fluxes in the surge tank and in the penstock, so:

$$v A = u A_s + Q_{turbine} \quad (2.66)$$

where:

u : velocity in the surge tank

A_s : area of the surge tank

$Q_{turbine}$: discharge in the turbine

3) Water surface velocity

The last equation describes the velocity of the water surface in the surge tank:

$$u = \frac{dz}{dt} \quad (2.67)$$

By combining (2.65), (2.66) and (2.67), the system of equations governing mass oscillations is obtained:

$$\left\{ \begin{array}{l} \frac{L}{g} \frac{dv}{dt} + z + Fv^2 = 0 \end{array} \right. \quad (2.65)$$

$$\left\{ \begin{array}{l} Q_{turbine} = v A - \frac{dz}{dt} A_s \end{array} \right. \quad (2.68)$$

2.4.3 Direct integration

Direct integration of the above equations is possible only for the case of sudden closure of the turbine. For other cases, non-rigorous methods should be adopted.

- Direct integration neglecting tunnel friction

At time $t = 0 - \varepsilon$, $Q_{turbine}$ is equal to Q_0 , whereas at $t = 0 + \varepsilon$, $Q_{turbine}$ is equal to 0. So, the continuity equation (2.68) becomes:

$$v = \frac{A_s}{A} \frac{dz}{dt} \quad (2.69)$$

and, deriving:

$$\frac{dv}{dt} = \frac{A_s}{A} \frac{d^2z}{dt^2} \quad (2.70)$$

Since $F = 0$, (2.65) becomes:

$$\frac{L}{g} \frac{dv}{dt} + z = 0 \quad (2.71)$$

By substituting (2.70) in (2.71), the resulting equation is:

$$\frac{L A_s}{g A} \frac{d^2z}{dt^2} + z = 0 \quad (2.72)$$

(2.72) is a second-order linear homogeneous differential equation, with constant coefficients. Its general solution is:

$$z = C_1 \cos\left(\frac{2\pi}{T}t\right) + C_2 \sin\left(\frac{2\pi}{T}t\right) \quad (2.73)$$

Imposing the boundary condition $z(0) = 0$, C_1 results equal to 0, so (2.73) becomes:

$$z = C_2 \sin\left(\frac{2\pi}{T}t\right) \quad (2.74)$$

Imposing C_2 equal to z^* , the resulting equation is:

$$z = z^* \sin\left(\frac{2\pi}{T}t\right) \quad (2.75)$$

Since $v = \frac{dz}{dt}$, it yields:

$$v = z^* \frac{2\pi}{T} \cos\left(\frac{2\pi}{T}t\right) \quad (2.76)$$

As the period of mass oscillation T is described by the equation:

$$T = 2\pi \sqrt{\frac{L}{g} \frac{A_s}{A}} \quad (2.77)$$

(2.76) can be rewritten as:

$$v = z^* \frac{2\pi}{2\pi \sqrt{\frac{L}{g} \frac{A_s}{A}}} \cos\left(\frac{2\pi}{T}t\right) \quad (2.78)$$

By imposing $v_0 = \frac{z^*}{\sqrt{\frac{L}{g} \frac{A_s}{A}}}$, it yields:

$$v = v_0 \cos\left(\frac{2\pi}{T}t\right) \quad (2.79)$$

(2.75) and (2.79) are plotted in Figure 2.13

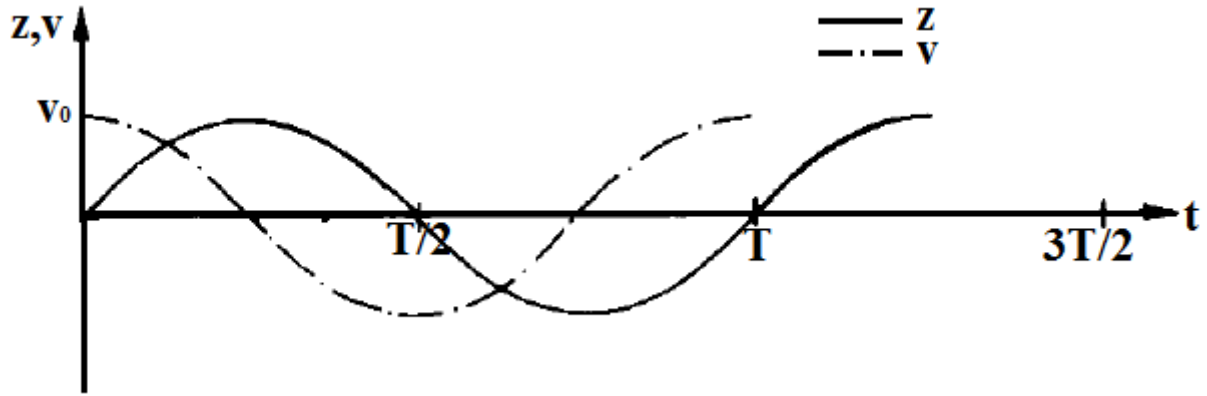


Figure 2.13 - Oscillation of water level in the surge tank following the sudden closure of turbine valve, when tunnel friction is neglected

▪ Direct integration including tunnel friction

By combining (2.65), (2.68) and (2.70), it yields⁴:

$$\left(\frac{v}{v_0}\right)^2 = \frac{L A}{2 g A_s} \frac{v_0^2}{(F v_0^2)^2} - \frac{z}{F v_0^2} + C e^{-z(2gA_s F v_0^2)/(L A v_0^2)} \quad (2.80)$$

When the oscillation starts, $v = v_0$. Therefore, $\frac{dv_0}{dt} = 0$. Because of this, (2.65) becomes:

$$z = -F v_0^2 \quad (2.81)$$

Considering this, the value of constant C may be found and (2.80) becomes:

$$\left(\frac{v}{v_0}\right)^2 = -\frac{z}{F v_0^2} + \frac{L A v_0^2}{2 g A_s (F v_0^2)^2} \left[1 - e^{-z(2gA_s F v_0^2)(z+F v_0^2)/(L A v_0^2)}\right] \quad (2.82)$$

As the turbine stops, the water level in the upstream surge tank rises, and (2.82) gives the velocity v in the tunnel corresponding to the water level z , et vice versa.

2.4.4 Rule of thumb

In the first steps of the design of the surge tank, a rule of thumb may be useful to find the maximum upsurge and downsurge.

Nielsen (2015) proposes the following formula:

$$z = \Delta Q \sqrt{\frac{L/A}{g A_s}} \quad (2.83)$$

⁴ The details of the integration can be found in Jaeger (1977), Chapter 7

As mentioned before, z is the difference between the water level in the surge tank and the water level in the upper reservoir, and it is positive when the water level in the surge tank exceeds the water level in the upper reservoir. ΔQ is equal to $Q_{tunnel} - Q_{turbine}$.

When the turbine closes, $Q_{turbine}$ is equal to 0, so $\Delta Q = Q_{tunnel}$ and z is positive, hence, the maximum upsurge takes place. When the turbine starts up, Q_{tunnel} is initially equal to 0 because of water inertia, so $\Delta Q = -Q_{turbine}$ and z is negative, hence, the maximum downsurge takes place.

2.5 Stability

As mentioned in the introduction, all over Europe, the demand is to keep the grid frequency at 50 Hz, with some tolerance (usually ± 0.1 Hz). If demand and production are unbalanced, a change in frequency will occur. To avoid this, if the demand changes, the production should be adapted fast. When the surge tank design is not satisfying, this may result in instability of mass oscillations.

The occurrence of instability may be explained referring to Figure 2.14

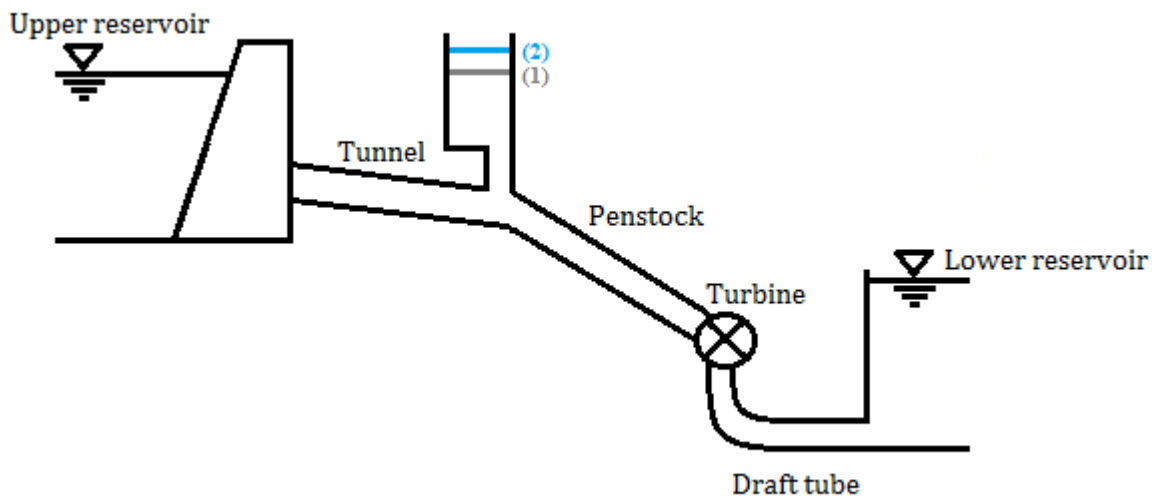


Figure 2.14 - Water level variation in the surge tank consequently to a partial closure of the turbine guide vanes, theoretical case (no friction in the tunnel)

The equation describing the power is:

$$P = \eta \rho g Q H \quad (2.84)$$

If, for instance, there is a decrease in the demand, the guide vanes are partially closed, in order to reduce the discharge. Because of water inertia, this results in an increase of the water level in the surge tank, which goes from level (1) to level (2). The increase in the head generates an increase in the power produced. In order to adjust this unwanted effect, the governor closes further the guide vanes, determining a further increase in the head, and, therefore, in the power produced.

If the surge tank size is too small, this situation can evolve into instability and disturbance, resulting in a change in the frequency of the grid. To avoid this risk, the surge tank should be stable, which means that the surges resulting from load changes should be damped out and, under any condition, should not be sustained or amplified.

2.5.1 The time-constants T_w and T_a

To guarantee stability, water inertia should not be too large. In order to test this, two time-constants may be used.

T_w , called the inflow time of masses of water, is defined as the time it takes to accelerate the masses of water from the nearest water surface upstream the turbine to nearest water surface downstream the turbine from zero discharge to initial discharge Q_0 , for a given head H_0 (Nielsen, 2015).

The formula that describes it is:

$$T_w = \frac{Q_0}{gH_0} \sum \frac{L}{A} \quad (2.85)$$

where

Q_0 : initial discharge

H_0 : initial head

$\sum \frac{L}{A}$: sum of the ratios length/area, considering the pipes between the two closest free water surfaces upstream and downstream the turbine

T_w is related to the magnitude of the inertia of the water masses.

The second time-constant is related to the rotating masses of the system, i.e. the turbine and the generator. Due to their inertia, any adjustment to the rotational speed cannot be instantaneous. This implies a stabilizing effect of the rotating masses, as they resist any change, giving the governor more time to react to these changes. This time-constant, called acceleration time of the rotational masses T_a , is defined as the time it takes to accelerate the turbine and the generator from zero angular speed to initial angular speed ω_0 , assuming maximum torque (Nielsen, 2015).

The corresponding formula is:

$$T_a = J \frac{\omega_0^2}{P_{max}} \quad (2.86)$$

where

J : moment of inertia

ω_0 : initial angular speed

P_{max} : maximum power

If $\frac{T_a}{T_w} > 4 - 6$, the regulation of the system is satisfying and a fast adaptation of the production (i.e. of the discharge) is guaranteed; hence, the plant should be safe against instability.

2.5.2 Algebraic investigation of the limit of stability

The three equations needed are:

- the dynamic equation

$$\frac{L}{g} \frac{dv}{dt} + z + Fv^2 = 0 \quad (2.65)$$

- the continuity equation

$$Q = v A - \frac{dz}{dt} A_s \quad (2.68)$$

- the governor equation

$$P = \eta \rho g Q H \quad (2.84)$$

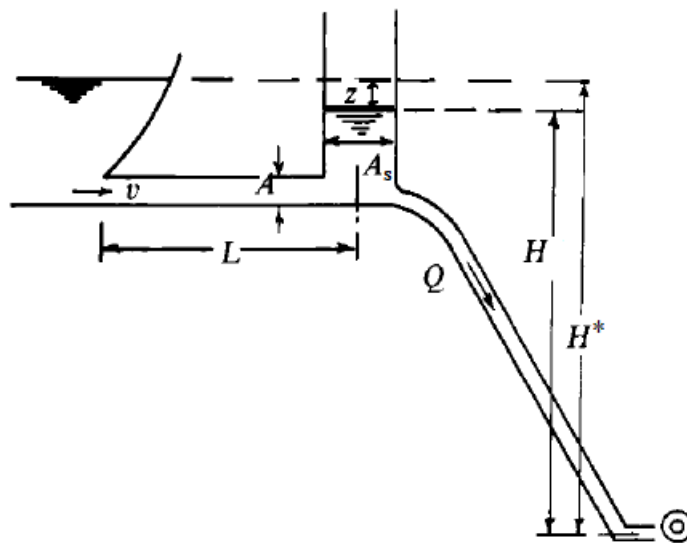


Figure 2.15 - Outline of stability analysis

Referring to Figure 2.15, it is possible to rewrite (2.84) as:

$$P = \eta \rho g Q (H^* + z) \quad (2.87)$$

where z is negative, as $WL_{surge\ tank} < WL_{reservoir}$.

Since ρ , g , η and H^* are constant, the power can be seen as a function of (Q, z) .

Representing the governor equation on Q - z plane, $Q = \text{constant}$ would be a straight line, as the blue one in Figure 2.16.

$Q = Q_0 \sqrt{\frac{H^* + z}{H^*}}$, the equation representing the case where the governor does not alter the open area of the cross-section of the turbine nozzle, is a function increasing with z . If represented by the approximation $Q = Q_0 \left(1 + \frac{z}{2H^*}\right)$, on the Q - z it will be a rising straight line, as the purple one. However, the governor equation to keep the power output constant is $Q = \frac{\eta_0 Q_0 H}{\eta (H^* + z)}$, where the subscript “0” refers to initial conditions. This equation may be represented as a falling curve, such as the green one.

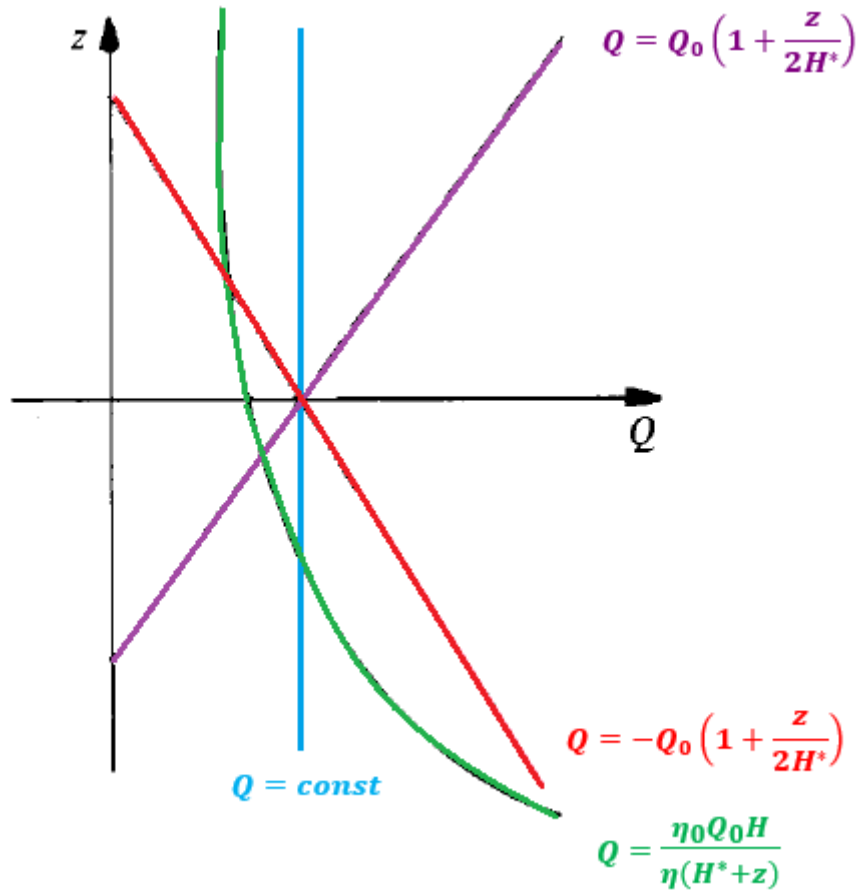


Figure 2.16 - Governor characteristics

It has been demonstrated that for $Q = \text{const}$, the mass oscillations are stable as long as friction is taken into account (Frank and Schueller, 1938). Stability is guaranteed also if the governor equation is a rising curve, such as the purple one, independently of the size of the surge tank. The risk of instability, therefore, occurs only when the governor equation is represented by a falling curve, such as the green and the red one.

To avoid the instability, the surge tank should satisfy the size requirement to guarantee the stability of the system. There are many criteria to define the minimum size of a surge tank to guarantee stability, although the standard method is Thoma equation.

2.5.3 Thoma method

The Ph.D. thesis by Thoma (1910) investigates the phenomenon of instability of mass oscillations and provides a criterion to find the minimum size of the surge tank to avoid it.

As presented in Chaudry (1987), Thoma equation is:

$$A_{Thoma} = \frac{L}{2 c g A H_{net}} \quad (2.88)$$

where:

A_{Thoma} : Thoma area

A : cross-sectional area of the tunnel

L : length of the tunnel

c : head loss coefficient

H_{net} : net head

The total head loss can be written as:

$$\Delta H = c Q^2 \quad (2.89)$$

According to Gauckler-Manning-Strickler equation:

$$Q = M R^{2/3} \sqrt{S} A \quad (2.90)$$

where:

M : Manning number

R : Hydraulic radius

S : linear hydraulic head loss

As the linear hydraulic loss is equal to the friction loss divide by the length of the tunnel, i.e. $S = \frac{h_f}{L}$, (2.90) can be rewritten as:

$$h_f = \frac{L Q^2}{A^2 M^2 R^{4/3}} \quad (2.91)$$

The hydraulic radius is a function of the area of the tunnel, and can be expressed as:

$$R = \frac{\sqrt{A}}{2\sqrt{\pi}} \quad (2.92)$$

So, (2.91) becomes:

$$h_f = \frac{2^3 \sqrt{2} \pi^{2/3} L}{A^{8/3} M^2} Q^2 \quad (2.93)$$

It yields:

$$c = \frac{2^3 \sqrt{2} \pi^{2/3} L}{A^{8/3} M^2} \quad (2.94)$$

By substituting (2.94) in Thoma equation:

$$A_{Thoma} = \frac{1}{2 g 2\sqrt[3]{2} \pi^{2/3}} \frac{A^{5/3} M^2}{H_{net}} \quad (2.95)$$

The first term consists of constants, so it may be replaced as it follows:

$$A_{Thoma} = 0.00942962 \frac{A^{5/3} M^2}{H_{net}} \quad (2.96)$$

It is recommended to adopt a safety factor, so:

$$A_{surge\ tank,min} \geq 1.5 A_{Th} \quad (2.97)$$

which can be written as:

$$A_{surge\ tank,min} \geq 0.014144 \frac{A^{5/3} M^2}{H_{net}} \quad (2.98)$$

The success of this method in practical applications may be explained by its effectiveness and simplicity. However, it is based on simplifications and neglects many features, like: influence of the penstock, velocity head of the water, and variable turbine efficiency during oscillations. In many cases, this may result in over-dimensioning of the surge tank, whose consequence is higher costs than necessary.

3. Literature review: Italian literature on surge tank stability

Italian academics actively contributed to the theme of stability in surge tanks. In this chapter, some of the most relevant papers are briefly presented.

Particularly significant was the conference, held in Padova in 1947, about how to dimension surge tanks in order to prevent instability. The conference papers are:

- Scimemi, E., *Sulla validità della regola di Thoma nelle vasche di oscillazione degli impianti idroelettrici (About the validity of Thoma method in surge tanks for hydropower plant)*

This paper is based on a series of experiments performed by the author. The aim is to test whether surge tanks whose size is smaller than Thoma area would lead to undamped oscillations. Four plants are tested and instability occurred just in one of them, where the surge tank size is $1/6$ of the Thoma area. It yields that, in practice, it may be possible to adopt surge tanks smaller than the size recommended by Thoma method, without incurring in instability.

- Ghetti, A., *Ricerche sperimentali sulla stabilità di regolazione dei gruppi idroelettrici con derivazione in pressione e pozzo piezometrico (Experimental researches on the regulation stability of hydropower systems with headrace tunnel and surge tank)*

The author aims to verify the validity of Thoma method by some experiments performed on a small plant set up in the hydraulic laboratory of the University of Padova. The study considers features neglected by Thoma, like the influence of the variable turbine efficiency during oscillations. It yields that the minimum surge tank size to guarantee the stability is from $1/2$ to $1/3$ of the Thoma area for the analysed plant.

- Evangelisti, G., *Problemi tecnici e sperimentali intorno alle vasche di oscillazione (Technical and experimental problems about surge tanks)*

In a hydropower plant, two oscillating systems coexist, reciprocally coupled: the hydraulic system, consisting in the surge tank and the upstream and downstream pipes, and the electromechanical system, consisting in the turbine, the generator, the governor and the grid. Since the two systems are coupled, they influence each other. Hence, overall stability may be possible even if one of the two systems is unstable when separately considered. The author addresses the problem with a mathematical approach, developing a more precise method to perform the approximate integration of the governing equations. By means of this, he demonstrates that stability is possible even if the requirement from Thoma equation is not satisfied. For this to happen, it is necessary that the electromechanical system influences with its stability the hydraulic system. However, this will yield to worse regulation. Therefore, for a good performance of the plant, it is advisable to keep Thoma method as a practical rule.

- Arredi, F., *Lo studio della stabilità dei sistemi adduttori-generatori degli impianti idroelettrici col criterio di Leonhard (Study of the stability of the adduction-electromechanical systems with Leonhard criterion)*

The Leonhard criterion is a method to solve linear equations, therefore, it can be applied to mechanical/hydraulic/electric systems when small oscillations are considered. Before this paper, the criterion has been applied to electric systems and turbine regulators, but the author is the first to try to use it to investigate the stability of a hydropower plant. Although the analysis yields to conclusions already reached in other papers (for instance, that, in a hydropower plant, the stability of the

electromechanical system can influence the hydraulic system), the main achievement is the demonstration of the applicability of the Leonhard criterion for stability studies in hydropower.

- Ghetti, A., *Sulla stabilità delle oscillazioni negli impianti idroelettrici provvisti di un sistema complesso di condotte e pozzi piezometrici (About the stability of mass oscillations in hydropower plants having a complex system of pipes and surge tanks)*

The paper aims to extend the application of Thoma method to more complex hydropower schemes, with two upstream surge tanks: one close to the penstock (surge tank 1) and one between the upper reservoir and the other surge tank (surge tank 2). A plant may have two upstream surge tanks because, for instance, a second surge tank has been added, instead of increasing the size of the existing one. The author develops the analysis by using a theoretical approach, and he shows that, if surge tank 1 has an area equal or larger than the Thoma area, the stability is guaranteed independently of the size of surge tank 2. However, stability can be guaranteed even if surge tank 1 has a smaller size, as long as not smaller than $0.5 \cdot A_{\text{Thoma}}$. The size of surge tank 1 necessary to guarantee stability depends also on the location of surge tank 2. In fact, as surge tank 2 gets closer to the upper reservoir, the size of surge tank 1 should be increased.

Giuseppe Evangelisti, professor at the university of Bologna since 1937 to 1974, conducted many studies on the topic and left a rich and relevant scientific output. Some of the most significant papers are briefly presented below.

- In *Alcune osservazioni sul colpo d'ariete e sulla regolazione delle turbine idrauliche (Comments on the water hammer and on the regulation of the turbine, 1941)*, a new method to find an approximate solution of the governing equations is presented, with the aim to provide a more general and complete approach to the problems in the regulation of the turbine.
- In *Sulla stabilità di regolazione delle installazioni idroelettriche (On the stability of the regulation of the hydroelectric installations, 1946)*, the influence of the penstock on stability is investigated from a mathematical point of view, and the conclusion is that the closer the surge tank is to the penstock, the larger will be its stabilizing effect.
- A mathematical approach is adopted also to study a case with two upstream surge tanks in *Adduzioni in pressione e stabilità di regolazione negli impianti idroelettrici (Under pressure adductions and stability of regulation in hydropowerplants, 1949)*. Ghetti already wrote about the topic in the paper *Sulla stabilità delle oscillazioni negli impianti idroelettrici provvisti di un sistema complesso di condotte e pozzi piezometrici (1947)*, mentioned above. Evangelisti, however, aims to investigate the influence of the surge tank location with respect to the headrace tunnel on stability, rather than discussing the dimensioning of surge tanks.
- A very comprehensive discussion of the problem of stability is presented in *Pozzi piezometrici e stabilità di regolazione (Surge tanks and stability of regulation, 1950)*, which can be seen as a summary of the main results achieved by the author on this subject. In the first paragraph, the author presents the topic and the governing equations. Then, in the second one, he describes Thoma method, discussing also the influence of the features that the method neglects, like the variable turbine efficiency. The last paragraph aims to investigate the influence of the involved elements (turbine-generator, regulator and penstock) and, finally, presents three case studies, where the discussed theory is applied. The paper leads, among the others, to a particularly relevant conclusion, already anticipated in previous papers by the same author: the stability analysis should be carried on isolated power plants, as the ones connected to the grid are influenced by the stability of the grid itself.
- In all the papers presented above, the hypothesis of small oscillations is constantly present, and this makes possible to linearize the governing equation, making their solution simpler. In *Sopra la stabilità*

delle grandi oscillazioni nei pozzi piezometrici (On the stability of big oscillations in surge tanks, 1951), this hypothesis is ruled out and the non-linear equations are analysed. The stability conditions for this case are found.

- The paper *Sopra la stabilità dei sistemi complessi di gallerie in pressione e pozzi piezometrici (On the stability of complex systems of pressure pipes and surge tanks, 1955)* investigates the stability criteria in more complex schemes, like: systems with more than one headrace tunnel, systems with two upstream surge tanks, systems with n upstream surge tanks, systems with an upstream and a downstream surge tank.

4. Method

In this chapter, Roskrepp power plant is presented. Then, after a description of the LVtrans freeware, the model is introduced, and its calibration and validation are discussed.

4.1 Roskrepp power plant

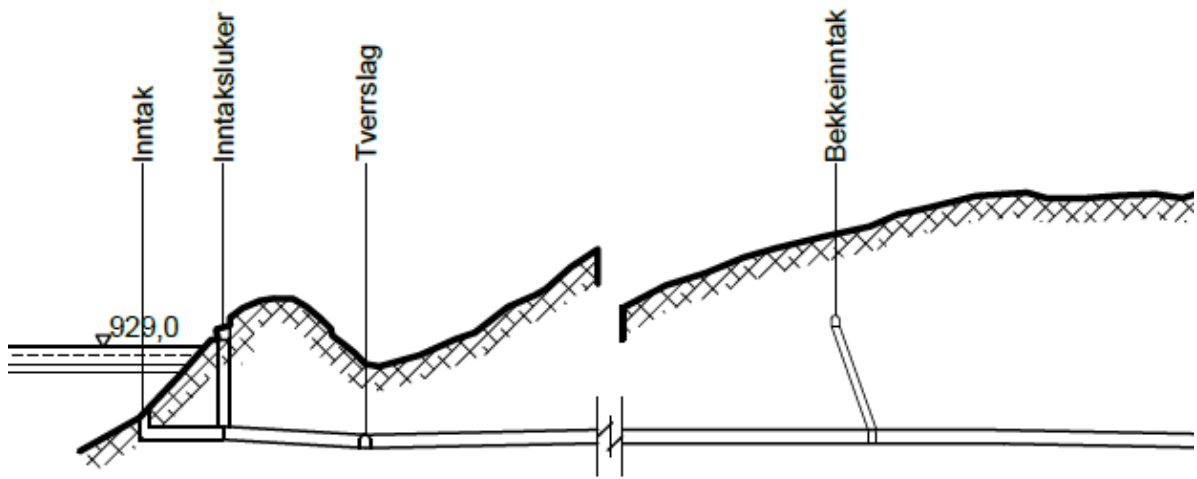
Roskrepp power plant has been built in 1979 in the South of Norway, in Vest-Agder County, at the top of the Kvina river. It is the smallest plant owned by Sira-Kvina company, with its installed capacity of 50 MW. However, it is strategically relevant, since it is the first of several power plants located along the Kvina river.

It is usually operated during winter, when the production is more profitable because of the high energy demand. The technical data of interest are summarized in Table 4-1 below.

Table 4-1 - Technical data of Roskrepp power plant

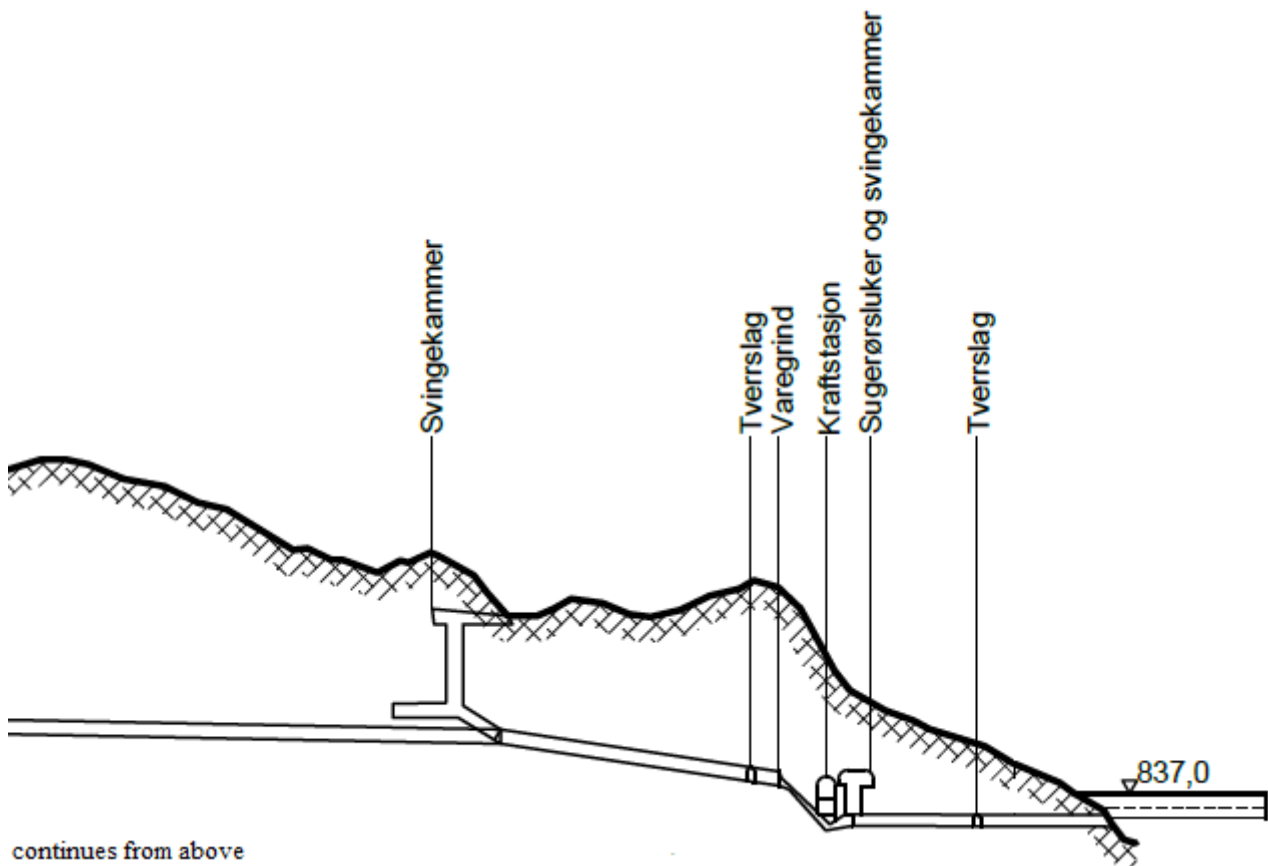
Turbine type	Francis
Installed capacity	50 MW
Annual average generation	105 GWh
RPM	250
Pole pairs number	12
Design head	83 m
Design discharge	67 m ³ /s

The drawing of the power plant is shown in Figure 4.1 and Figure 4.2 below.



continues below

Figure 4.1 - Roskrepp power plant, part 1



continues from above

Figure 4.2 - Roskrepp power plant, part 2

All the elements of the power plant and their characteristics are presented in the following paragraphs. The necessary information was found in the report (Roskrepp kraftverk - falltapsmålinger, 1980) and in the drawings of the power plant.

4.1.1 Upper and lower reservoir

The main intake is located at the dam in Lake Roskreppfjord, whereas the outlet is in Lake Øyarvatn, as shown in Figure 4.3 below.



Figure 4.3 - Intake and outlet location

The water levels of the upper and lower reservoirs are summarized in Table 4-2 below.

Table 4-2 - Characteristics of the reservoirs

	HRWL [masl]	LRWL [masl]
Upper reservoir	929	890
Lower reservoir	837	825

4.1.2 Brook intake

The power plant includes a brook intake in Skjerevatn lake, as shown in Figure 4.4 below.

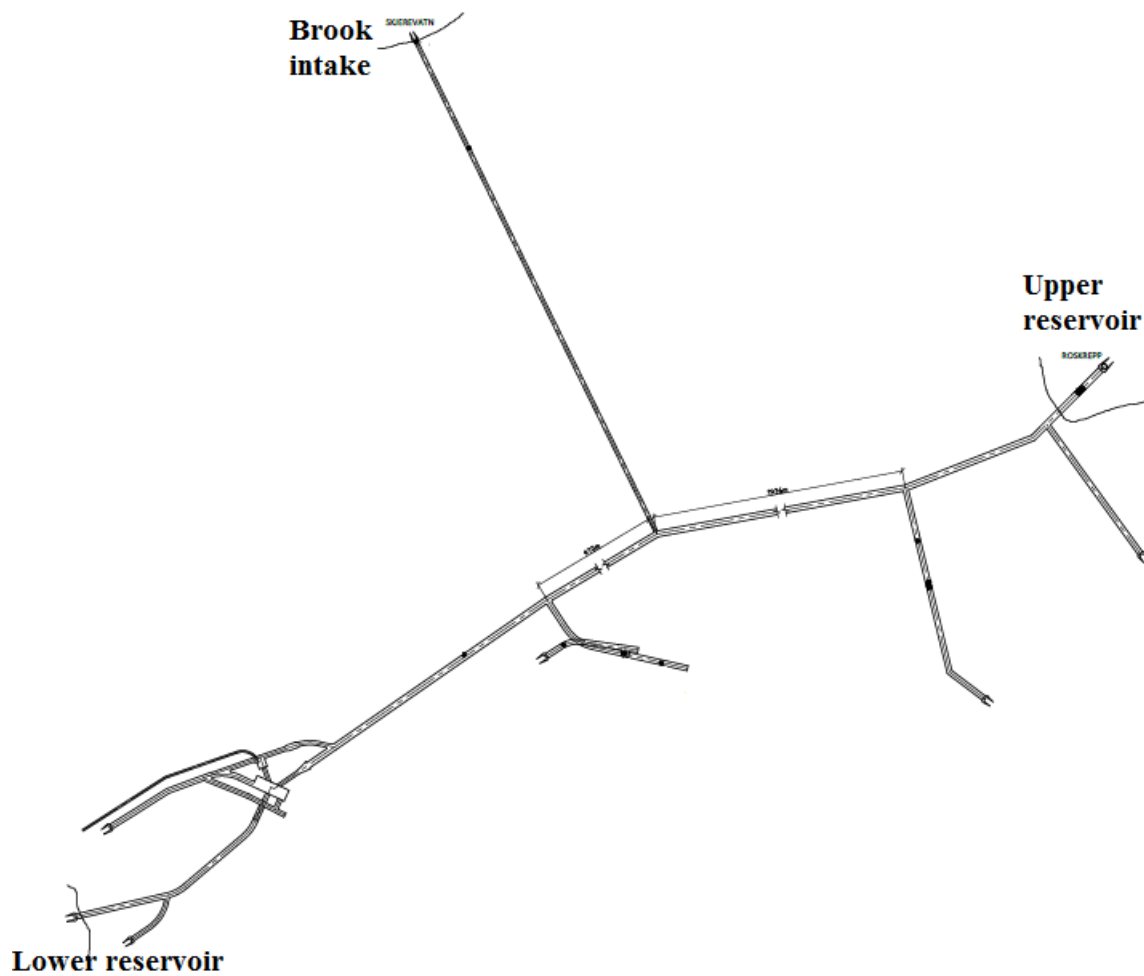


Figure 4.4 - Roskrepp power plant, plan view

The brook intake conveying the water to the headrace tunnel is displayed in Figure 4.5.

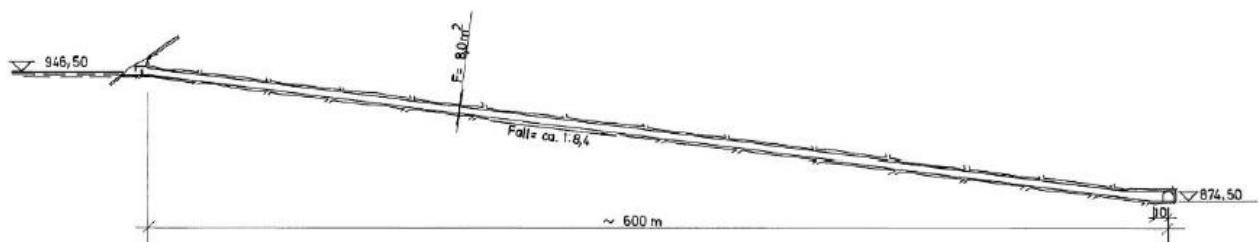


Figure 4.5 - Brook intake of Roskrepp power plant

The characteristics of the brook intake are summarized in Table 4-3 below.

Table 4-3 - Characteristics of the brook intake

Length	604.2 m
Cross-section area	8 m ²
Slope	1:8.4

4.1.3 Upstream surge tank

The upstream surge tank is located around 350 m upstream from the turbine and it is a two-chamber surge tank. Two alternatives were considered at design stage, as shown in Figure 4.6.

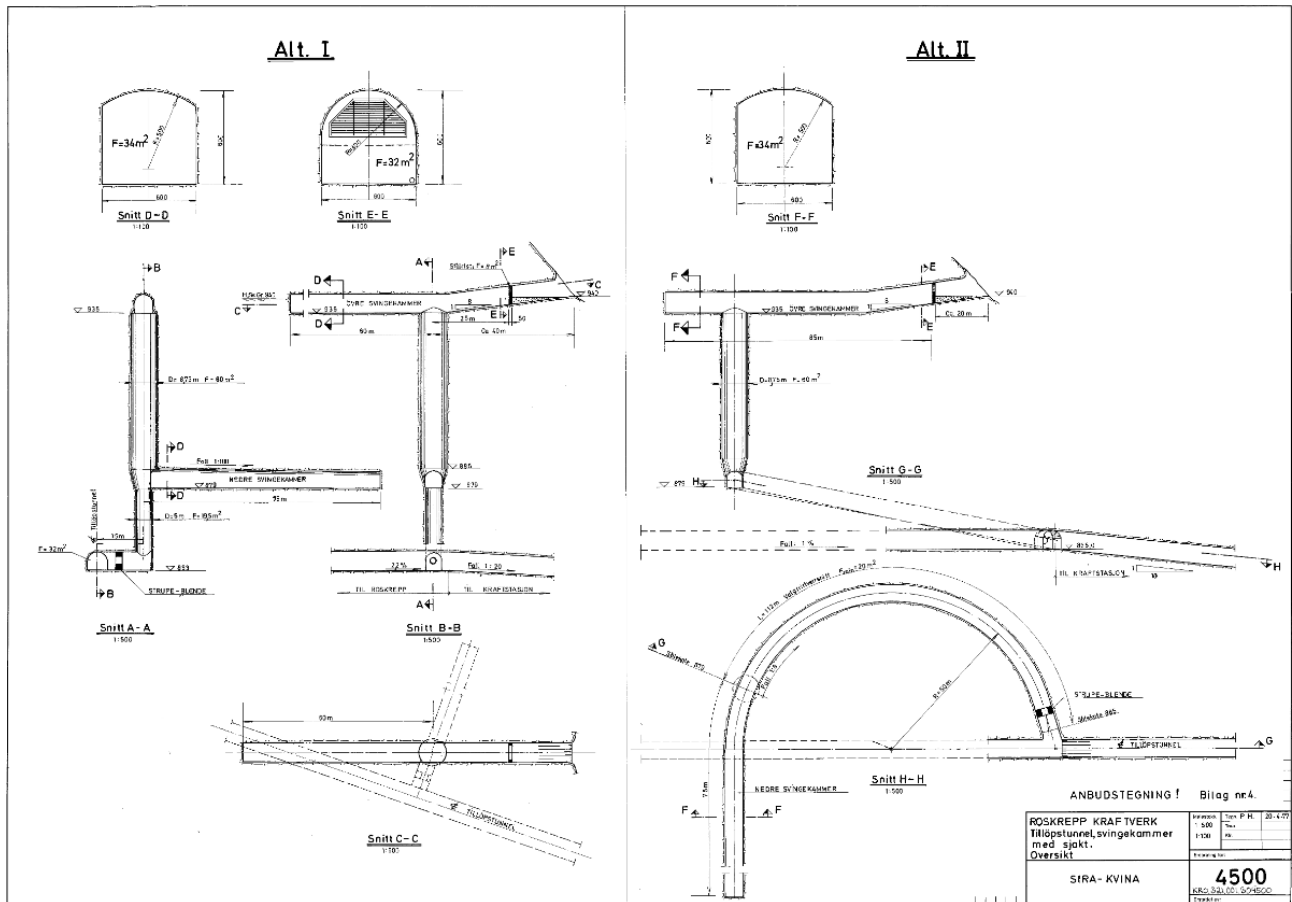


Figure 4.6 - Surge tank design - alternative I and II

This design was typical in Norway in that period, hence, the engineers were familiar with it. They preferred it to a differential surge tank because it is simpler to build and requires lower construction costs. The cross-section areas of the different parts of the surge tank are summarized in Table 4-4 below.

Table 4-4 - Upstream surge tank, cross-section areas

	From	To	Cross-section area [m ²]
Lower chamber	865 masl	885 masl	34
Vertical shaft	885 masl	935 masl	60
Upper chamber	935 masl	941 masl	34

In the interest of simplicity, a simplified design is used for the model, shown in figure 4.7.

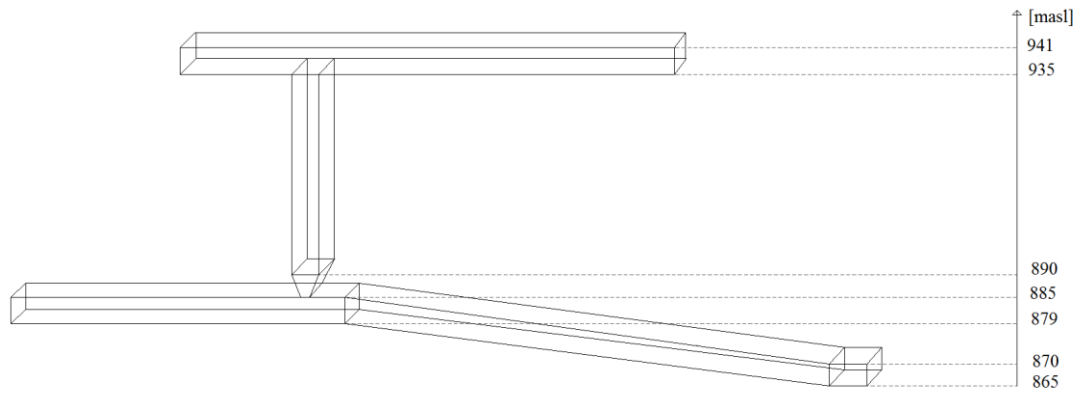


Figure 4.7 - Simplified design of the upstream surge tank

4.1.4 Turbine

The installed turbine is a Francis turbine. Its parameters are summarized in the following table:

Table 4-5 - Characteristics of the turbine

Design head	83 m
Design discharge	67 m ³ /s
Efficiency	0.947

4.1.5 Downstream surge tank

The downstream surge tank is located around 24 m downstream the turbine and consists in a vertical surge shaft, with a service gallery on the top, as shown in Figure 4.8 below.

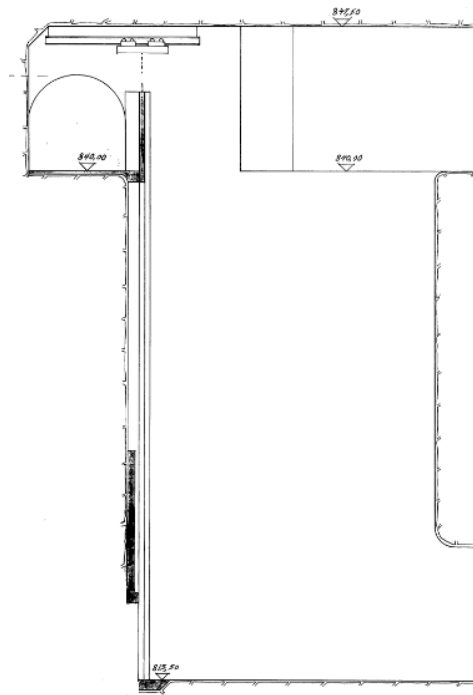


Figure 4.8 - Downstream surge tank, side view

Its main characteristics are summarized in Table 4-6 below:

Table 4-6 - Characteristics of the downstream surge tank

	From	To	Cross-section area [m ²]
Vertical shaft	813.5 masl	840 masl	90

4.1.6 Pipes

- Headrace tunnel

Originally, the entire headrace tunnel had a layer of asphalt on the invert, so its section was equal to section C-C shown in Figure 4.9.

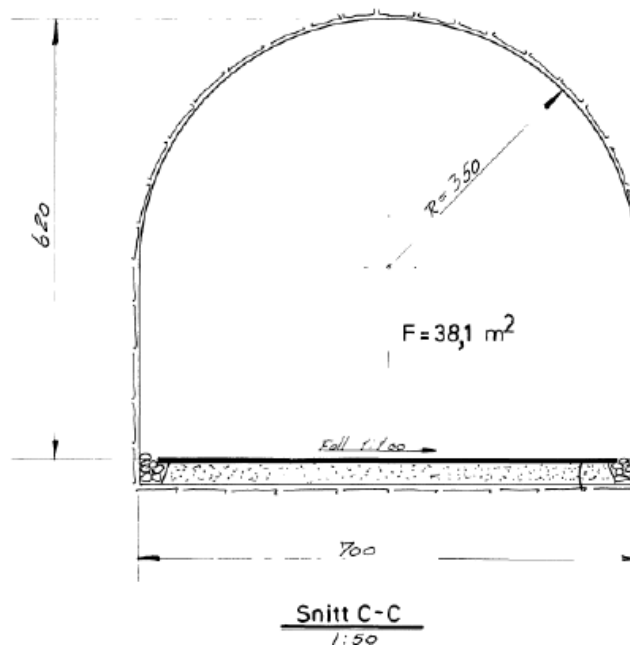


Figure 4.9 - Original cross-section of the headrace tunnel

However, the pressure destroyed the asphalt cover and, in 2007, the tunnel was renovated. In some parts, the asphalt has been removed, so now their section is equal to section D-D, displayed in Figure 4.10.

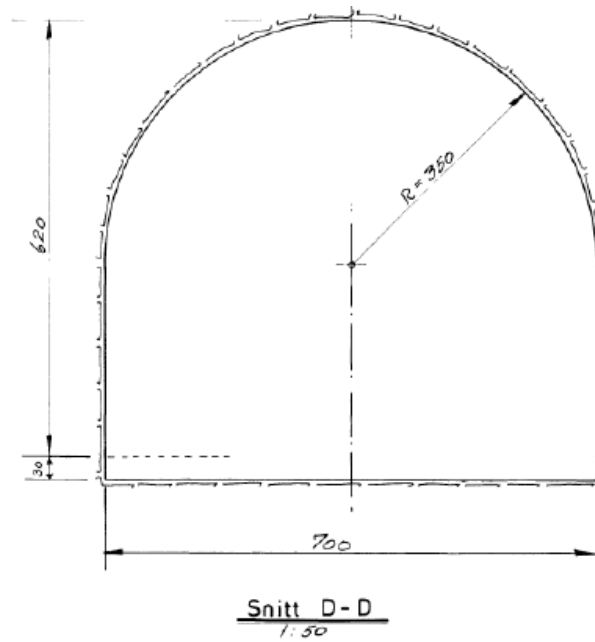


Figure 4.10 - Cross section of the headrace tunnel after the asphalt removal

Figure 4.11 below shows the headrace tunnel and the type of cross-section in each segment.

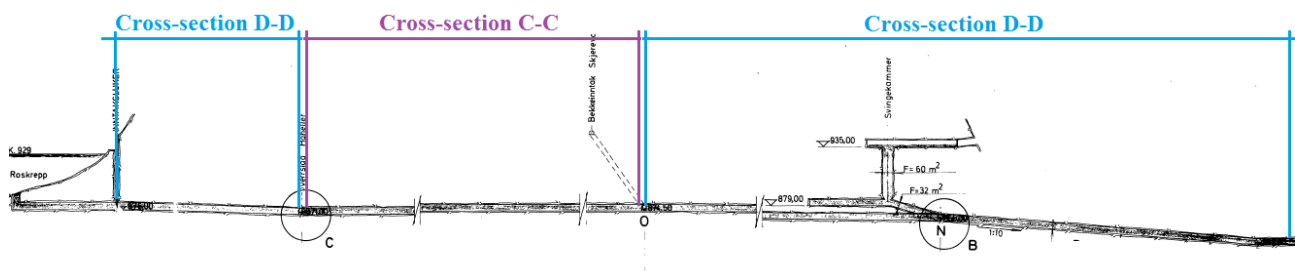


Figure 4.11 - Headrace tunnel and its cross-sections

The characteristics of the two cross-sections are summarized in Table 4-7.

Table 4-7 - Characteristics of the headrace tunnel cross-sections

Cross-section	Area [m ²]	Equivalent diameter [m]
C-C	38.1	6.97
D-D	40	7.16

It should be underlined that these data are uncertain, as the headrace tunnel is a drill and blast tunnel and, as mentioned above, there are not “as-built” drawings available.

- Draft tube

The draft tube is the pipe installed at the exit of the turbine and it has a variable cross-section area, as shown in Figure 4.12.

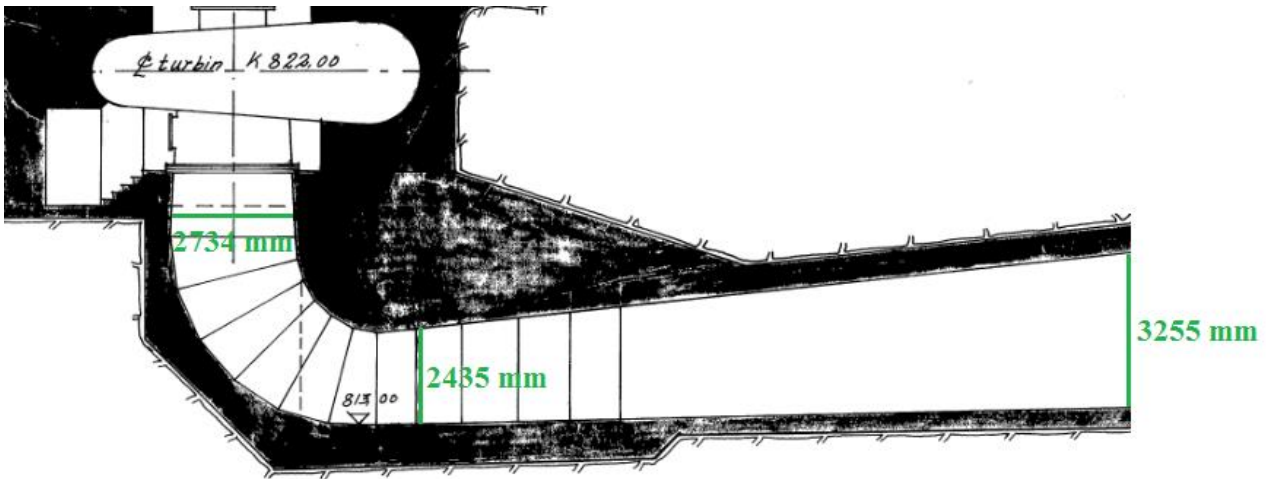


Figure 4.12 - Draft tube, side view

- Tailrace tunnel

The tailrace tunnel connecting the downstream surge tank with the lower reservoir is shown in Figure 4.13 below.

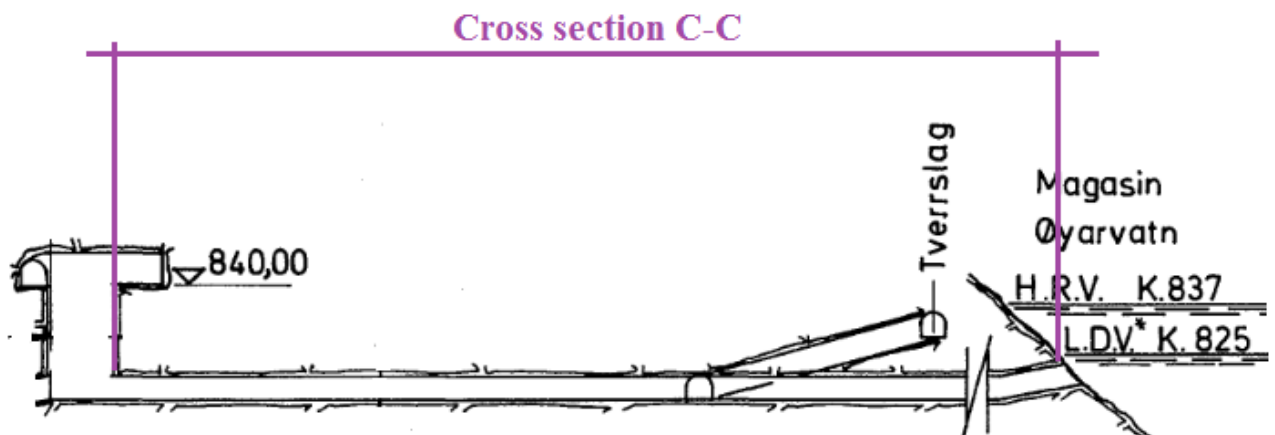


Figure 4.13 - Tailrace tunnel and its cross-section

It is long around 300 m and has a section similar to the section C-C described above for the headrace tunnel, with an area of 38.1 m².

4.2 LVtrans

LVtrans is a program developed in LabVIEW environment by Dr. Ing. Bjørnar Svingen for the Rainpower company. It can be used for any system which consists mainly of fluid-filled pipes and open channels, but its primary application is hydropower. Each element of a hydropower plant is represented as a node, having its own icon, function, and parameters, and it is connected to the other nodes by means of pipes. It is based on the method of characteristics, which makes the solution almost exact from an analytical point of view, keeping the computational time adequately low.

The program is object-oriented, which means that the user does not need to change the source code, but can directly change the nodes. In fact, during simulations, the node can be accessed and the data can be viewed in graph form, logged and changed. The simulations can be performed in real time or at higher speeds, and the time interval of the computations can be changed.

The interface of the program is shown in Figure 4.14 and Figure 4.15 below.

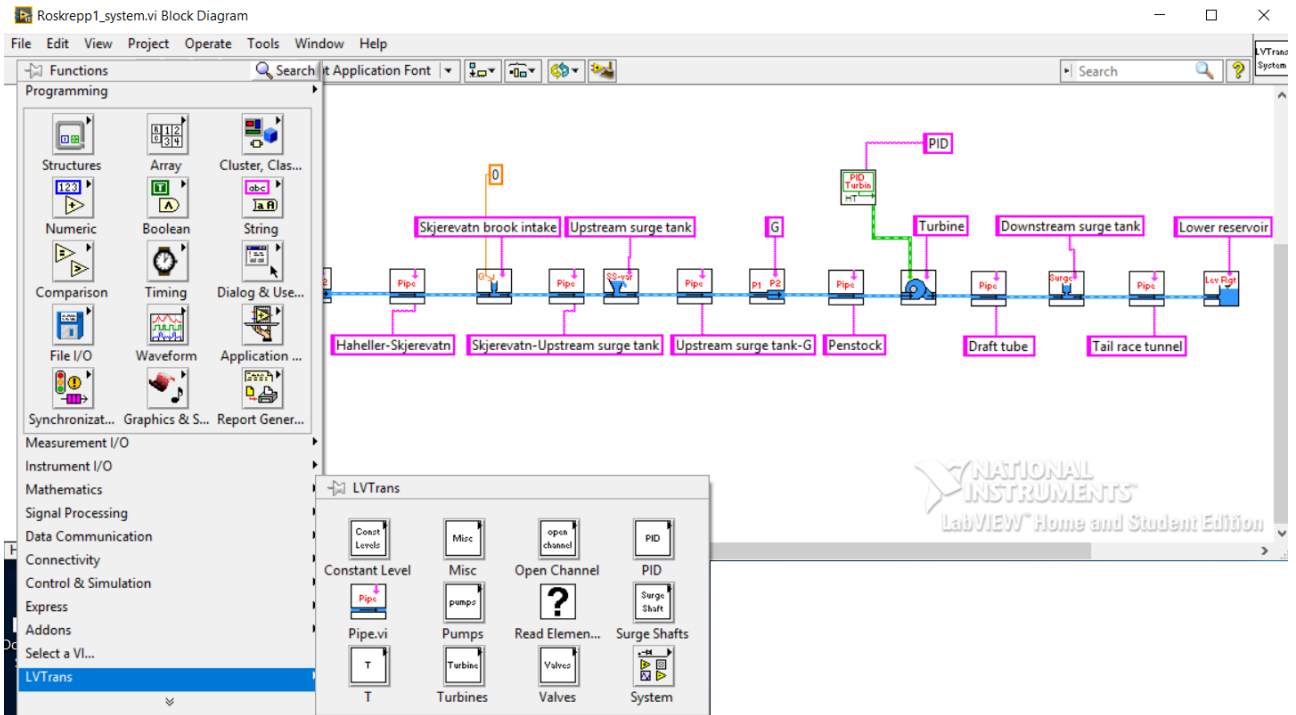


Figure 4.14 - Program interface, block diagram window

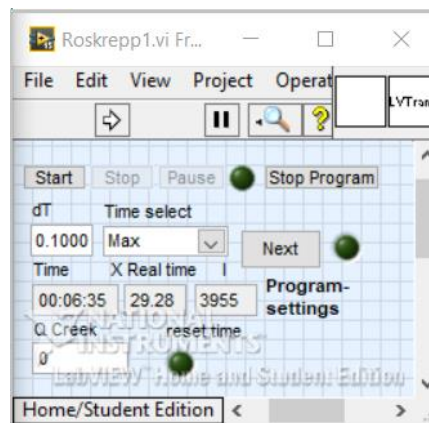
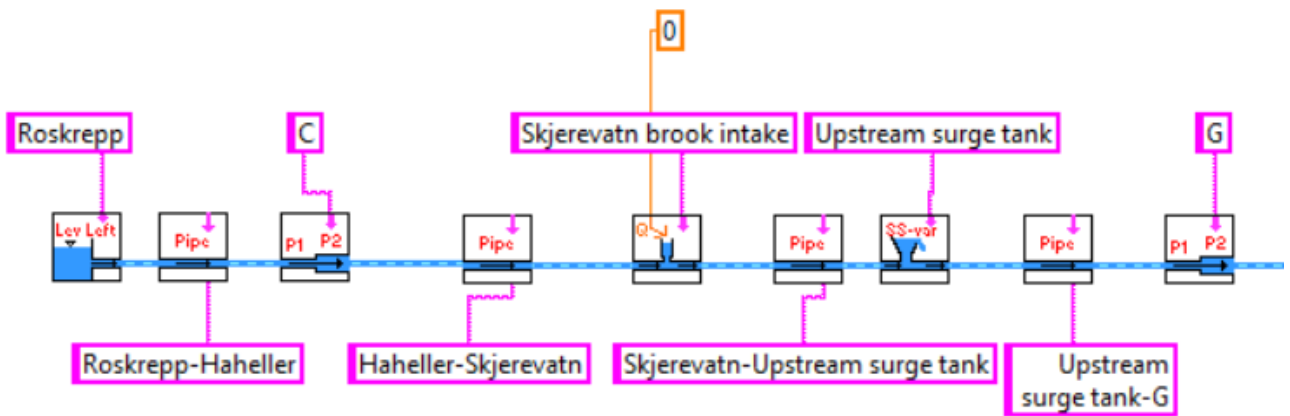


Figure 4.15 - Program interface, simulation settings window

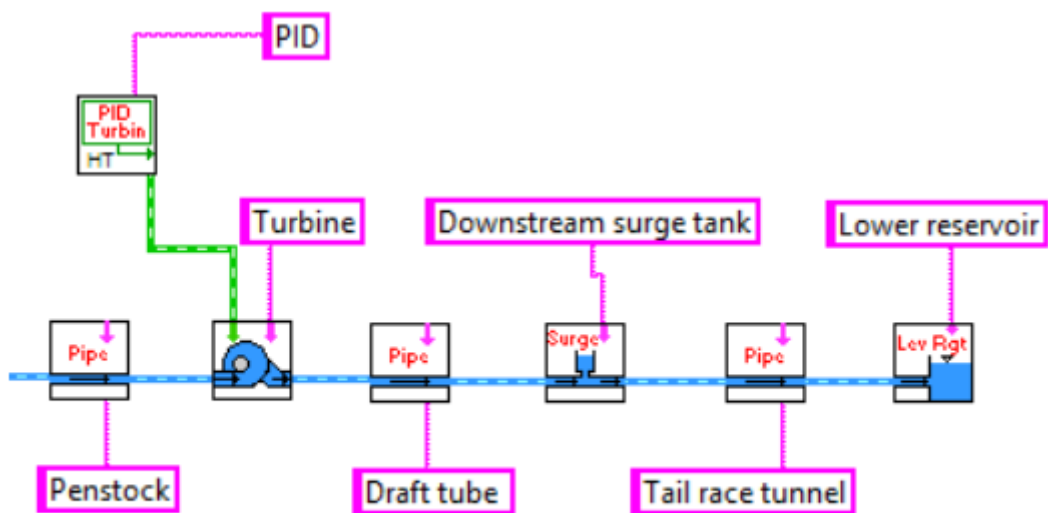
The model is based on the drawings of the power plant, provided by Sira-Kvina company. Since they are not “as-built” drawings but design drawings, lack of precision affects them. To rectify this issue, the model has been calibrated, as described in section 4.3.

The model built in LVtrans is presented in Figure 4.16 and Figure 4.17 below.



continues below

Figure 4.16 - LVtrans model of Roskrepp power plant, part 1




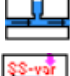






continues from above

Figure 4.17 - LVtrans model of Roskrepp power plant, part 2

An overview of the model components is provided in Table 4-8 below.

Table 4-8 - Components of the model

Component	Symbol
Reservoirs	
Tunnels and pipes	
Contractions/expansions	
Brook intake	
Upstream surge tank	
Downstream surge tank	
Francis turbine	
PID governor	

4.3 Calibration

The aim of the calibration is to make the model outputs as similar as possible to the ones of the prototype. The procedure adopted in this thesis is the optimization of model performances, carried out by comparing measurements and simulations. First, the calibration is performed for the steady-state situation, then for the transient situation.

The calibration is performed using measurements of the power output and of the pressure in front of the turbine, taken during a measurement campaign performed in September 2017. The same dataset includes the measurements of the draft tube pressure. However, these cannot be used directly for the calibration, since LVtrans is not able to simulate the correct draft tube pressure. The reason is that the turbine model in the freeware already contains a draft tube, but the only element that the model accepts downstream a turbine is a pipe. So, the model has two draft tubes. This does not compromise the simulation results, but makes impossible to use draft tube pressure measurements directly for the calibration.

The curve showing the power output during the measurements is displayed in Figure 4.18.

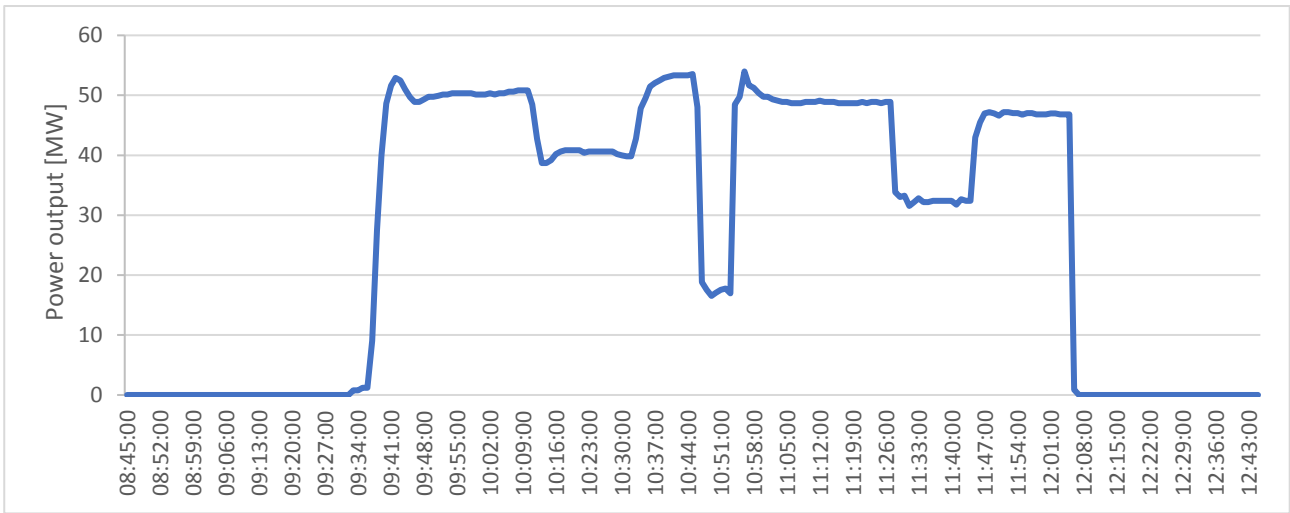


Figure 4.18 - Power output during the measurements, September 19th, 2017

The water level variation in the upper and lower reservoirs is shown, respectively, in Figure 4.19 and Figure 4.20.

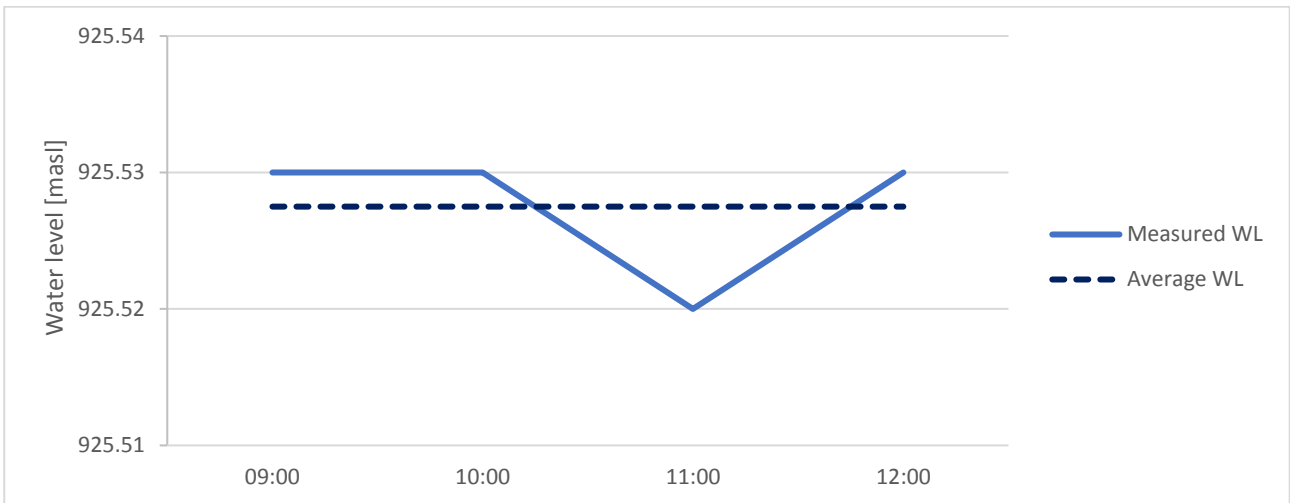


Figure 4.19 - Water level in the upper reservoir during the measurements

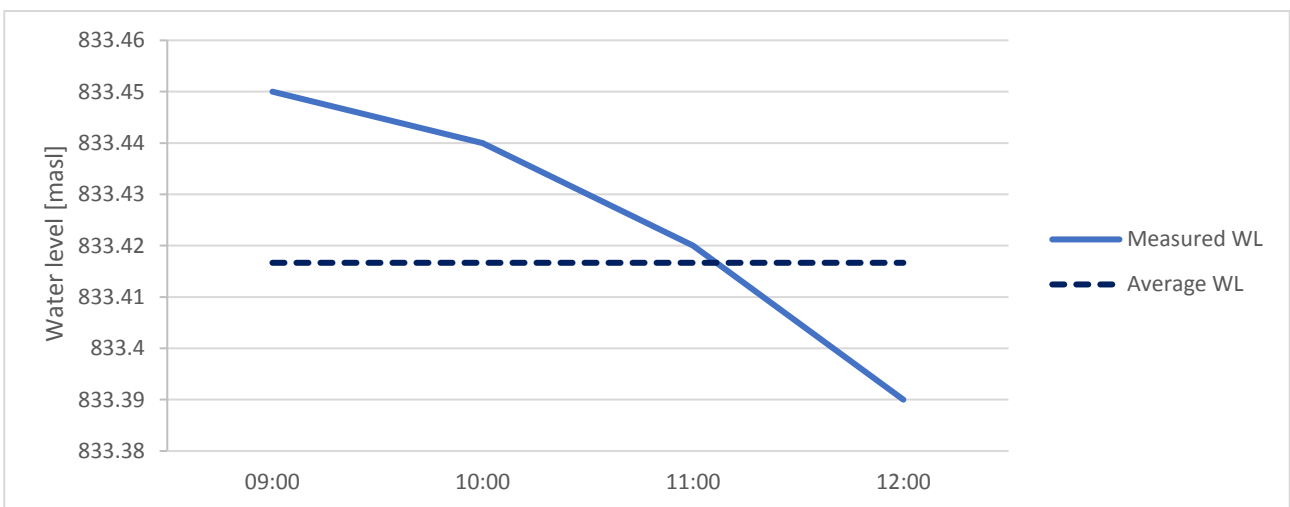


Figure 4.20 - Water level in the lower reservoir during the measurements

As the variation is small, the choice is to input the average values in the simulations.

A complete overview of all the parameters used in the model, included the calibrated ones, can be found in Annex 1.

4.3.1 Calibration of steady-state operation

The measurements used for the steady-state calibration are summarized in table 4-9 below.

Table 4-9 - Measured power output and pressure in front of the turbine

From	to	Power [MW]	Pressure [kPa]	Static head [mWC]
09:53:00	10:05:00	50.3	913.02	916.07
10:19:00	10:29:00	40.7	946.62	919.5
10:42:00	10:46:00	53.4	901.4	914.89
10:50:00	10:51:00	17.1	993	924.22
11:11:00	11:23:00	48.8	920.4	916.82
11:36:00	11:40:00	32.4	964.9	921.36
11:54:00	12:03:00	46.9	928.2	917.62

In the interest of simplicity, average values are used.

In order to convert the pressure in front of the turbine into the corresponding static head, the following formula is applied:

$$h_{static} = \frac{p}{\rho g} + z_{sensor} \quad (4.1)$$

where:

h_{static} : static head, in [mWC]

p : pressure in front of the turbine, in [Pa]

z_{sensor} : sensor elevation, equal to 823 masl

The static head is a function of:

- water levels in the reservoirs
- discharge
- head losses

As the water levels in the reservoirs and the discharge value during the measurements are known, the head losses are the only parameter to be calibrated.

To make the simulation results to match with the measurements, the coefficients of distributed and singular losses are calibrated by a trial and error procedure, starting from initial values found in literature. The comparison between the measurements and the outputs of the calibrated model is shown in Table 4-10 below.

Table 4-10 - Calibration of steady-state operation: comparison between measurements and calibrated model

Power				Upstream hydraulic head			
Measurements [MW]	Simulation [MW]	Absolute error [MW]	Relative error [%]	Mesaurements [masl]	Simulation [masl]	Absolute error [masl]	Relative error [%]
17.10	17.02	-0.08	0.47	924.22	924.33	0.11	0.01
32.40	33.91	1.51	4.66	921.36	921.37	0.01	0.00
40.70	41.99	1.29	3.17	919.49	919.13	-0.36	0.04
46.90	47.31	0.41	0.87	917.62	917.23	-0.39	0.04
48.80	48.80	0.00	0.00	916.82	916.61	-0.22	0.02
50.30	49.92	-0.38	0.76	916.07	916.11	0.04	0.00
53.40	52.10	-1.30	2.43	914.89	915.05	0.16	0.02

The results from the calibration are considered satisfying, as the maximum absolute error for the power output is 1.51 MW, corresponding to a relative error of 4.66%, and the maximum absolute error for the static head in front of the turbine is 39 cm, corresponding to a relative error of 0.04%.

4.3.2 Calibration of transient operation

The transient-state calibration is performed referring to a shutdown, from 46.9 MW to 0 MW. Parameters upstream and downstream the turbine influence the transients, so the calibration should be performed on the pressure in front of the turbine and downstream the turbine.

As mentioned above, LVtrans is not able to simulate the correct draft tube pressure. To exploit the measurements for the calibration, the static head downstream the turbine is adjusted, as shown in Figure 4.21. The details of this adjustment can be found in Leroquais (2018)

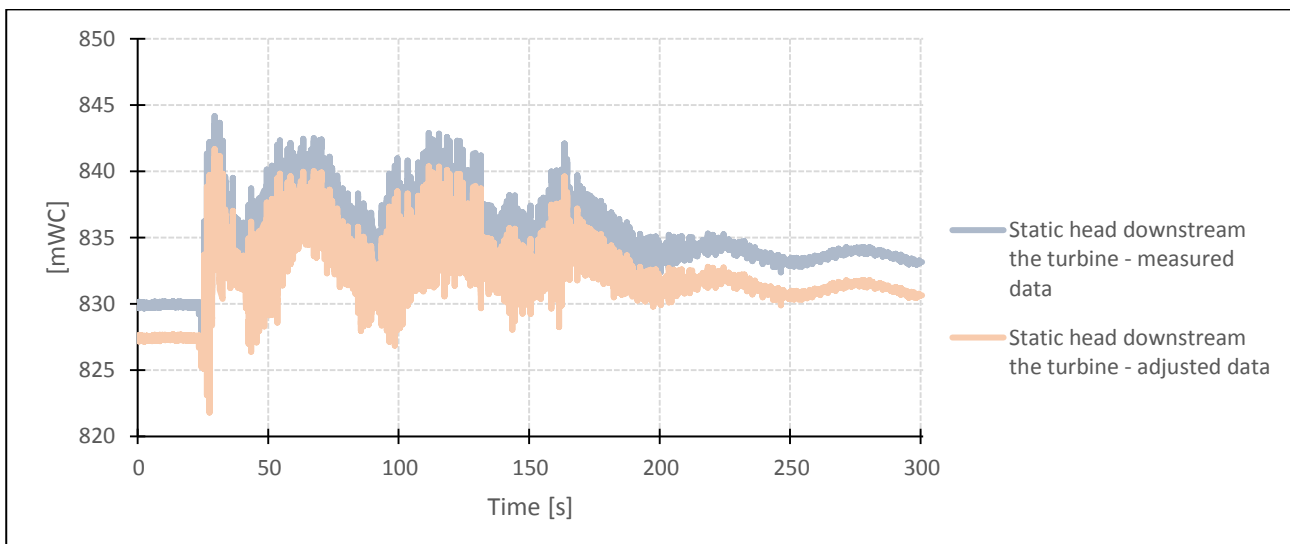


Figure 4.21 - Shutdown: adjusted static head downstream the turbine

This adjustment is performed to make the data comparable with the ones logged from the turbine in the model, which represents the pressure at the outlet of the draft tube.

- Upstream the turbine

The upstream surge tank and the brook intake have the main impact on the pressure in front of the turbine. Some other parameters influence it, but either they are known, or they have been calibrated in the steady-state calibration, or they are considered to play a minor role.

The parameters calibrated in this section are presented in Table 4-11 below.

Table 4-11 - Parameters to be calibrated upstream the turbine

	Parameter	Description	Unit
Brook intake	$D_{\text{equivalent}}$	Diameter of the equivalent water table surface	[m]
	C_{vp}	Concentrated loss for positive flow (water level in the brook intake increasing)	[-]
	C_{vm}	Concentrated loss for negative flow (water level in the brook intake decreasing)	[-]
Upstream surge tank	A	Cross-section area of the vertical shaft	[m ²]
	C_{vp}	Concentrated loss for positive flow (water level in the surge tank increasing)	[-]
	C_{vm}	Concentrated loss for negative flow (water level in the surge tank decreasing)	[-]

As for the steady-state calibration, the approach is a trial and error procedure, pursuing a fit as good as possible with the measured data.

The final parameter combination is presented in Table 4-12 and the response of the calibrated model is shown in Figure 4.22

The full calibration procedure is presented in Annex 2.

Table 4-12 - Calibrated set of parameters upstream the turbine

	$D_{\text{equivalent}}$ [m]	C_{vp} [-]	C_{vm} [-]
Brook intake	18	35	100000
	$A_{\text{vertical shaft}}$ [m ²]	C_{vp} [-]	C_{vm} [-]
Upstream surge tank	55	100	100

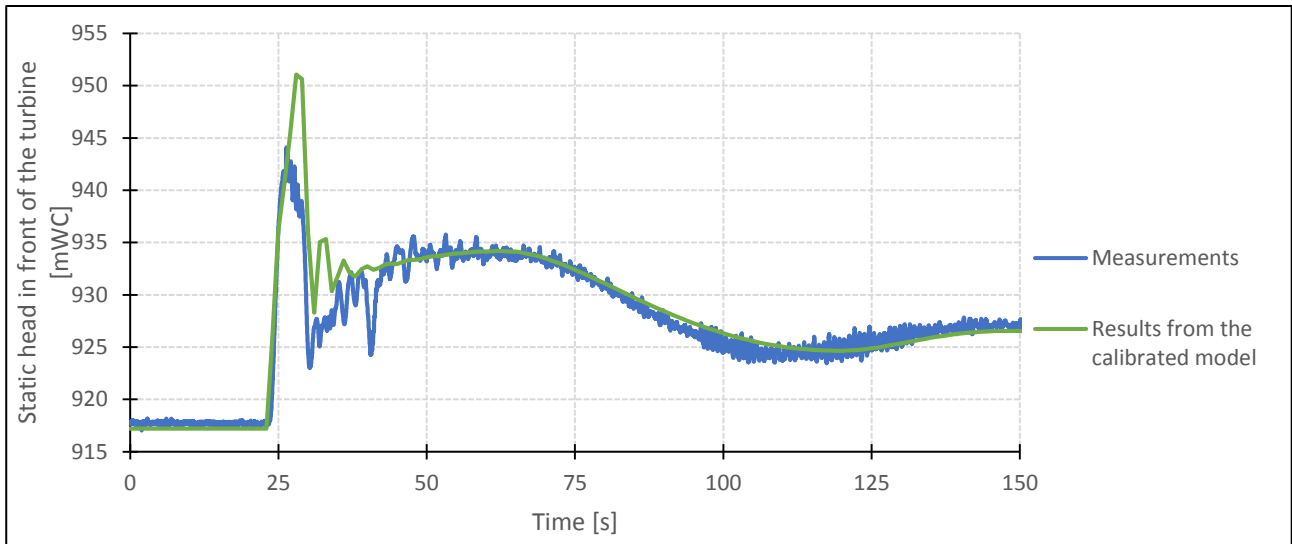


Figure 4.22 - Shutdown: static head in front of the turbine, comparison between measurements and model output

By referring to Figure 4.22, it is possible to identify discrepancies between the prototype response and the model response.

The first spike, which is due to the water hammer, is not well reproduced by the model. In fact, the value in the measurements is 944 mWC, whereas the value in the simulation is over 950 mWC.

As the focus of this thesis is on the stability of mass oscillations, the correct simulation of the water hammer is irrelevant, so the response of the calibrated model is considered satisfying for the aim of the thesis.

- Downstream the turbine

Among all the parameters, the ones of the downstream surge tank play the main role in influencing the pressure downstream the turbine.

They are presented in Table 4-13 below.

Table 4-13 - Parameters to be calibrated downstream the turbine

	Parameter	Description	Unit
Downstream surge tank	D	Cross-section diameter	[m]
	Cvp	Concentrated loss for positive flow (water level in the surge tank increasing)	[-]
	Cvm	Concentrated loss for negative flow (water level in the surge tank decreasing)	[-]

The approach is the same adopted for the calibration of the parameters upstream the turbine, and it is presented in detail in Annex 2.

The final parameter combination is presented in Table 4-14 and the response of the calibrated model is shown in Figure 4.23.

Table 4-14 - Calibrated set of parameters downstream the turbine

	D [m]	C _{vp} [-]	C _{vm} [-]
Downstream surge tank	10.3	1000	1000

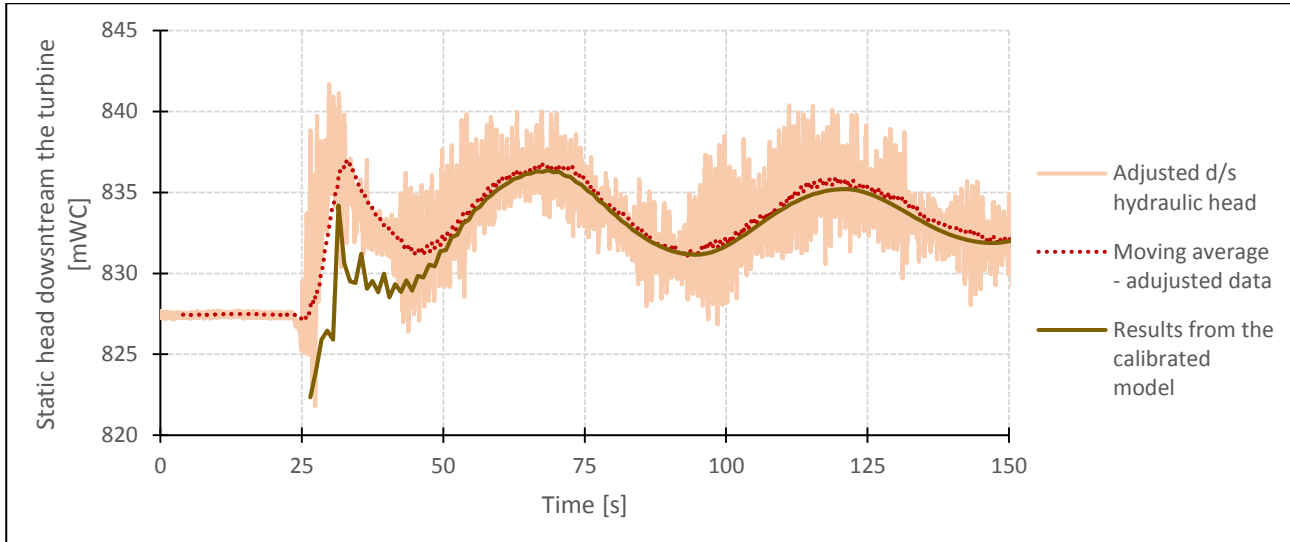


Figure 4.23 - Shutdown: static head downstream the turbine, comparison between measurements and model output

As for the case upstream the turbine, it is easy to find some differences between the prototype and the model response by referring to Figure 4.23.

The first drop, occurring between the 25th and the 50th is not well reproduced by the model.

The cause of the drop is the water hammer, and, as mentioned before, a model able to correctly reproduce the water hammer is out of the scope of this thesis.

From the 50th to the 150th second, the results from the simulation fit well the measurements. Therefore, the output of the calibrated model is considered satisfying for the aim of the thesis.

4.4 Validation

As LVtrans simulates power plants as 1D models, many limitations affect the goodness of the validation. The first challenge regards the operation: the model has been calibrated on the steady-state operation and on a shut-down from 46.9 MW to 0 MW, so it will not be possible to obtain the same accuracy for start-ups and load changes. The main reason is that the characteristics of the turbine in LVtrans are generic values and not the real values from the power plant.

A second challenge is the governor type: Roskrepp has an old-fashioned governor, whereas the one simulated in LVtrans is a modern one. Therefore, the real governor behaves differently with respect to the simulated one, and this will result in differences in the operation.

The validation is performed on a small load change from 48.89 MW to 32.4 MW, measured around 11:30 a.m. on September 17th, 2017. The load change was operated by closing the guide vanes in two steps, as shown in Figure 4.24.

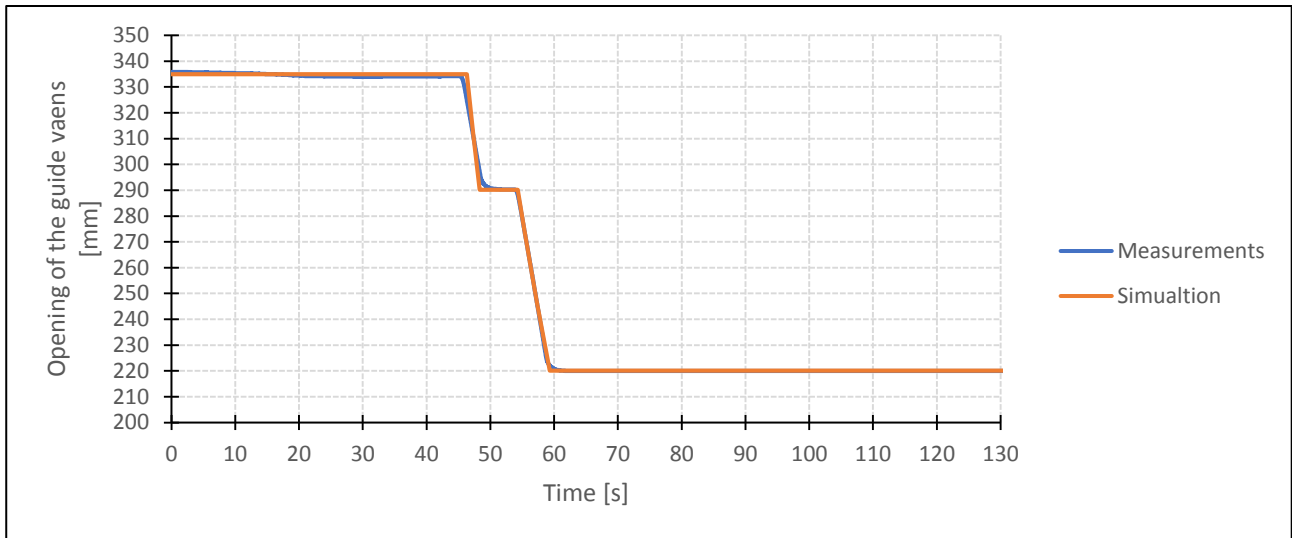


Figure 4.24 - Small load change: guide vanes opening, comparison between measurements and model

Figure 4.25 shows the static head in front of the turbine in the simulation against the one in the measurements.

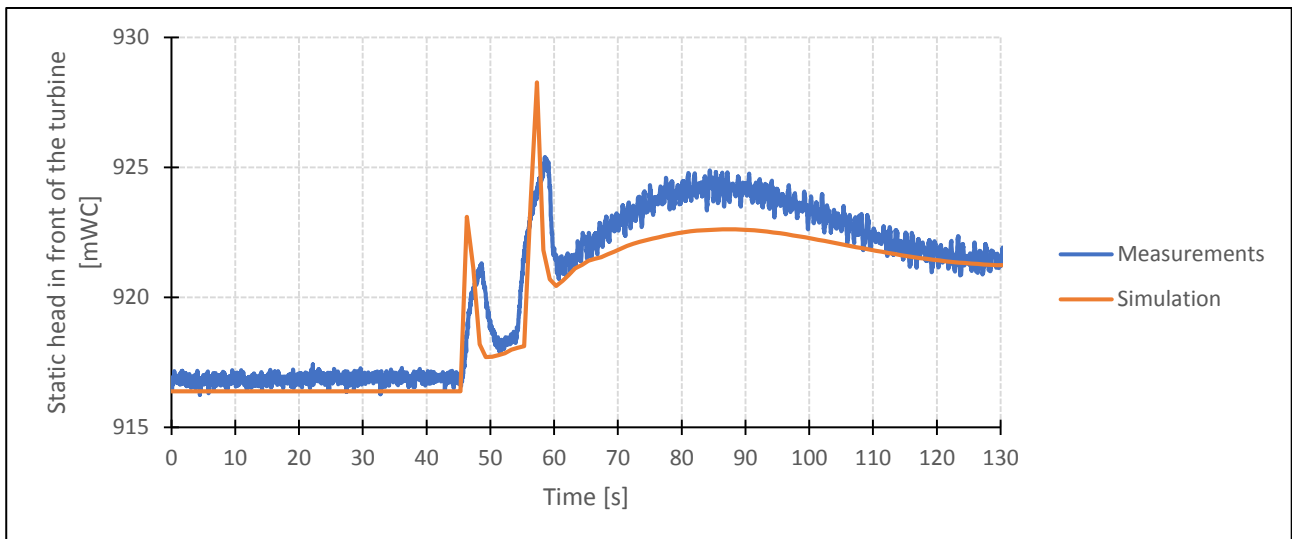


Figure 4.25 - Small load change: static head in front of the turbine, comparison between measurements and model output

Referring to the figure above, it can be seen that the two spikes occurring at second 45th and 55th are higher in the simulation than in the measurements. These spikes are caused by water hammer, and, as the correct simulation of water hammer is out of the scope of the thesis, the fit is considered acceptable.

The goodness of the validation is evaluated comparing the period of mass oscillations and the maximum amplitude due to mass oscillations between the measurements and the simulation.

Such comparison is shown in Table 4-15 below.

Table 4-15 - Validation: comparison between measurements and validated model

	Measurements [s]	Simulation [s]	Absolute error [s]	Relative error [%]
Period	64	68	4	6.25
	Measurements [masl]	Simulation [masl]	Absolute error [masl]	Relative error [%]
Max amplitude due to mass oscillations	924.88	922.61	2.27	0.25

Considering the challenges in validating a 1D model described at the beginning of the paragraph, the validation is considered acceptable and the results satisfying.

5. Results and discussion

The author found more convenient to include results and discussion in the same chapter, hence, in this chapter, the simulated scenarios are presented and discussed. The influence on stability of the brook intake and of the downstream surge tank is investigated. Finally, a comparison between dynamic analysis and Thoma method is carried out.

Since the focus is on stability, all the simulations presented in this chapter were performed in isolated mode, to avoid that the grid influences the power plant with its inherent stability.

5.1 Influence on stability

To evaluate what is the impact of the brook intake and of the downstream surge tank on stability, two scenarios are analysed:

- scenario A, start-up to 50 MW, i.e. full load
- scenario B, start-up to the maximum possible power output for a stable system

Scenario B may be particularly interesting for the owner of the project, since its aim is to investigate the possibility to increase the power output without any intervention on the surge tanks.

The turbine in Roskrepp power plant has a manual block for the guide vanes, in order to limit their opening. For this kind of designs, if the opening is forced beyond the block, the turbine is not covered any longer by its guaranty. For what concerns Roskrepp power plant, the guaranty has already expired, so the opening beyond the manual block could be performed. Besides, by cutting the blades and the splitters of the turbine, the discharge could be further increased. Instability may be the only limit to the power output increase: the aim of scenario B is to test this possibility.

However, the model shows a limitation in this scenario. To increase the power output to meet the set power, the discharge is incremented. As a result, the head losses increase as well.

At one point, their growth is so vast that they affect the power output to such large extent, that the result is a decreasing power output for an increasing set power.

Because of this limit, it was possible to test a maximum power output of 52.11 MW.

For this analysis, the discharge in the brook intake is assumed equal to 0 m³/s.

5.1.1 Influence of the brook intake

To verify how the brook intake influences the stability of the power plant, three designs are analysed and compared:

1. the existing design, with one brook intake
2. a design without any brook intakes
3. a design with two brook intakes, the existing one and an additional one, midway through the existing brook intake and the upstream surge tank

- Scenario A: start-up to 50 MW

The water level variation in the upstream and downstream surge tank for scenario A is shown, respectively, in Figure 5.1 and Figure 5.2

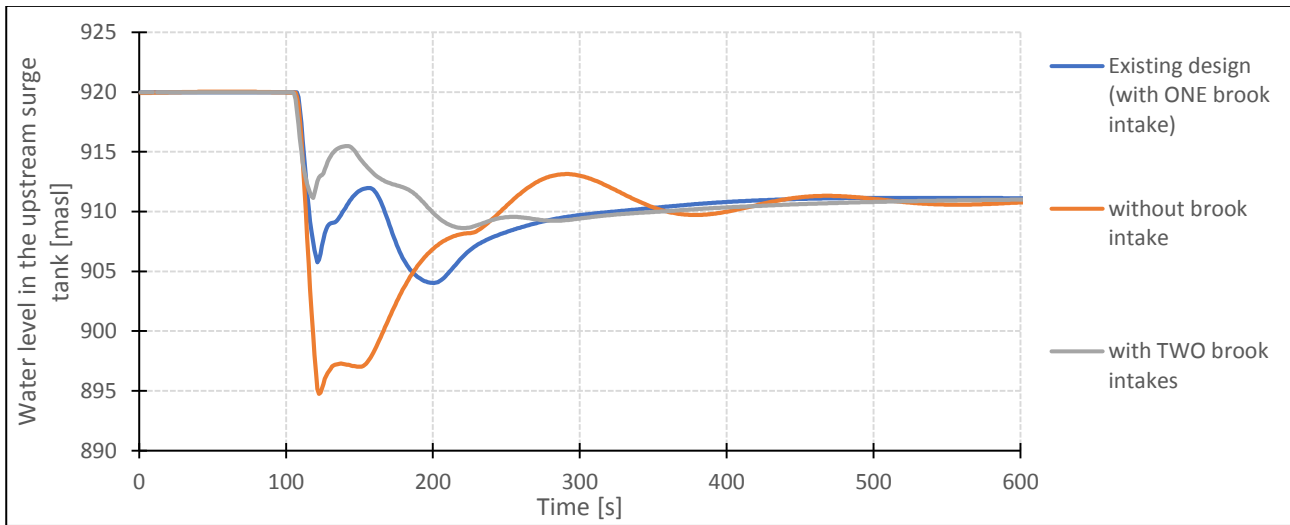


Figure 5.1 - Influence of the brook intake, scenario A: water level variation in the upstream surge tank

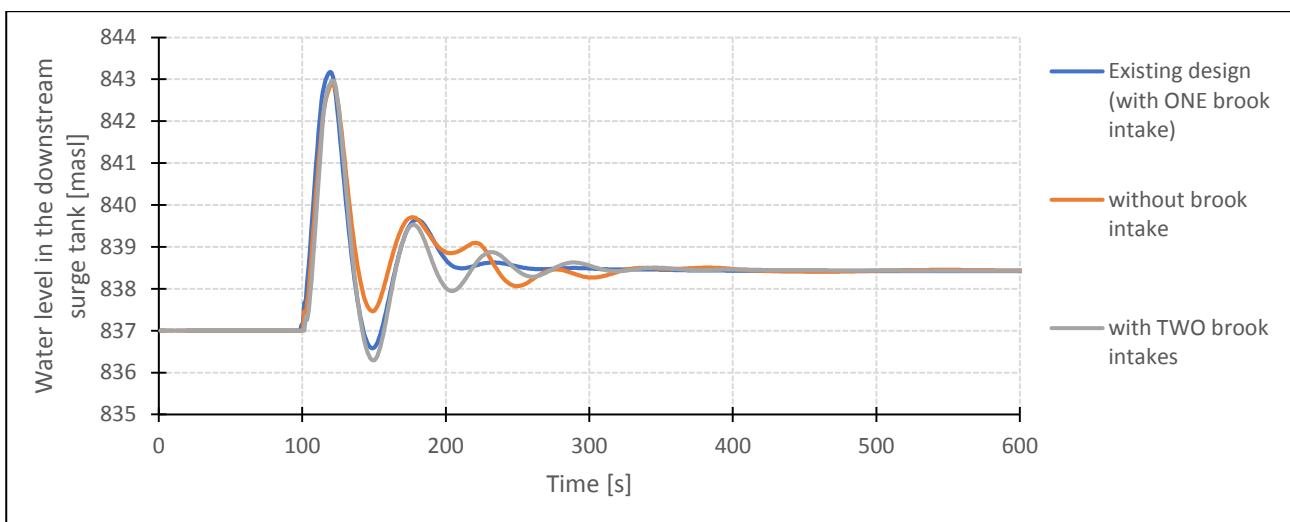


Figure 5.2 - Influence of the brook intake, scenario A: water level variation in the downstream surge tank

By referring to Figure 5.1, it is possible to acknowledge that the presence of the brook intake has a stabilizing effect, as the amplitude and the period of the oscillations are reduced in the case with one brook intake (blue line) and even more in the case with two brook intakes (gray line). However, all the three cases are stable.

For what concerns the downstream surge tank, the brook intake presence has not a big impact, as can be seen in Figure 5.2

The stabilizing effect of the brook intake can be explained by the fact that mass oscillations occur between the two closest water surfaces. If a brook intake is present between the upper reservoir and the surge tank, the mass oscillations have less space to develop. The part of pipe affected by mass oscillations for every case is shown in Figure 5.3, Figure 5.4 and Figure 5.5 below.

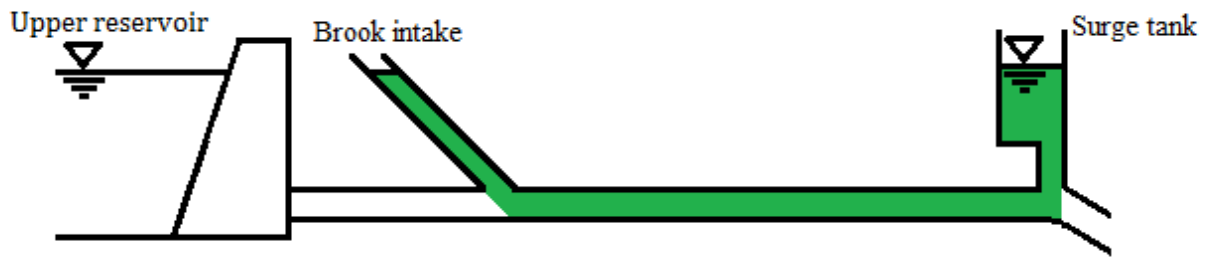


Figure 5.3 - Part of pipe affected by mass oscillations in the existing design, with one brook intake

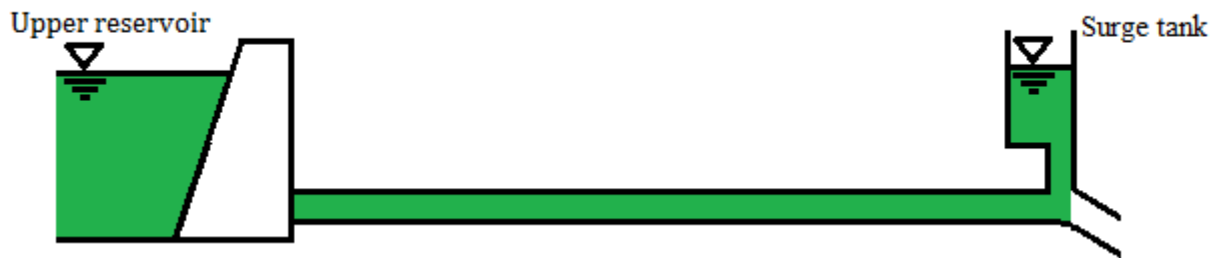


Figure 5.4 - Part of pipe affected by mass oscillations in the design without any brook intake

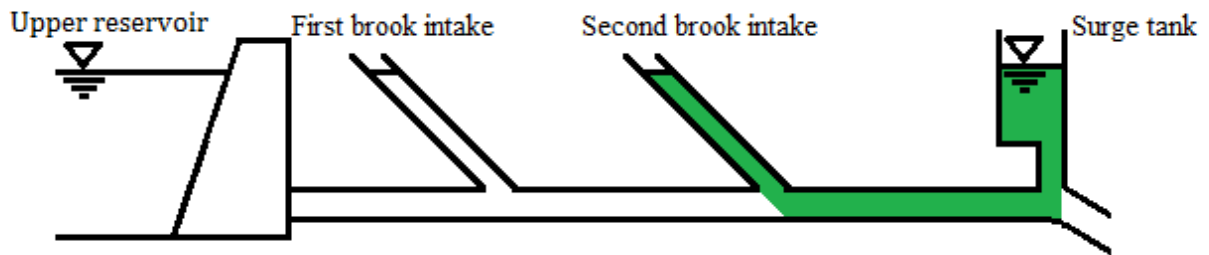


Figure 5.5 - Part of pipe affected by mass oscillations in the design with two brook intakes

- Scenario B: start-up to 52.11 MW

The water level variation in the upstream and downstream surge tank for scenario B is shown, respectively, in Figure 5.6 and Figure 5.7.

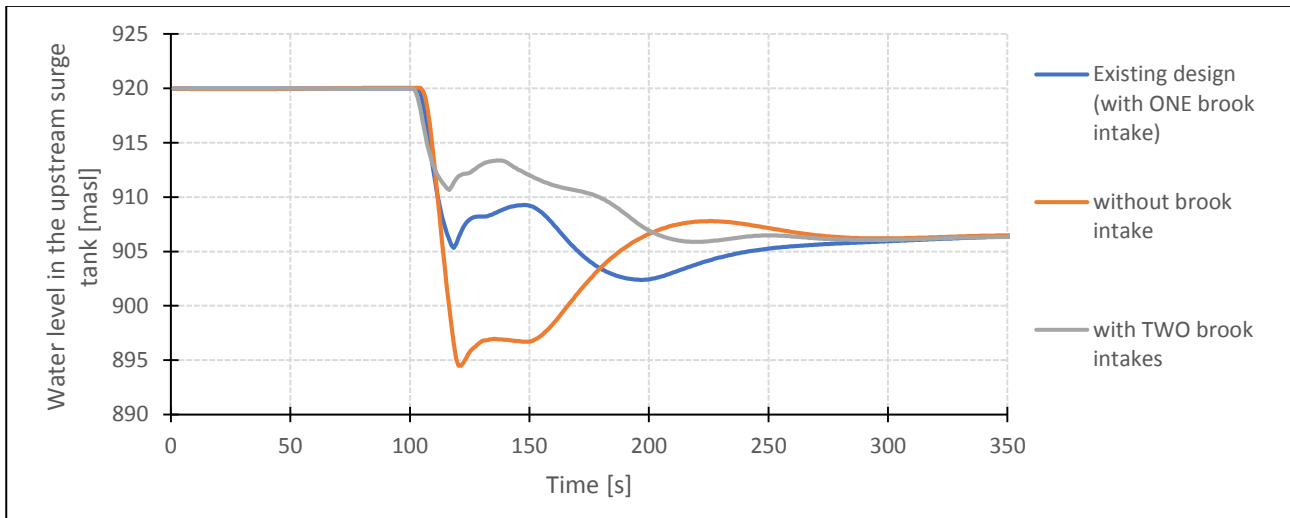


Figure 5.6 - Influence of the brook intake, scenario B: water level variation in the upstream surge tank

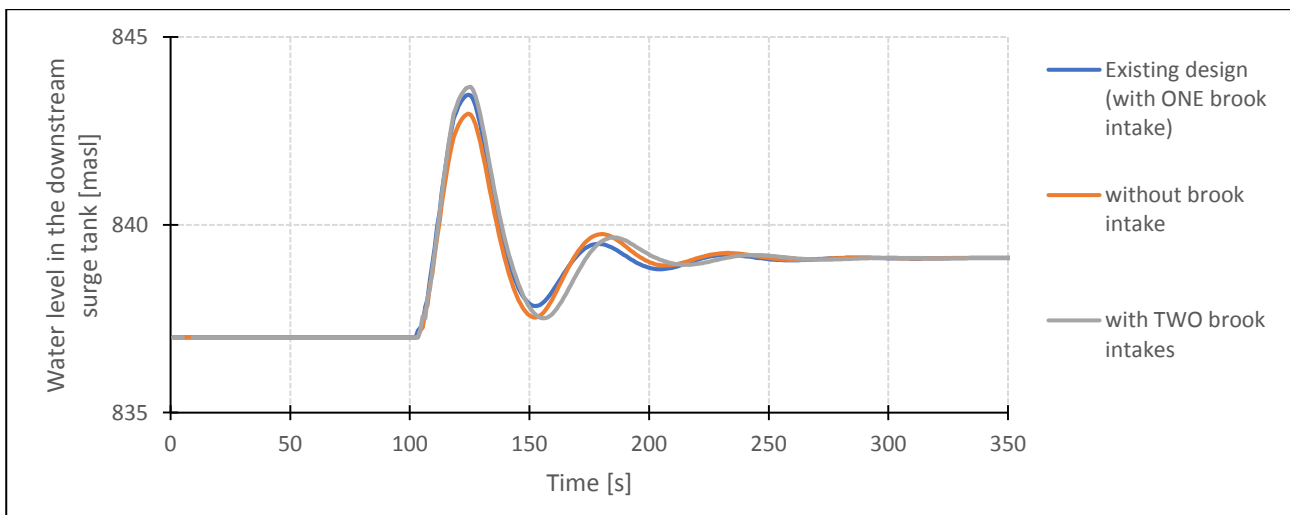


Figure 5.7 - Influence of the brook intake, scenario B: water level variation in the downstream surge tank

By referring to Figure 5.6, it can be seen that the stabilizing effect of the brook intake noticed in scenario A is confirmed: again, the amplitude and the period of the oscillations are reduced more and more as the number of brook intakes increases. However, all the three cases are stable.

As can be seen in Figure 5.7, the water level in the downstream surge tank is not strongly influenced by the presence of one or two brook intakes.

5.1.2 Influence of the downstream surge tank

To evaluate the influence of the downstream surge tank on the system stability, two schemes are compared:

1. the existing design, with the upstream and downstream surge tank
2. a design with the upstream surge tank, but without the downstream one

- Scenario A: start-up to 50 MW

The water level variation in the upstream surge tank for scenario A is shown in Figure 5.8.

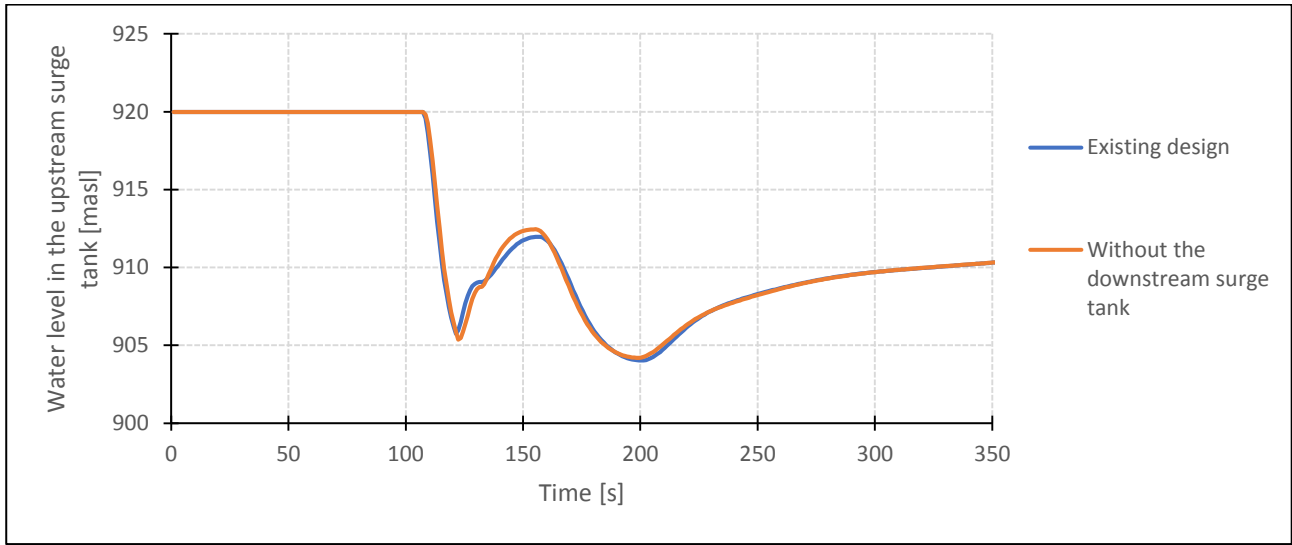


Figure 5.8 - Influence of the downstream surge tank, scenario A: water level variation in the upstream surge tank

As Figure 5.8 shows, the absence of the downstream surge tank has a limited impact on the water level in the upstream surge tank and its stability is not compromised.

- Scenario B: start-up to 52.11 MW

The water level variation in the upstream surge tank for scenario B is shown in Figure 5.9.

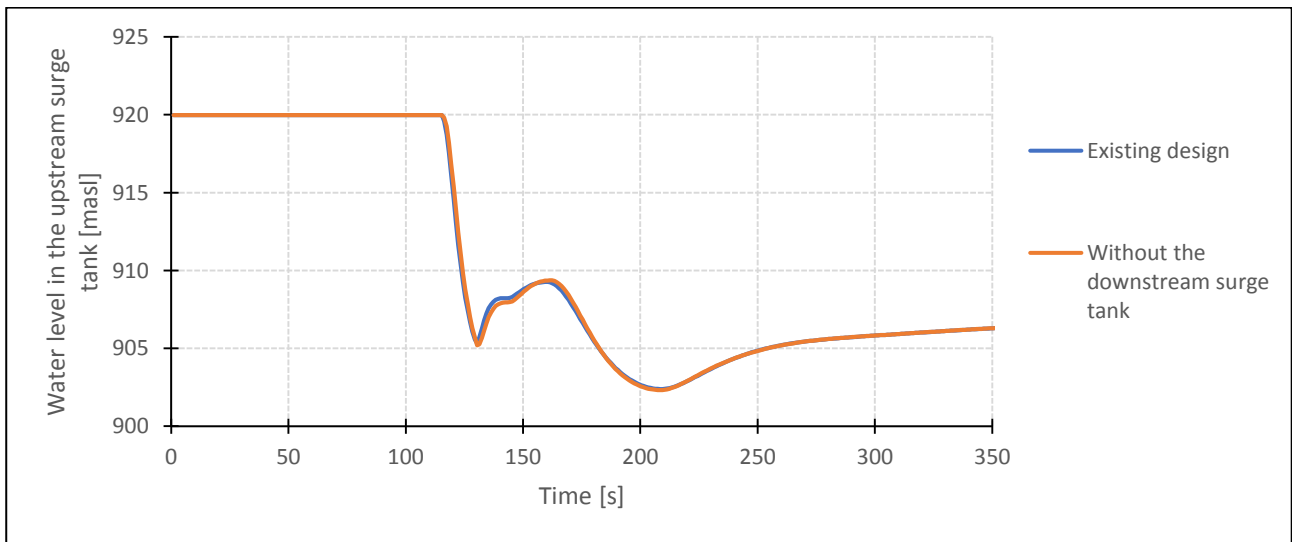


Figure 5.9 - Influence of the downstream surge tank, scenario B: water level variation in the upstream surge tank

Figure 5.9 confirms the findings of scenario A: the influence of the downstream surge tank on the water level in upstream surge tank is very limited.

5.2 Possibility of abolishing the upstream surge tank

As discussed in section 5.1.1, the brook intake proves to have a stabilizing effect. The aim of the following analysis is to test whether the brook intake could be used as a surge shaft, allowing the abolition of the upstream surge tank. Hence, where a brook intake is present, it could be exploited to guarantee stability to the system, without the need of a surge tank to damp out mass oscillations.

In the following analysis, the focus is set on the system stability. To discuss if the abolition of the upstream surge tank is actually feasible, more factors should be taken into account, such as:

- the pressure spike resulting from water hammer
- the maximum upsurge and downsurge of the water level in the brook intake and in the downstream surge tank, that may lead to overflow and air entrainment in the tunnel

These aspects are considered out of the scope of the thesis. However, a more comprehensive analysis should include them, in order to have the complete picture to choose on the abolition of the upstream surge tank.

As this is a theoretical investigation, two options for the value of the diameter of the brook intake are tested: the real value and the calibrated value.

5.2.1 Real value for $D_{\text{brook intake}}$

The cross-sectional area of the brook intake is 8 m^2 , which corresponds to a diameter of 3.2 m. Since the brook intake has a slope of 1:8.4 and LVtrans is not able to take into account the slope, the diameter of the equivalent water table surface should be used in the simulation.

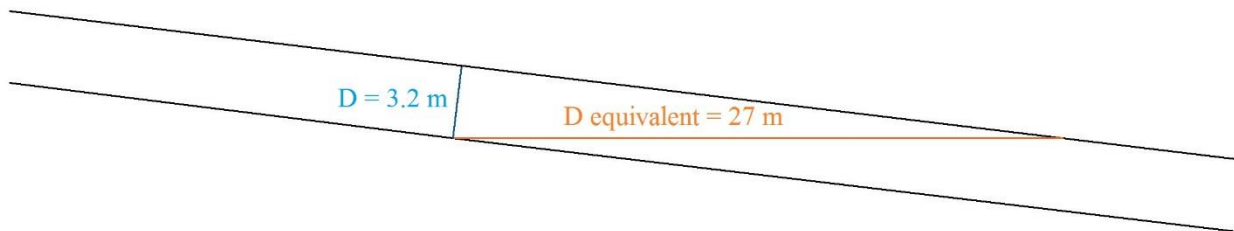


Figure 5.10 - Brook intake: diameter and diameter of the equivalent water table surface

The scheme is tested for a start-up to full load, considering different discharges in the brook intake, from $0 \text{ m}^3/\text{s}$ to the maximum possible discharge, $30 \text{ m}^3/\text{s}$.

The water level variation in the brook intake and in the downstream surge tank following the start-up to full load is shown, respectively, in Figure 5.11 and Figure 5.12

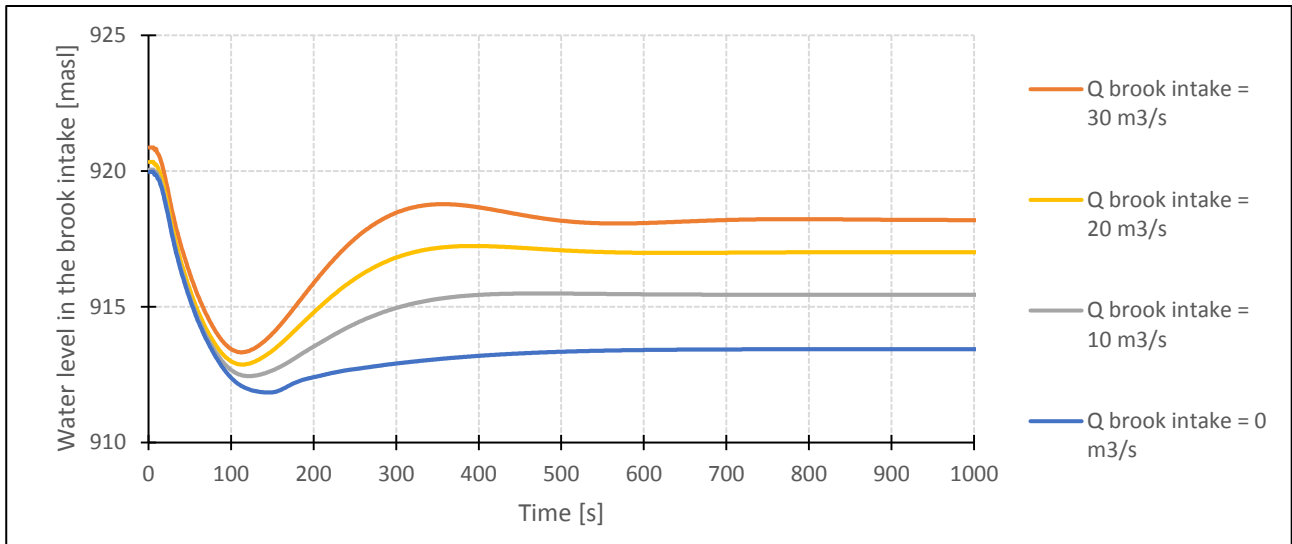


Figure 5.11 - Abolition of the upstream surge tank, start-up to full load: water level variation in the brook intake ($D_{\text{brook intake}} = 27 \text{ m}$)

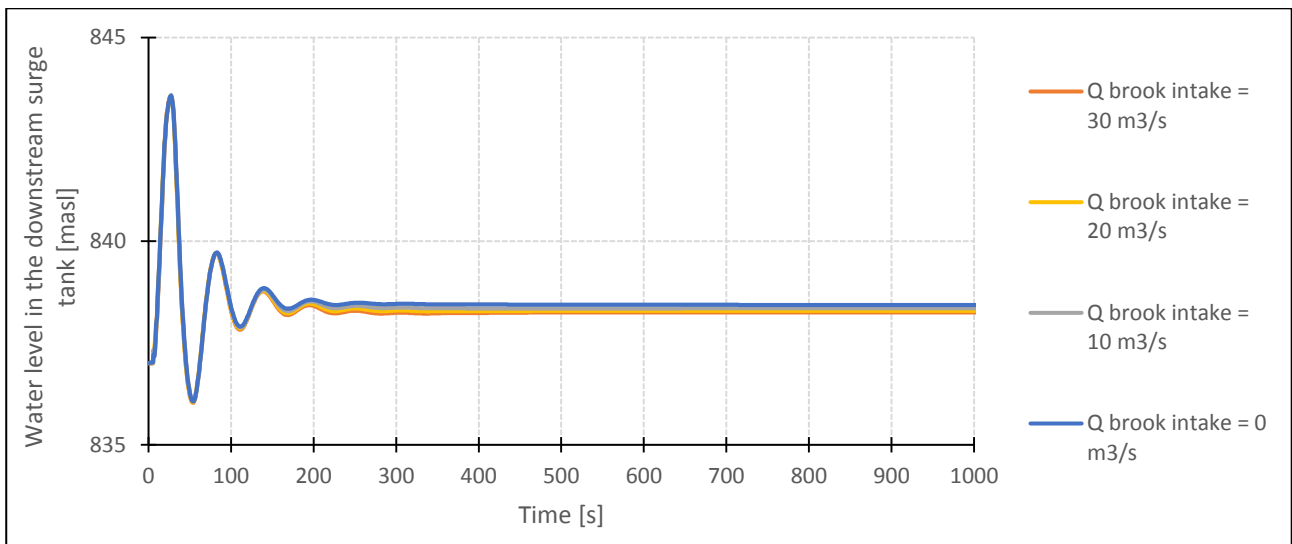


Figure 5.12 - Abolition of the upstream surge tank, start-up to full load: water level variation in the downstream surge tank ($D_{\text{brook intake}} = 27 \text{ m}$)

The above figures show that the system stability is guaranteed in every case, also in the worst-case scenario, the one with maximum discharge in the brook intake.

5.2.2 Calibrated value for $D_{\text{brook intake}}$

As seen in paragraph 4.3.2, the calibrated value of $D_{\text{brook intake}}$ is 18 m. This option is considered worth exploring as it is more conservative than the one analysed in the above paragraph.

As above, the scheme is tested for a start-up to full load, considering different discharges in the brook intake, from $0 \text{ m}^3/\text{s}$ to the maximum possible discharge, $30 \text{ m}^3/\text{s}$.

The water level variation in the brook intake and in the downstream surge tank following the start-up to full load is shown, respectively, in Figure 5.13 and Figure 5.14

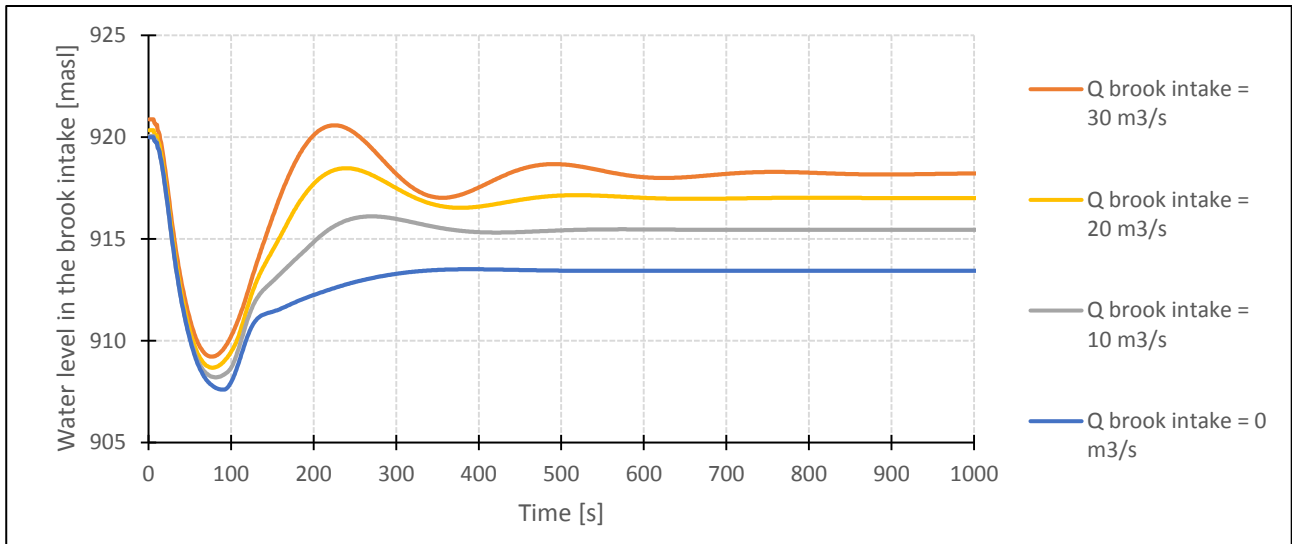


Figure 5.13 - Abolition of the upstream surge tank, start-up to full load: water level variation in the brook intake ($D_{brook\ intake} = 18\ m$)

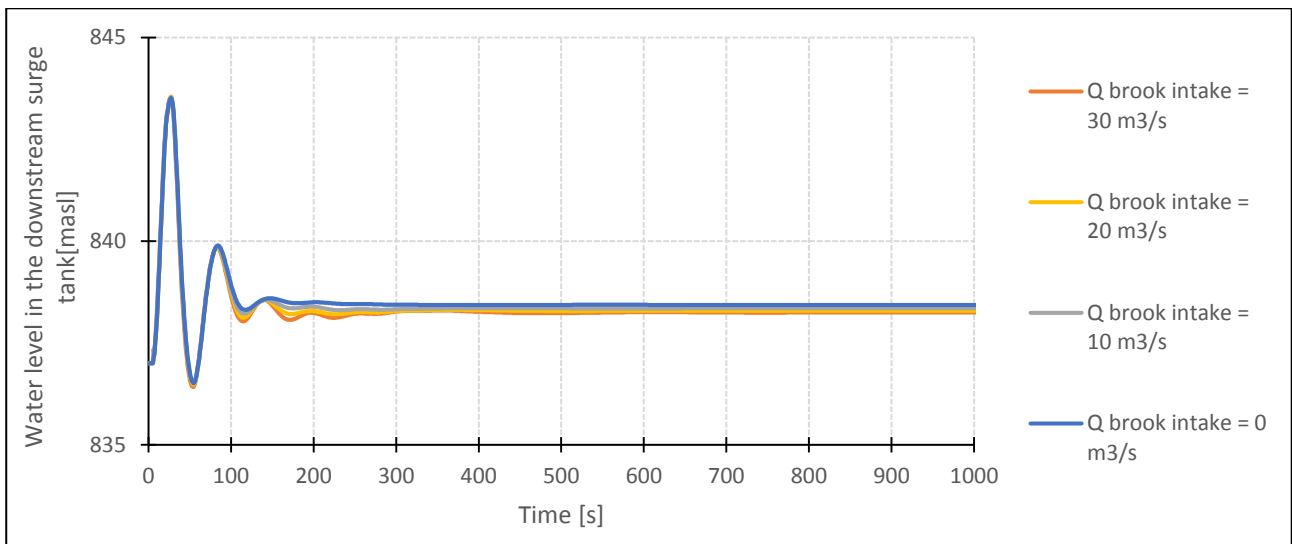


Figure 5.14 - Abolition of the upstream surge tank, start-up to full load: water level variation in the downstream surge tank ($D_{brook\ intake} = 18\ m$)

Even though this case is more conservative, the system is stable for each tested value of $Q_{brook\ intake}$. It yields that, in terms of stability, the abolition of the upstream surge tank is possible.

5.3 Stability analysis

In this section, the standard criterion to define the size of surge tanks, Thoma method, is compared with direct simulation in four different scenarios:

- scenario a, the existing design with no discharge in the brook intake
- scenario b, the existing design with maximum possible discharge in the brook intake ($Q_{brook\ intake} = 30\ m^3/s$)
- scenario c, a design without any brook intakes
- scenario d, a design without the downstream surge tank ($Q_{brook\ intake} = 0\ m^3/s$)

Scenario b, c and d represent the worst-case scenarios; therefore, they are quite relevant for the purpose of the analysis.

5.3.1 Thoma method

Thoma method, described in paragraph 2.5.3, is here applied to Roskrepp power plant to identify the recommended size of the surge tank. In the interest of simplicity, in this analysis, the upstream surge tank is considered as a simple surge shaft.

The formula to be used is the (2.98):

$$A_{surge\ tank, \min} \geq 0.014144 \frac{A^{5/3} M^2}{H_{net}} \quad (2.98)$$

The net head is obtained from the formula $H_{net} = \frac{P}{\rho g \eta Q}$, where P is the capacity, 50 MW, and η the turbo-generator efficiency, which is assumed equal to 0.9. So, H_{net} results equal to 84.52 m.

For what concerns Manning number, in the report from Roskrepp power plant, two values are available: 31.1 $m^{1/3}/s$ for the headrace tunnel without asphalt layer, 36.1 $m^{1/3}/s$ for the headrace where the asphalt layer is present. In order to obtain a value to be used in Thoma equation, a weighted average is computed, as shown in Table 5-1 below. Also, the weighted average of the areas of the different sections of the headrace tunnel is computed.

Table 5-1 - Computation of weighted averages of area and Manning number for the headrace tunnel

Part of the headrace tunnel	Roskrepp-Haheller (adit)	Haheller-Skjerevatn (brook intake)	Skjerevatn-Upstream surge tank	Upstream surge tank-G
L [m]	275	1926	970	341
A [m ²]	7.15	6.97	7.15	7.15
M [m ^{1/3} /s]	31.1	36.1	31.1	31.1
Area (weighted average) [m ²]	M (weighted average) [m ^{1/3} /s]			
7.05	33.84			

Head loss measurements can be very uncertain. In order to assess the impact of this uncertainty, a sensitivity analysis is performed. The range considered for the Manning number is 25-40 $m^{1/3}/s$, that, according to Benson (1989), is the range for a drill and blast unlined tunnel.

In Figure 5.15 below, the impact of the variation of Manning number on the Thoma area is shown.

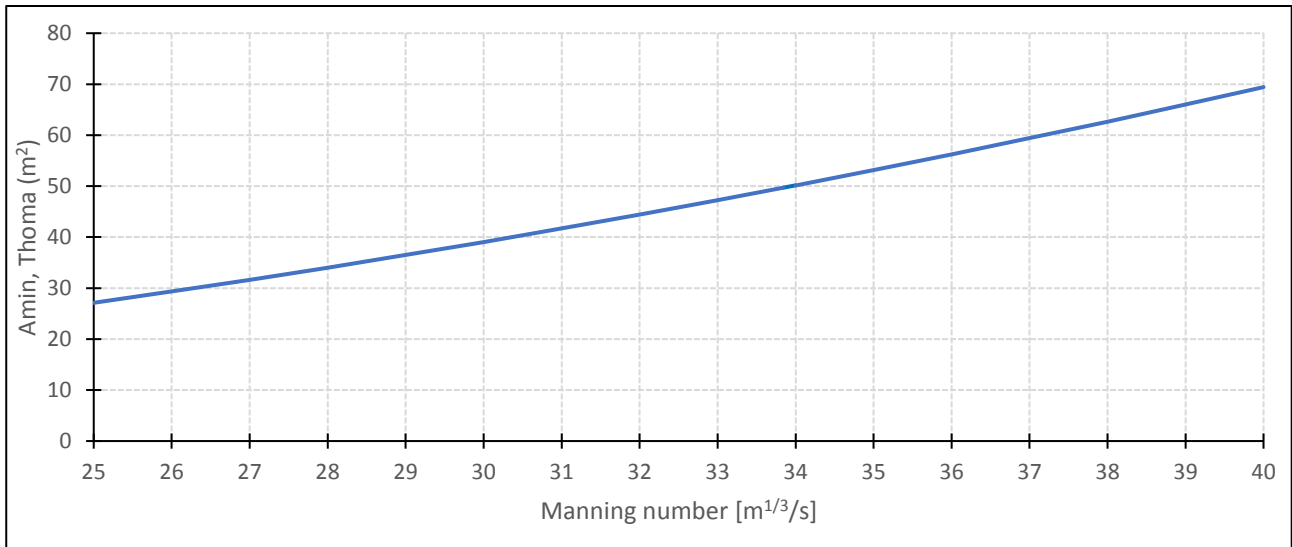


Figure 5.15 - Sensitivity analysis: sensitivity of A_{Thoma} to the variation of Manning number

As shown in Figure 5.15, Thoma area is very sensitive to the variation of Manning number. In the interest of simplicity, in the next analysis, the adopted value of A_{Thoma} is the one obtained by using as Manning number the weighted average. The obtained A_{Thoma} value is shown in Table 5-2 below. However, the analysis is carried out bearing in mind that a small error in the head loss measurements has a significant impact on the computed value of A_{Thoma} .

Table 5-2 - Thoma area and correspondent diameter for Roskrepp power plant

M [m ^{1/3} /s]	Amin, Thoma [m ²]	Diameter [m]
33.84	50.3	8.0

The value of A_{Thoma} is used in the model and the response is compared with the one from the model where the actual upstream surge tank (the one from the drawings) is implemented. This comparison can be found in Annex 3 and shows that the two models give very similar outputs for the water level variation in the surge tanks, in all the analysed scenarios. This was expected, as the vertical shaft of the upstream surge tank in the design drawings has a cross-section of 60 m², value quite similar to the one obtained in the computations above.

5.3.2 Direct simulation

For each of the mentioned scenarios, different values for the surge shaft diameter are tested. The aim is to find the minimum diameter that guarantees the stability of the system

- scenario a, the existing design with no discharge in the brook intake

As shown in paragraph 5.2, the existing design would be stable without the upstream surge tank, independently from the discharge in the brook intake. Hence, for scenario a and for scenario b (presented below), it may be interesting to find the minimum value of the brook intake diameter that guarantees the stability of the system. This analysis is relevant just from an academic point of view, as it would be unlikely that the power company is interested in reducing the brook intake diameter. In fact, this would decrease the discharge of the brook intake and, hence, the power production.

The water level variation in the brook intake and in the downstream surge tank for scenario a is shown, respectively, in Figure 5.16 and Figure 5.17. To better visualize the different behaviour of the system when stable and when unstable, three different cases are compared: the minimum diameter required for stability, the minimum diameter minus 20 cm and the minimum diameter minus 40 cm. This kind of plot is adopted for every similar analysis that follows.

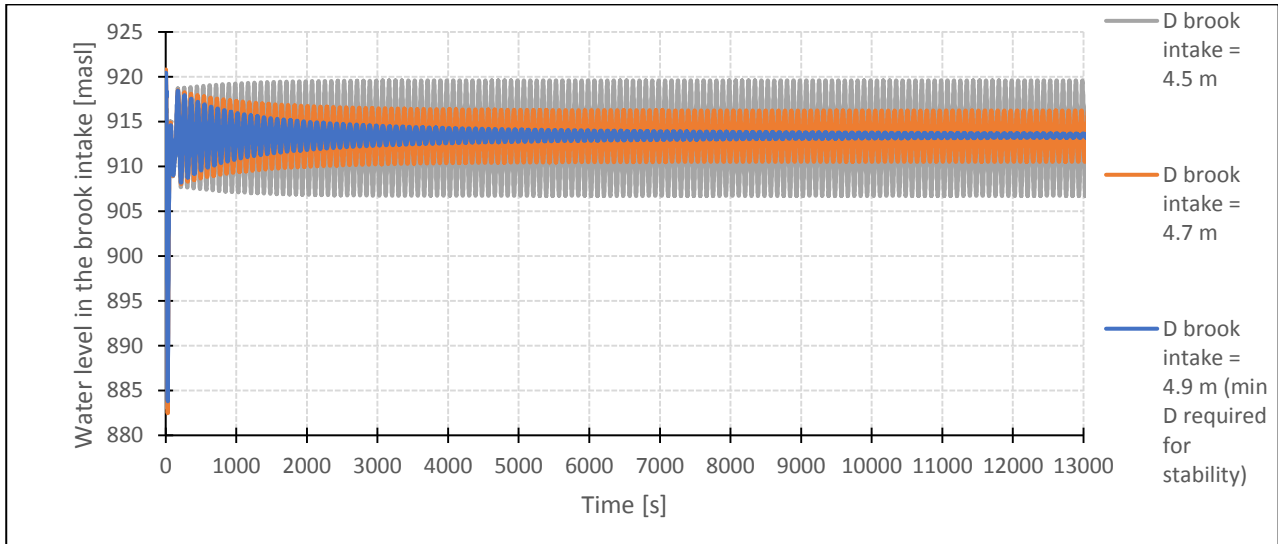


Figure 5.16 - scenario a: water level variation in the brook intake, comparison of different $D_{brook\ intake}$

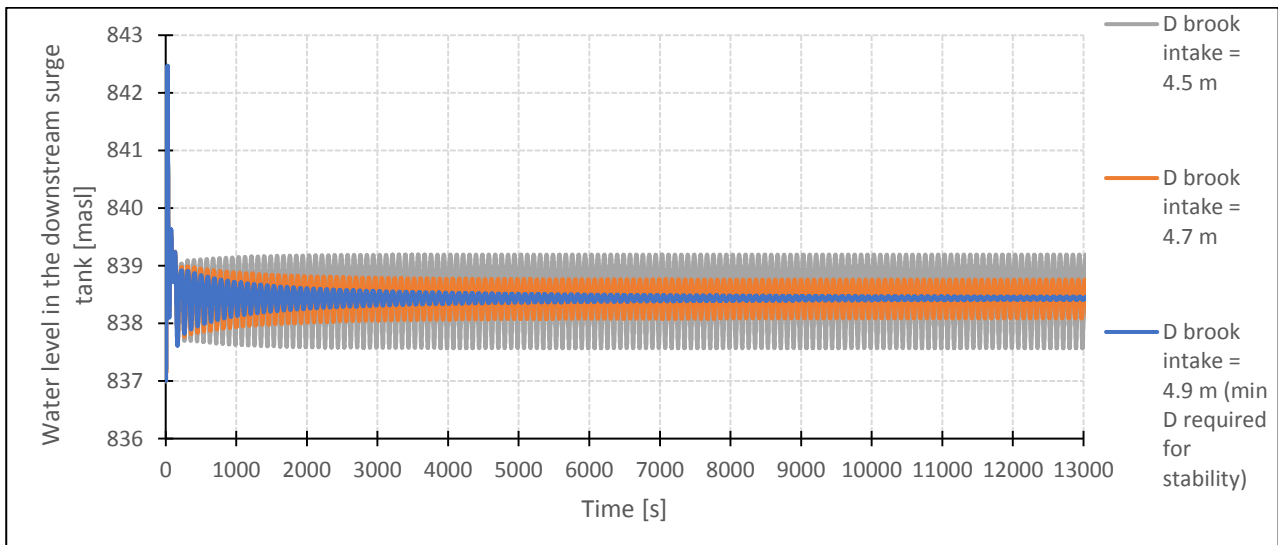


Figure 5.17 - scenario a: water level variation in the downstream surge tank, comparison of different $D_{brook\ intake}$

The above figures show that, for scenario a, a brook intake diameter equal to 4.9 m is sufficient to guarantee the stability of the system.

- scenario b, the existing design with maximum possible discharge in the brook intake

The water level variation in the brook intake and in the downstream surge tank for scenario b is shown, respectively, in Figure 5.18 and Figure 5.19.

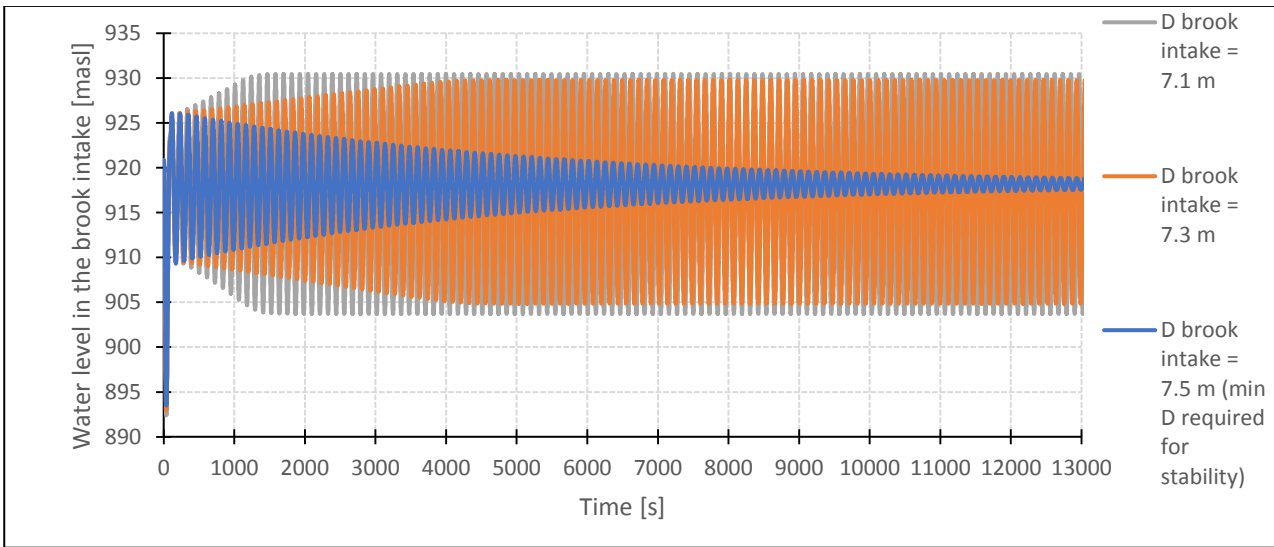


Figure 5.18 - scenario b: water level variation in the brook intake, comparison of different $D_{\text{brook intake}}$

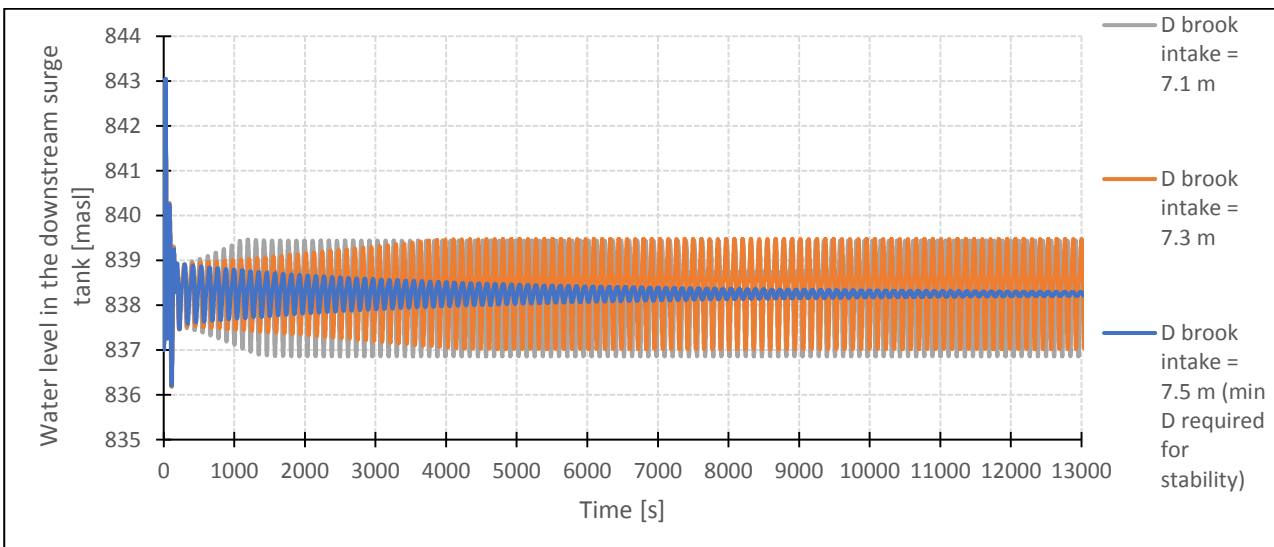


Figure 5.19 - scenario b: water level variation in the downstream surge tank, comparison of different $D_{\text{brook intake}}$

As shown by the above figures, the system stability is guaranteed when the brook intake diameter is, at least, equal to 7.5 m.

- scenario c, design without any brook intakes

The water level variation in the upstream and downstream surge tank for scenario c is shown, respectively, in Figure 5.20 and Figure 5.21 below.

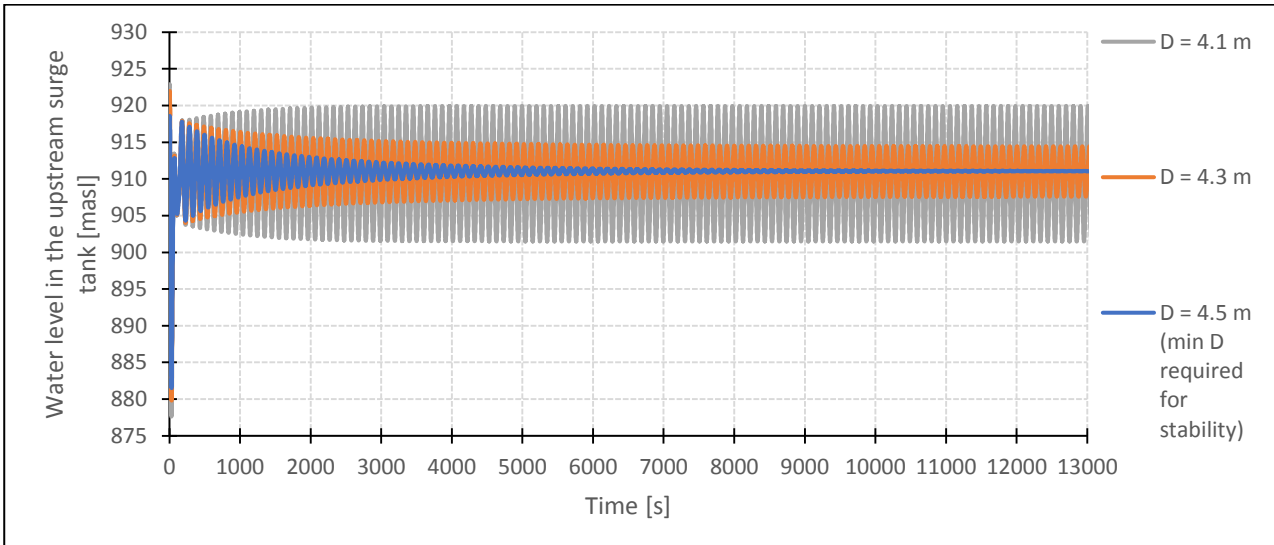


Figure 5.20 - scenario c: water level variation in the upstream surge tank, comparison of different $D_{\text{upstream surge shaft}}$

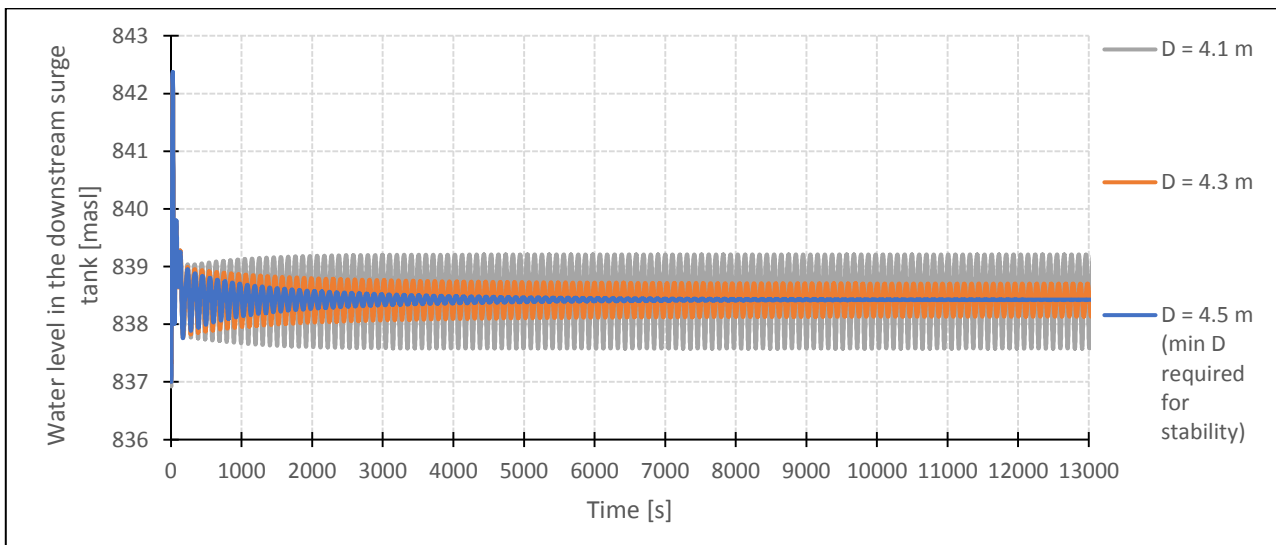


Figure 5.21 - scenario c: water level variation in the downstream surge tank, comparison of different $D_{\text{upstream surge shaft}}$

As shown by the above figures, for this scenario, the system is stable for a minimum upstream surge shaft diameter equal to 4.5 m.

- scenario d, design without the downstream surge tank

The water level variation in the upstream surge tank for scenario d is shown in Figure 5.22

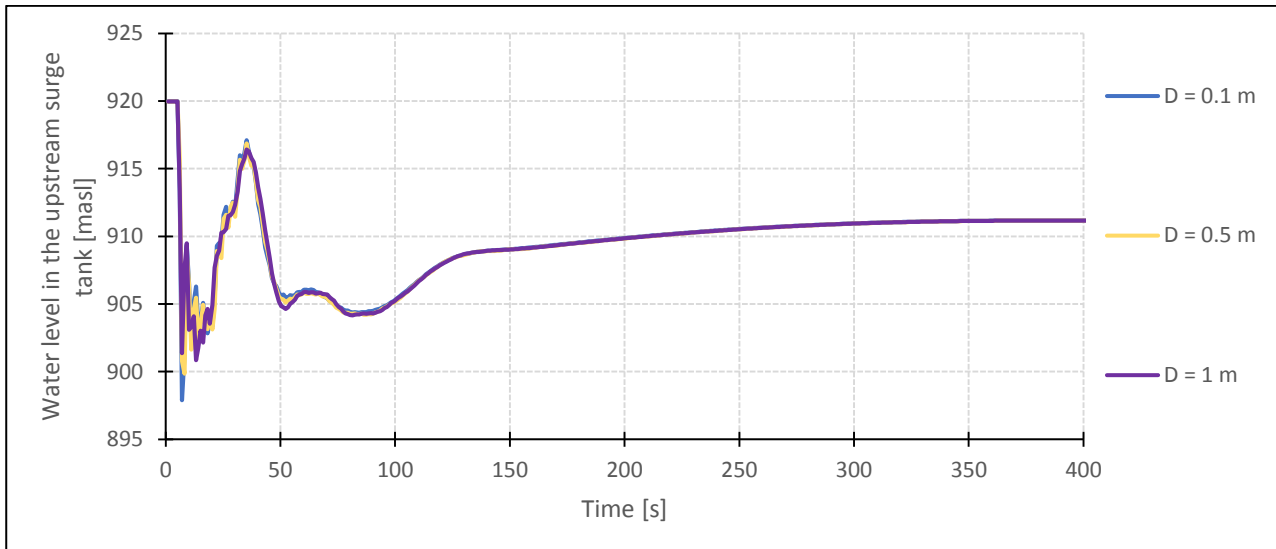


Figure 5.22 - scenario d: water level variation in the upstream surge tank, comparison of different $D_{\text{upstream surge shaft}}$

Figure 5.22 above shows that, even for very small upstream surge shaft diameters, the system is stable. Therefore, the possibility to abolish the upstream surge shaft is investigated, to test whether the stability would be guaranteed also in that case.

First, the design with the calibrated value for the diameter of the brook intake ($D_{\text{brook intake}} = 18 \text{ m}$) is simulated, as shown in Figure 5.23.

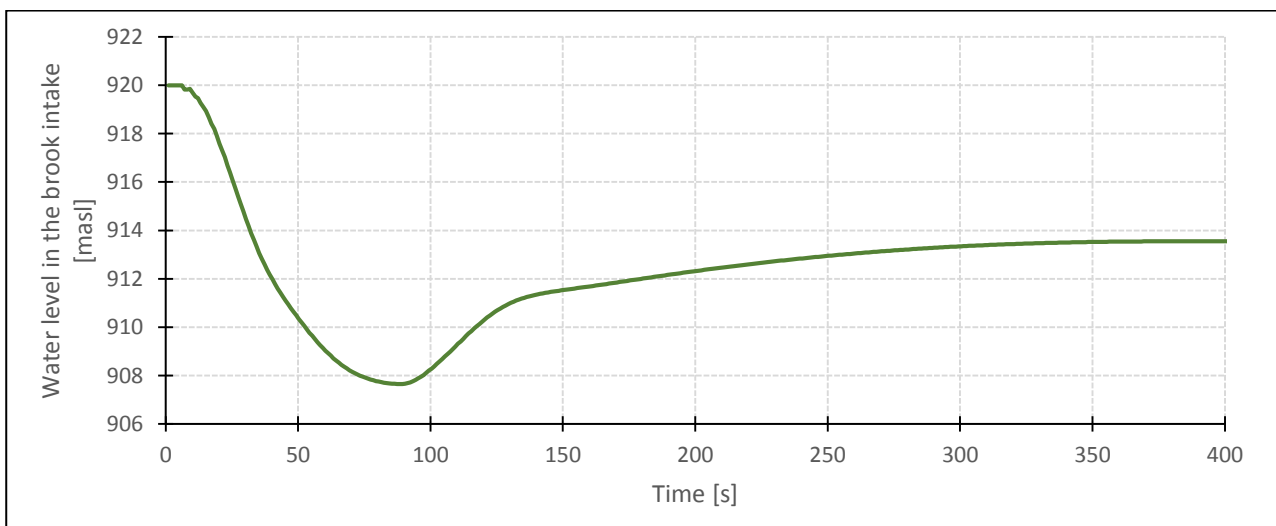


Figure 5.23 - scenario d: water level variation in the brook intake when $D_{\text{brook intake}} = 18 \text{ m}$

As shown in Figure 5.23 above, the system stability is ensured if the brook intake diameter is equal to 18 m. Hence, it may be interesting to find which value represents the minimum brook intake diameter that guarantees stability.

The water level variation in the brook intake for scenario d is shown in Figure 5.24 below.

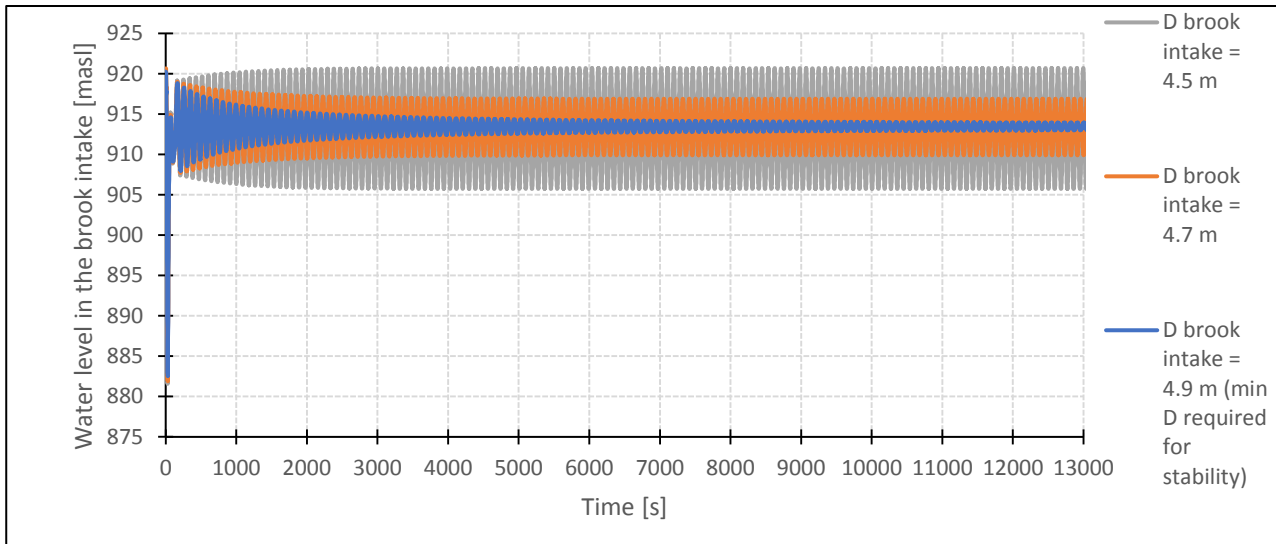


Figure 5.24 - scenario d: water level variation in the brook intake, comparison of different $D_{brook\ intake}$

As shown by the above figure, when neither the upstream nor the downstream surge tank are present, a minimum brook intake diameter of 4.9 m can guarantee the stability of the system. The same value was obtained for scenario a. The conclusion of the analysis on the influence of the downstream surge tank in paragraph 5.1.2 was that the absence of the downstream surge tank does not compromise the stability of the system. In the light of the above, this conclusion is confirmed and strengthened: the absence of the downstream surge tank does not have any influence on the system stability.

5.3.3 Comparison

Table 5-3 below shows, for each scenario, the comparison between the areas of the upstream surge shaft selected with Thoma method and the ones selected with direct simulation.

Table 5-3 - Comparison between Thoma method and direct simulation

	Thoma method	Direct simulation
	A	A
	[m ²]	[m ²]
scenario a, the existing design with no discharge in the brook intake	49.7	0
		(Upstream surge tank not needed)
scenario b, the existing design with maximum possible discharge in the brook intake	49.7	0
		(Upstream surge tank not needed)
scenario c, a design without any brook intakes	49.7	15.9
scenario d, a design without the downstream surge tank	49.7	0
		(Upstream surge tank not needed)

As shown in Table 5-3, for each scenario, the analysis performed by means of the direct simulation allows to choose a smaller area, and, in most of the cases, to abolish the upstream surge tank. This will result in a considerable reduction in the construction costs of the power plant.

Another observation is that, since Thoma method does not take into consideration the influences on stability (the discharge in the brook intake, the presence of the brook intake and the presence of the downstream surge), the proposed area is the same for each scenario. On the other hand, the direct simulation considers all the influences and, for each scenario, offers a tailored proposal.

5.3.4 Minimum diameter required for stability, case with reduced $D_{\text{brook intake}}$

This section aims to find, for each of the mentioned scenarios, the diameter of the upstream surge tank that represents the threshold for stability for critical conditions.

As the previous paragraphs have shown, the brook intake has a strong stabilizing effect. Therefore, it has been chosen to reduce its diameter and input in the model, when required (scenario a, b and d), an equivalent diameter equal to 3.2 m. This choice can be justified by the will of testing very unfavourable conditions, to discuss whether stability would be possible also in this case.

- scenario a, the existing design with no discharge in the brook intake

The water level variation in the upstream and downstream surge tank for scenario a is shown, respectively, in Figure 5.25 and Figure 5.26.

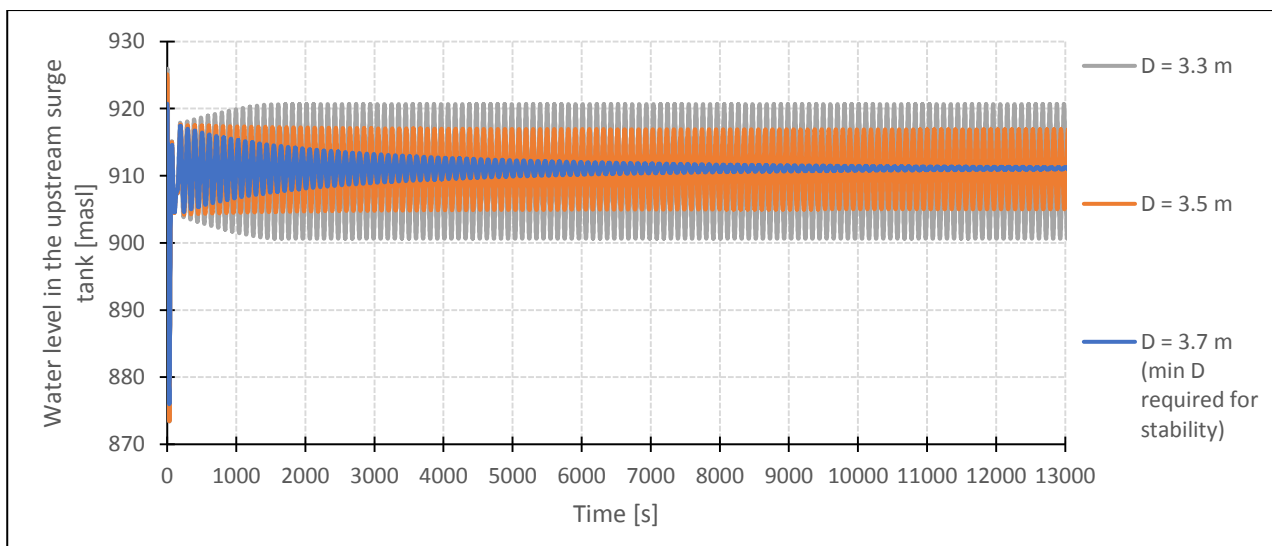


Figure 5.25 - scenario a: water level variation in the upstream surge tank, comparison of different $D_{\text{upstream surge shaft}}$ (case with reduced $D_{\text{brook intake}}$)

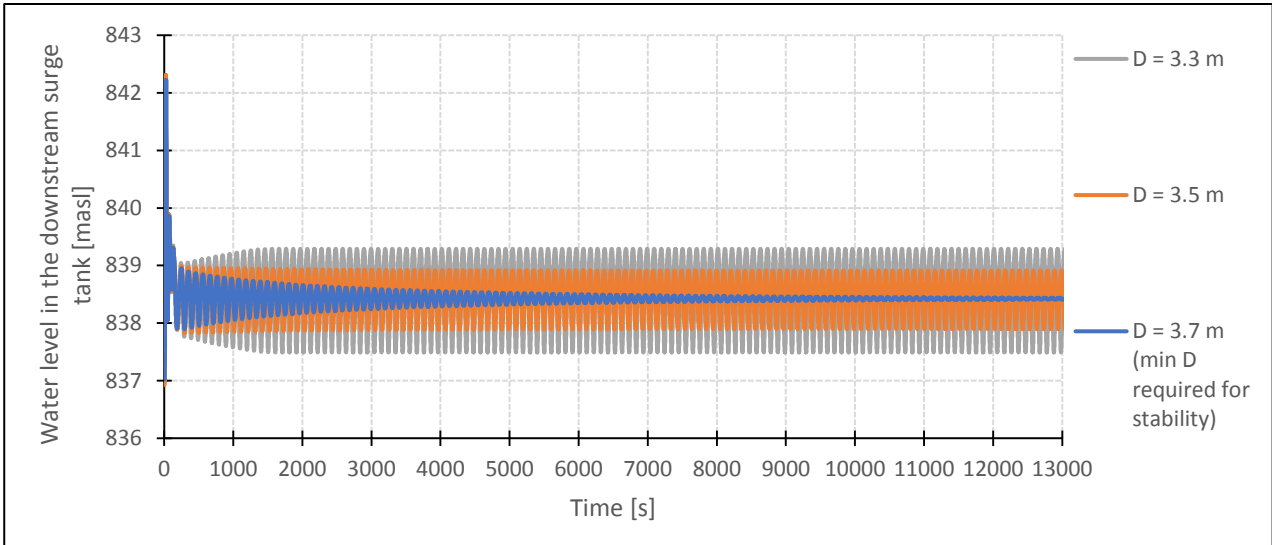


Figure 5.26 - scenario a: water level variation in the downstream surge tank, comparison of different $D_{upstream\ surge\ shaft}$ (case with reduced $D_{brook\ intake}$)

As shown by the above figures, when the discharge in the brook intake is equal $0\ m^3/s$, the minimum value for the upstream surge shaft diameter that guarantees the stability of the system is 3.7 m.

- scenario b: existing design with maximum possible discharge in the brook intake

The water level variation in the upstream and downstream surge tank for scenario b is shown, respectively, in Figure 5.27 and Figure 5.28.

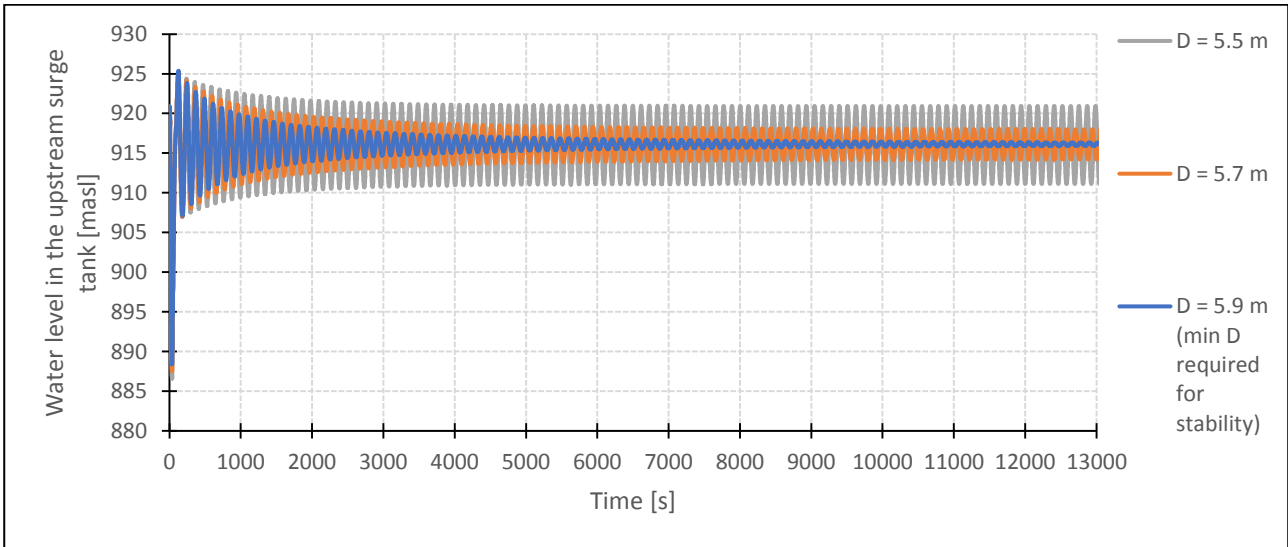


Figure 5.27 - scenario b: water level variation in the upstream surge tank, comparison of different $D_{upstream\ surge\ shaft}$ (case with reduced $D_{brook\ intake}$)

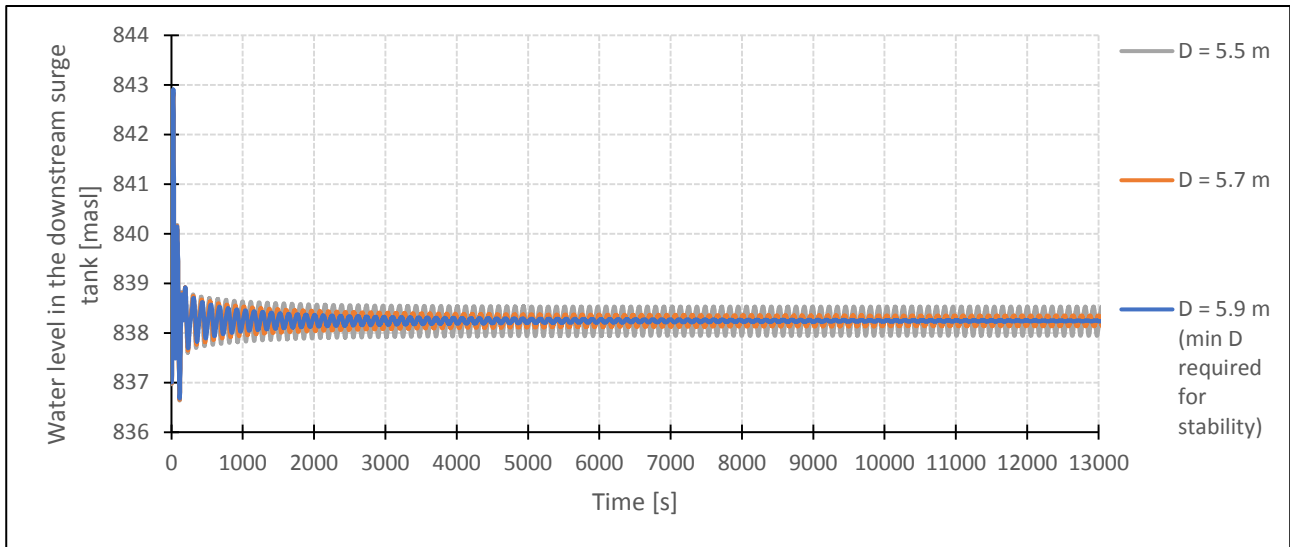


Figure 5.28 - scenario b: water level variation in the downstream surge tank, comparison of different $D_{\text{upstream surge shaft}}$ (case with reduced $D_{\text{brook intake}}$)

As shown by the above figures, 5.9 m is the minimum value for the upstream surge shaft diameter that guarantees the stability of the system, when the discharge in the brook intake is equal to the maximum possible value.

- scenario c: design without any brook intakes

This situation is the same as presented in scenario c in paragraph 5.3.2, as the brook intake is not present.

- scenario d, design without the downstream surge tank

The water level variation in the upstream surge tank for scenario d is shown in Figure 5.29.

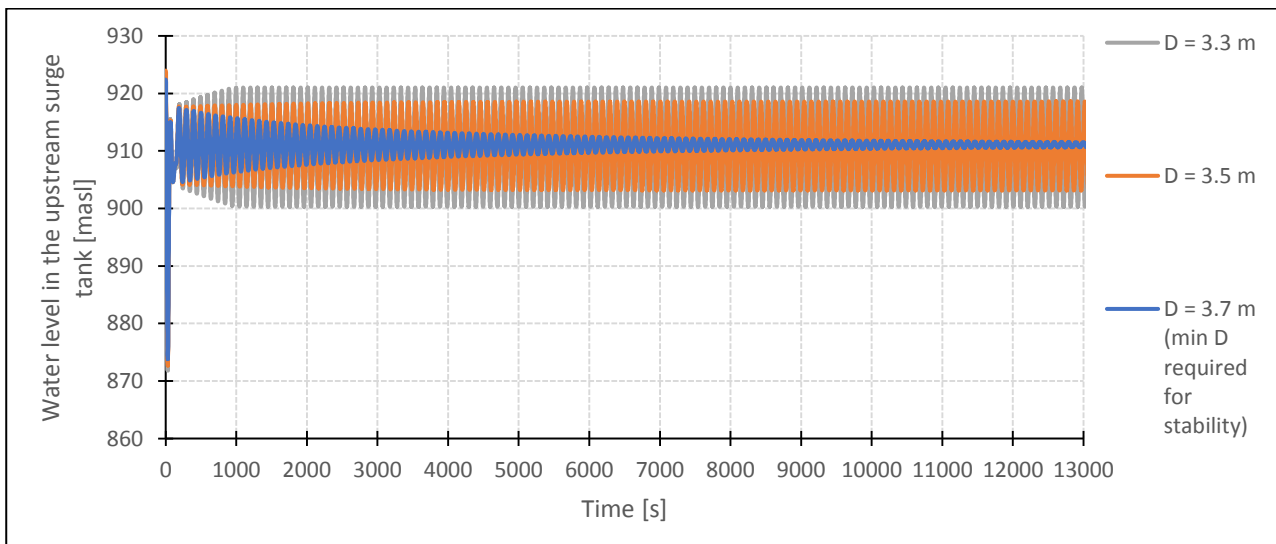


Figure 5.29 - scenario d: water level variation in the upstream surge tank, comparison of different $D_{\text{upstream surge shaft}}$ (case with reduced $D_{\text{brook intake}}$)

As shown in Figure 5.29, 3.7 m is the minimum diameter of the upstream surge shaft required for stability in case of absence of the downstream surge tank.

Table 5-4 below summarizes, for each scenario, the area of the upstream surge shaft that represents the threshold for stability.

Table 5-4 – Minimum area required for stability for each scenario

	Minimum diameter required for stability [m]	Minimum area required for stability [m ²]
scenario a, the existing design with no discharge in the brook intake	3.7	10.8
scenario b, the existing design with maximum possible discharge in the brook intake	5.9	27.3
scenario c, a design without any brook intakes	4.5	15.9
scenario d, a design without the downstream surge tank	3.7	10.8

By comparing the values resulting from the analysis, some considerations may be done on the three worst-case scenarios:

- scenario b

The largest destabilizing influence is exercised by the maximum discharge in the brook intake, as scenario b requires the largest upstream surge shaft area to guarantee stability. However, it is very seldom to have such a heavy discharge in the brook intake of Roskrepp power plant, and a more frequent value for $Q_{\text{brook intake}}$ is 1-2 m³/s.

- scenario c

The stabilizing influence of the brook intake discussed in paragraph 5.1.2, 5.2 and 5.3.2 is confirmed. In fact, when the brook intake is not present, a larger upstream surge shaft area is necessary to guarantee stability.

- scenario d

The same threshold value is obtained both for scenario a and d, as it happened in the case with the non-reduced value for $D_{\text{brook intake}}$ presented in paragraph 5.3.2. The lack of influence on system stability from the downstream surge tank is again confirmed.

6. Conclusions and suggestions for future work

In this chapter, conclusions are drawn from the results discussed in Chapter 5. Then, some suggestions for future work are proposed.

6.1 Conclusions

The thesis presents the method of direct simulation, performed in LVtrans, to investigate stability in power plants. The goal of the study was to suggest an alternative to Thoma method, currently adopted in most cases to identify the minimum size of surge tanks to guarantee stability.

The simulation results show that direct simulation allows to analyse the impact on stability of the brook intake and of the downstream surge tank. Taking into account the elements that affect stability, direct simulation provides a tailored surge shaft diameter for each case. On the contrary, Thoma method cannot account for these influences and suggests the same diameter for each case.

Moreover, when directly comparing the diameters selected by using the two methods, the ones selected with direct simulation result smaller for each analysed design scheme. In most cases, direct simulation shows even that the abolition of the upstream surge tank would be possible in terms of stability. This is particularly relevant for the hydropower industry, as smaller diameters or, even, the abolition of the upstream surge tank imply lower construction costs for the project.

In the analysis performed on the abolition of the upstream surge tank, it results that the brook intake, working as a surge shaft, could guarantee the stability of the system on its own. Therefore, if Roskrepp was a project at design stage, a scheme without the upstream surge tank would be recommended, after having verified that, in this case, the power plant would be safe against water hammer and overflow/air entrainment in the tunnel.

Considering the drawbacks, direct simulation requires the establishment, calibration, and validation of a numerical model: hence, it is data-demanding. For the analysed case study, this did not represent a problem, since data were available. However, as field measurement campaigns are time demanding and expensive, this may constitute a limit for the application of direct simulation.

To conclude, direct simulation appears a good alternative to Thoma method, as it provides a more accurate method to select the size of the surge tank and overcomes the problem of over-dimensioning. The data necessary to set up the model would be available as, when a new project is designed, the designers have control of what will be built. On the other hand, the calibration would be a challenge, as measurements are not available for new hydropower. Two options could be considered: either assuming that the model is correct, and performing a sensitivity analysis to assess the impact of uncertainty, or calibrating the numerical model against a physical one.

However, Thoma equation is still considered as an effective method for the early stages of the design, when few data are available.

6.2 Suggestions for future work

The suggestions for future work address two issues: how to improve the presented analysis and which aspects, according to the author, are worth exploring.

- how to improve the presented analysis

As mentioned many times, the focus of this thesis is on stability, therefore water hammer, maximum upsurge, and maximum downsurge have not been considered. Part of the role of a surge tank is to deal with these issues. Therefore, a more comprehensive analysis could be developed, to investigate if a surge tank whose size is found with direct simulation could be satisfying from all points of view.

Further work could be addressed to reduce the uncertainties affecting the model. First, as the discharge in the brook intake has a great influence on stability, an instrument to log its flow could be adopted. Second, since “as built” drawings are not available, they could be produced. In June 2018, a scanning campaign of the whole power plant was performed. This data will consistently reduce the uncertainty about the design of the plant and makes possible to build a more accurate model.

Moreover, as this study has been performed using a numerical model, it could be interesting to integrate it with a physical model, to exploit the advantages of hybrid modelling. So far, hybrid modelling has been used to study the mass oscillation amplitude. Adopting it to analyse stability may produce valuable results. Besides, a physical model could also provide more data for the verification of the numerical model for other kinds of transients, completing the analysis performed in this thesis.

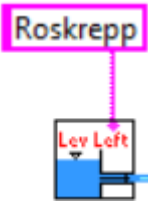
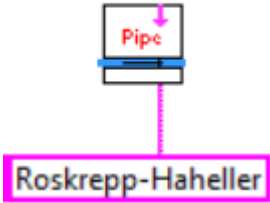
- aspects worth exploring

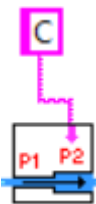

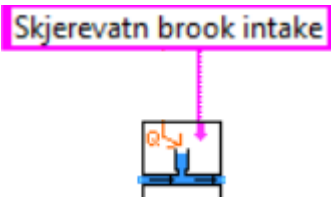
As usually done in practice, dampening time is not considered in this work as a critical factor for design. Hence, the minimum surge tank size for stability is recommended regardless of the dampening time. This choice is due to the fact that it is not proven yet if dampening time has an economic impact on the project. It would, therefore, be good to investigate whether the dampening time has a cost to the power plant. To assess that, analysis of the wear in the waterway and of the influence of mass oscillations on the wear would be needed.

Finally, a relevant aspect that deserves more in-depth analysis is the possibility to exploit brook intakes as surge shafts: in fact, when brook intakes prove they can effectively replace surge tanks, they guarantee a considerable reduction in the power plant construction costs.

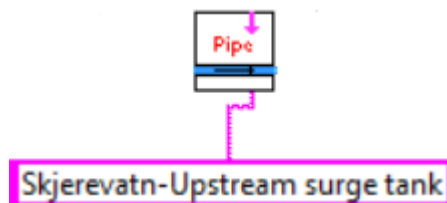
A. Annex

Annex 1: Parameters of the LVtrans model

Element	Symbol	Parameter	Description	Unit	Value
Upper reservoir		H0	Initial water level	[masl]	925.53
		Cvp	Concentrated loss coefficient for positive flow (water level in the reservoir increasing)	[-]	12000
		Cvm	Concentrated loss coefficient for negative flow (water level in the reservoir decreasing)	[-]	12000
Headrace tunnel from the upper reservoir to the Haheller adit		L	Length of the pipe	[m]	275
		D	Effective diameter	[m]	7.15
		f	Distributed friction coefficient	[-]	0.105
		Lambda	Elastic-dynamic friction constant	[-]	500000
		rho	Density of the water	[kg/m ³]	1000
		a	Celerity	[m/s]	1200
		Areal	Cross-sectional area	[m ²]	40
		P	Wetted perimeter	[m]	22.35
		Z0	Geodesic level for the left end	[masl]	890
		Z1	Geodesic level for the right end	[masl]	871
		Q0	Design discharge	[m ³ /s]	63
		H0	Initial pressure head	[m]	925.53

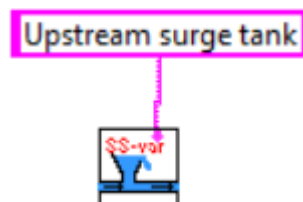
Contraction		Cvp	Concentrated loss coefficient for positive flow (water flowing downstream)	[-]	13000
		Cvm	Concentrated loss coefficient for negative flow (water flowing upstream)	[-]	13000
Headrace tunnel from the Haheller adit to the brook intake		L	Length of the pipe	[m]	1926
		D	Effective diameter	[m]	6.97
		f	Distributed friction coefficient	[-]	0.105
		Lambda	Elastic-dynamic friction constant	[-]	500000
		rho	Density of the water	[kg/m ³]	1000
		a	Celerity	[m/s]	1200
		Areal	Cross-sectional area	[m ²]	38
		P	Wetted perimeter	[m]	21.84
		Z0	Geodesic level for the left end	[masl]	871
		Z1	Geodesic level for the right end	[masl]	874.5
		Q0	Design discharge	[m ³ /s]	63
		H0	Initial pressure head	[m]	925.53
		Brook intake		H0	Initial water level
D	Diameter			[m]	18
f	Distributed friction coefficient			[-]	0.05
Cvp	Concentrated loss coefficient for positive flow (water flowing downstream)			[-]	35

Headrace tunnel
from the brook
intake to the
upstream surge
tank



Cvm	Concentrated loss coefficient for negative flow (water flowing upstream)	[-]	100000
L	Length of the pipe	[m]	970
D	Effective diameter	[m]	7.15
f	Distributed friction coefficient	[-]	0.105
Lambda	Elastic-dynamic friction constant	[-]	500000
rho	Density of the water	[kg/m ³]	1000
a	Celerity	[m/s]	1200
Areal	Cross-sectional area	[m ²]	40
P	Wetted perimeter	[m]	22.35
Z0	Geodesic level for the left end	[masl]	874.5
Z1	Geodesic level for the right end	[masl]	865
Q0	Design discharge	[m ³ /s]	63
H0	Initial pressure head	[m]	925.53
Cvp	Concentrated loss coefficient for positive flow (water level in the surge tank increasing)	[-]	100
Cvm	Concentrated loss coefficient for negative flow (water level in the surge tank decreasing)	[-]	100
H0	Initial pressure head	[m]	925.53
L-weir	Level of the weir (upper boundary)	[masl]	942

Upstream surge
tank

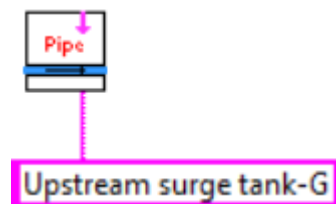


L0	Height from the geodesic level of the headrace tunnel of the cross-sectional area A0	[m]	0
L1	Height from the geodesic level of the headrace tunnel of the cross-sectional area A1	[m]	5
L2	Height from the geodesic level of the headrace tunnel of the cross-sectional area A2	[m]	7
L3	Height from the geodesic level of the headrace tunnel of the cross-sectional area A3	[m]	14
L4	Height from the geodesic level of the headrace tunnel of the cross-sectional area A4	[m]	20
L5	Height from the geodesic level of the headrace tunnel of the cross-sectional area A5	[m]	20.01
L6	Height from the geodesic level of the headrace tunnel of the cross-sectional area A6	[m]	25
L7	Height from the geodesic level of the headrace tunnel	[m]	69.99

of the cross-sectional area
A7

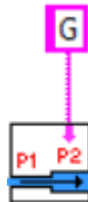
L8	Height from the geodesic level of the headrace tunnel of the cross-sectional area A8	[m]	70
L9	Height from the geodesic level of the headrace tunnel of the cross-sectional area A9	[m]	76
A0	Cross-sectional area at L0	[m ²]	42
A1	Cross-sectional area at L1	[m ²]	367.8
A2	Cross-sectional area at L2	[m ²]	325.8
A3	Cross-sectional area at L3	[m ²]	776
A4	Cross-sectional area at L4	[m ²]	450
A5	Cross-sectional area at L5	[m ²]	28
A6	Cross-sectional area at L6	[m ²]	55
A7	Cross-sectional area at L7	[m ²]	55
A8	Cross-sectional area at L8	[m ²]	666
A9	Cross-sectional area at L9	[m ²]	666
L	Length of the pipe	[m]	341
D	Effective diameter	[m]	7.15
f	Distributed friction coefficient	[-]	0.105
Lambda	Elastic-dynamic friction constant	[-]	500000
rho	Density of the water	[kg/m ³]	1000
a	Celerity	[m/s]	1200

Headrace tunnel from the upstream surge tank to the contraction G

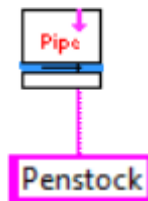


Areal	Cross-sectional area	[m ²]	40
P	Wetted perimeter	[m]	22.35
Z0	Geodesic level for the left end	[masl]	865
Z1	Geodesic level for the right end	[masl]	842
Q0	Design discharge	[m ³ /s]	67
H0	Initial pressure head	[m]	925.53
Cvp	Concentrated loss coefficient for positive flow (water flowing downstream)	[-]	13000
Cvm	Concentrated loss coefficient for negative flow (water flowing upstream)	[-]	13000
L	Length of the pipe	[m]	92
D	Effective diameter	[m]	4
f	Distributed friction coefficient	[-]	0.005
Lambda	Elastic-dynamic friction constant	[-]	500000
rho	Density of the water	[kg/m ³]	1000
a	Celerity	[m/s]	1200
Areal	Cross-sectional area	[m ²]	12.56
P	Wetted perimeter	[m]	12.56
Z0	Geodesic level for the left end	[masl]	842
Z1	Geodesic level for the right end	[masl]	822
Q0	Design discharge	[m ³ /s]	67
H0	Initial pressure head	[m]	925.53

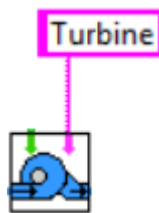
Contraction



Penstock

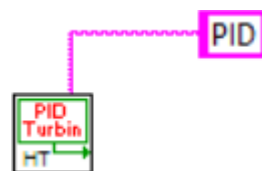


Francis turbine



Qr	Design discharge	[m ³ /s]	67
Hr	Design head	[m]	83
Hr_design	Design head for fine tuning	[m]	83
Nr	Angular velocity	[RPM]	250
Tr	Torque	[Nm]	1975358
Er	Electrical torque	[Nm]	1975358
a1r(deg)	Design angle of the guide vanes	[degrees]	19.9
b1r(deg)	Design angle of the turbine	[degrees]	73.1
r1	Design inlet radius	[m]	1.126
r2	Design outlet radius	[m]	1.187
Ta	Acceleration time of the rotational masses	[s]	6
Twt	Inflow time of masses of water	[s]	0.1
eta_h	Hydraulic efficiency	[-]	0.94
eta_r	Total efficiency	[-]	0.95
Nturb	Number of turbines	[-]	1
Poles	Number of poles	[-]	24

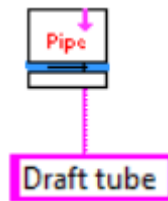
PID governor



Pr	Power at BEP	[MW]	51.7
Nr	Angular velocity	[RPM]	250
SP_Power	Initial power	[MW]	0
P_n_grid	Proportional constant when running on grid	[-]	1
Ti_n_grid	Integrative constant when running on grid	[-]	10
Td_n_grid	Derivative constant when running on grid	[-]	0
P_n_island	Proportional constant when running isolated	[-]	1

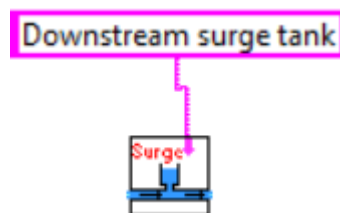
Ti_n_island	Integrative constant when running isolated	[-]	7
Td_n_island	Derivative constant when running isolated	[-]	0
T_close_hi	Closing time from full open	[-]	6
T_close_low	Closing time	[-]	6
T_open_hi	Opening time to full open	[-]	10
T_open_low	Opening time to full open	[-]	10
L	Length of the pipe	[m]	24
D	Effective diameter	[m]	2.85
f	Distributed friction coefficient	[-]	0.008

Draft tube



Lambda	Elastic-dynamic friction constant	[-]	500000
rho	Density of the water	[kg/m ³]	1000
a	Celerity	[m/s]	1200
Areal	Cross-sectional area	[m ²]	6.4
P	Wetted perimeter	[m]	9
Z0	Geodesic level for the left end	[masl]	822
Z1	Geodesic level for the right end	[masl]	813.5
Q0	Design discharge	[m ³ /s]	67
H0	Initial pressure head	[m]	833.42

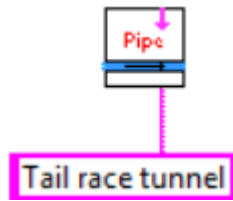
Downstream surge tank



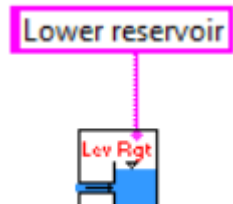
H0	Initial water level	[masl]	833.42
D	Diameter	[m]	10.3
f	Distributed friction coefficient	[-]	0.05
Cvp	Concentrated loss coefficient for positive flow (water)	[-]	1000

		flowing downstream)		
		Cvm	Concentrated loss coefficient for negative flow (water flowing upstream)	[-] 1000
		L	Length of the pipe	[m] 300
		D	Effective diameter	[m] 6.97
		f	Distributed friction coefficient	[-] 0.15
		Lambda	Elastic-dynamic friction constant	[-] 500000
		rho	Density of the water	[kg/m ³] 1000
		a	Celerity	[m/s] 1200
		Areal	Cross-sectional area	[m ²] 38.16
		P	Wetted perimeter	[m] 21.93
		Z0	Geodesic level for the left end	[masl] 813.5
		Z1	Geodesic level for the right end	[masl] 825
		Q0	Design discharge	[m ³ /s] 67
		H0	Initial pressure head	[m] 833.42
		H0	Initial water level	[masl] 833.43
		Cvp	Concentrated loss coefficient for positive flow (water level in the reservoir increasing)	[-] 12000
		Cvm	Concentrated loss coefficient for negative flow (water level in the reservoir decreasing)	[-] 12000

Tail race tube



Lower reservoir



Annex 2: Procedure of the calibration of transient operation

In the calibration process, the simulations are performed inputting different values for the parameters, with the aim to find the set of values that gives the best possible fit with the measurements.

In this section, the influence of each calibrated parameter is investigated, in order to motivate the choice of the values presented in paragraph 4.3.2.

During the shutdown, the turbine opening follows the pattern shown in Figure A.1.

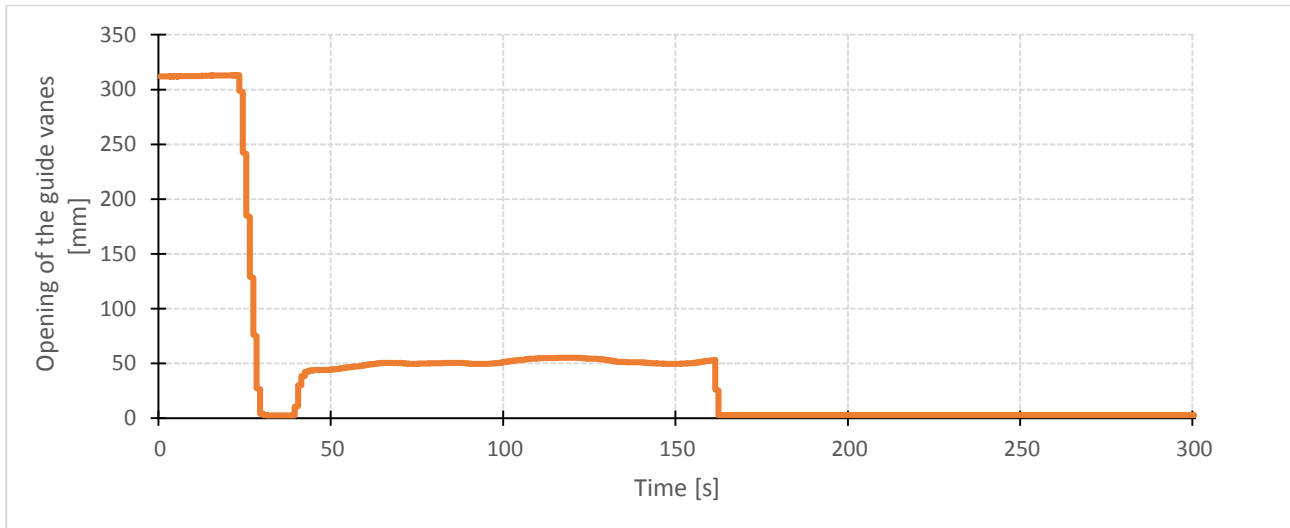


Figure A.1 - Turbine opening during the shutdown

First, it is completely closed in 6 seconds and stays shut for 10 seconds. After that, the turbine slightly reopens. At the end, the final and complete closure takes place, as the ball valve closes (around second 160th).

When a shutdown is simulated in LVtrans, the turbine opening does not follow this pattern. Therefore, the calibration is performed on the time interval from 0 to 150 seconds.

A2.1 Upstream the turbine

Figure A.2 shows the static head in front of the turbine during the shutdown, based on the measurements.

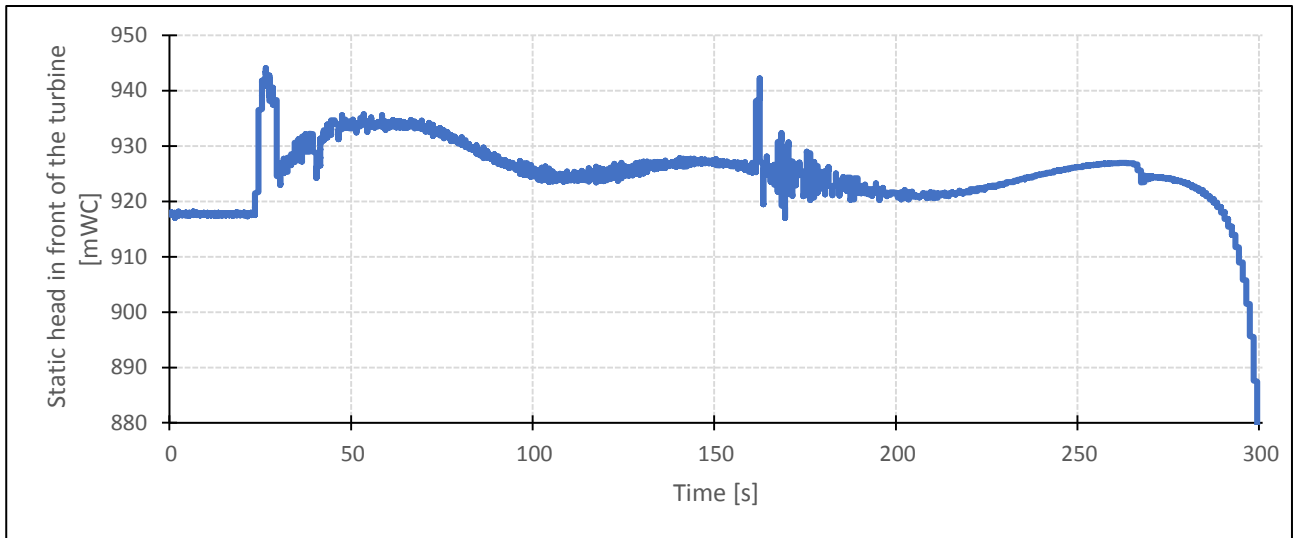


Figure A.2 - Measured static head in front of the turbine

A2.1.1 Calibration of the parameters of the brook intake

- $D_{\text{equivalent}}$

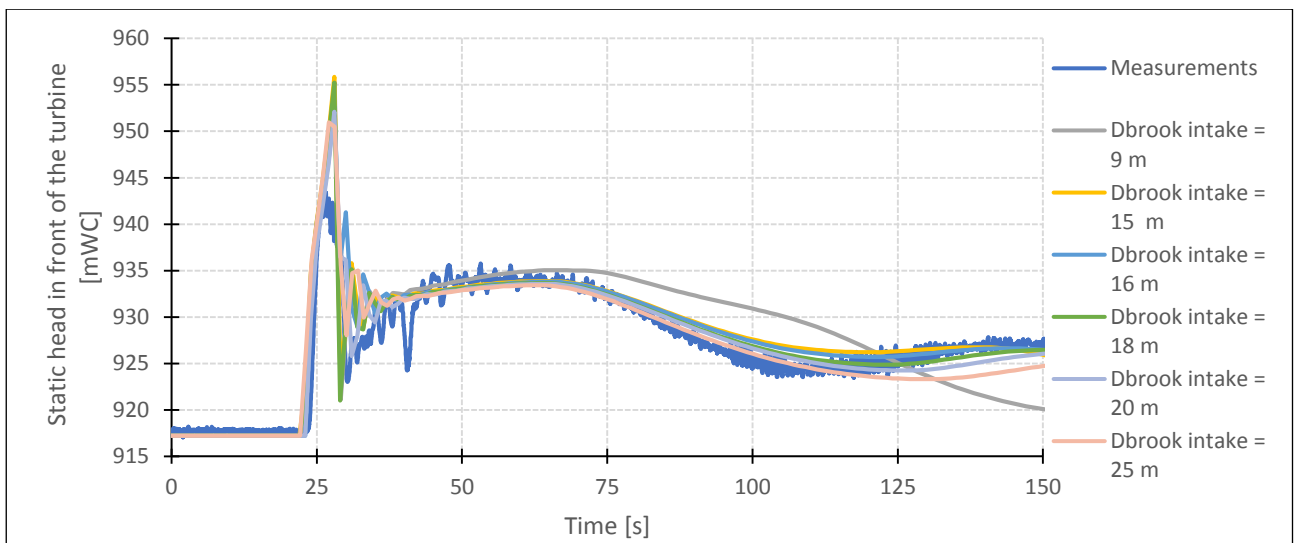


Figure A.3 - Static head in front of the turbine: measurements and simulations for different brook intake diameters

The best possible fit is guaranteed by $D_{\text{equivalent}} = 18 \text{ m}$, as a shown in Figure A.4 below.

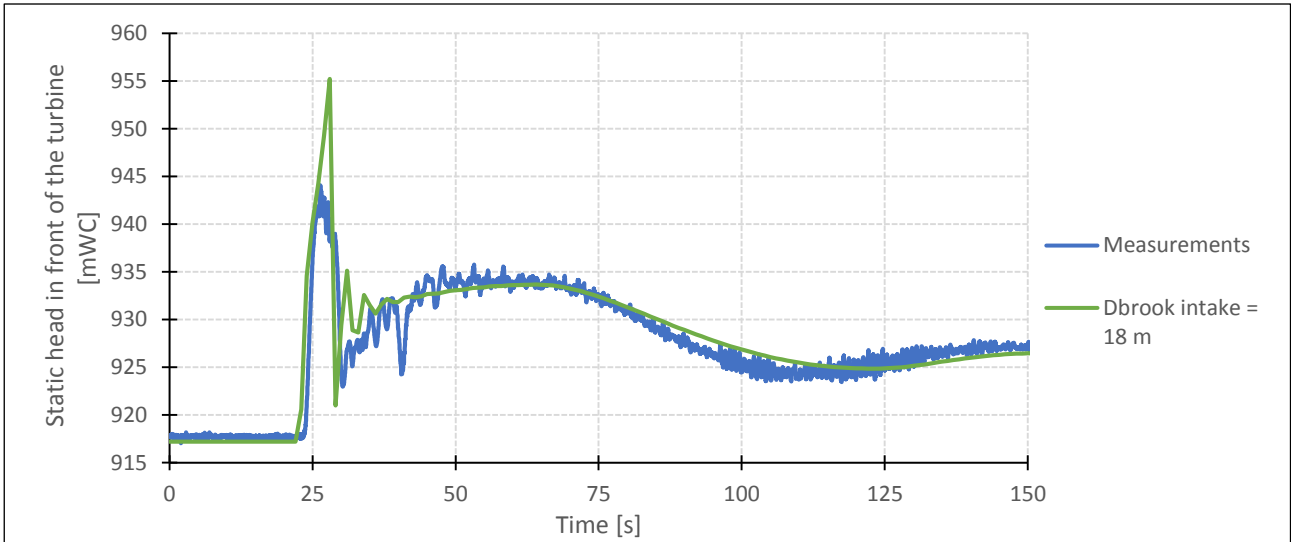


Figure A.4 - Static head in front of the turbine: measurements and model calibrated for the brook intake diameter

- C_{vp}

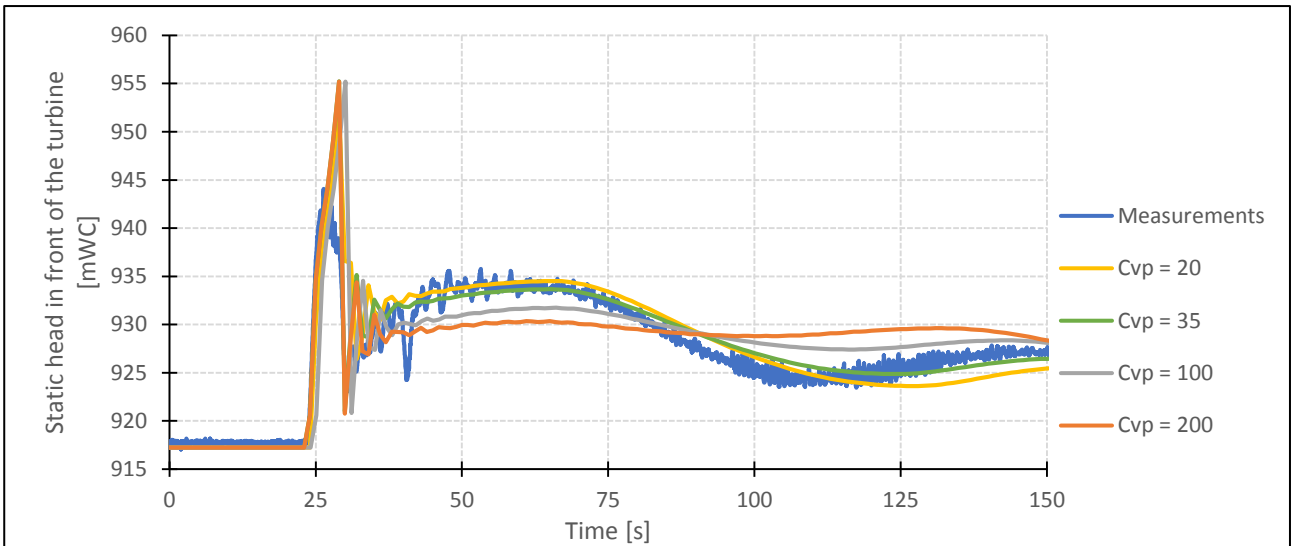


Figure A.5 - Static head in front of the turbine: measurements and simulations for different loss coefficients C_{vp} for the brook intake

The best possible fit is obtained for $C_{vp} = 35$, as a shown in Figure A.6 below.

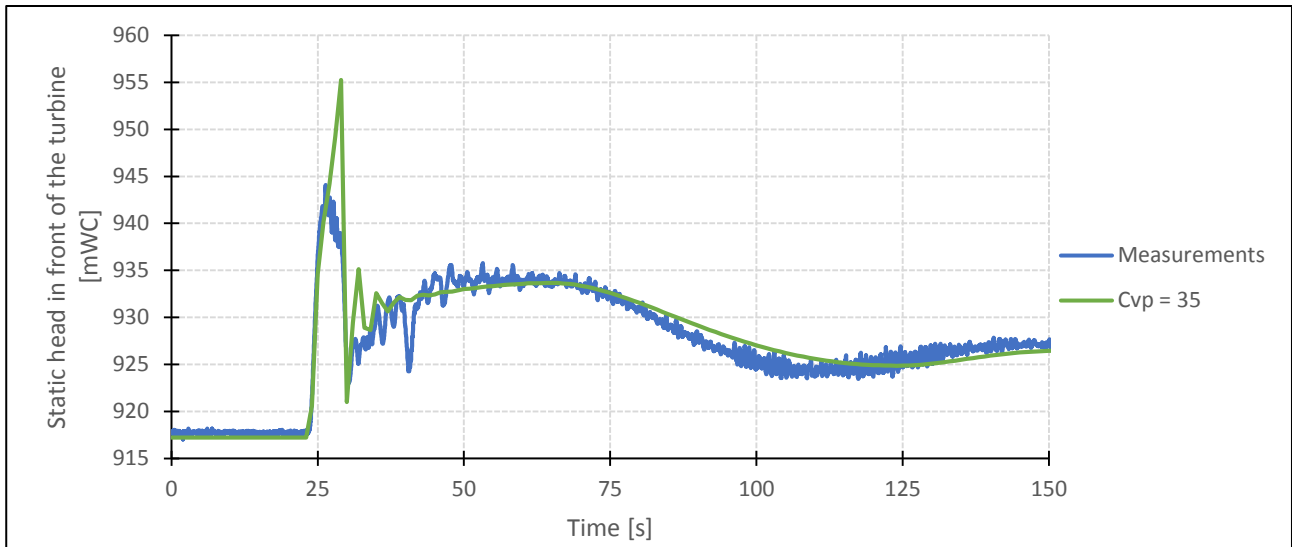


Figure A.6 - Static head in front of the turbine: measurements and model calibrated for the loss coefficient C_{vp} for the brook intake

- C_{vm}

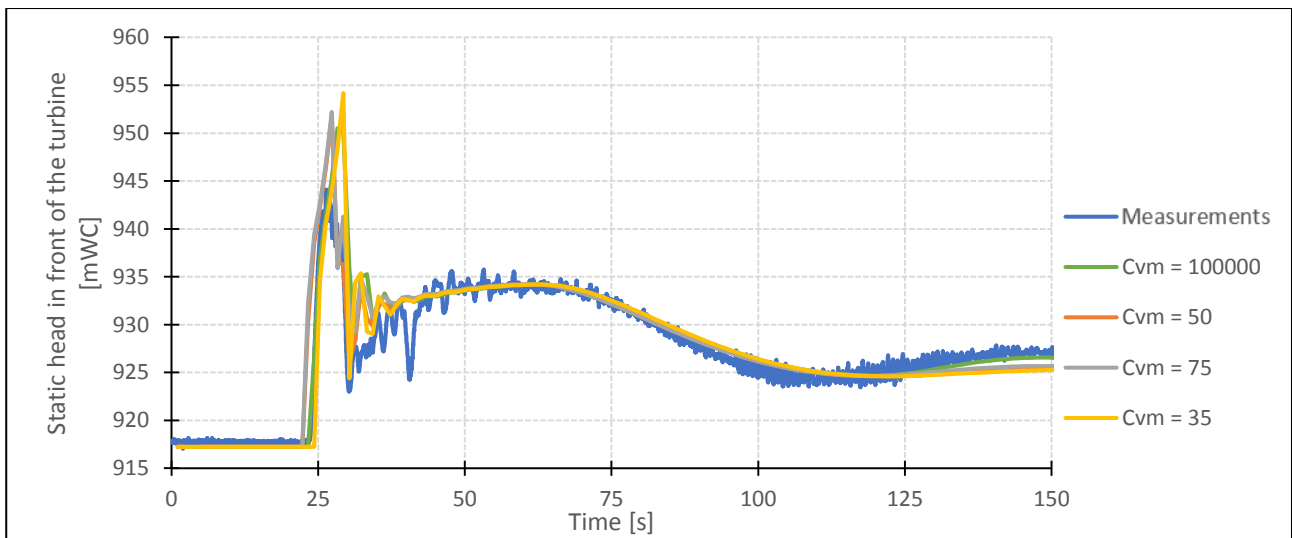


Figure A.7 - Static head in front of the turbine: measurements and simulations for different loss coefficients C_{vm} for the brook intake

Figure A.7 shows that for lower values of C_{vm} , the mass oscillations are not well-simulated after second 125th.

So, the best possible fit is obtained for $C_{vm} = 100000$, as shown in Figure A.8 below.

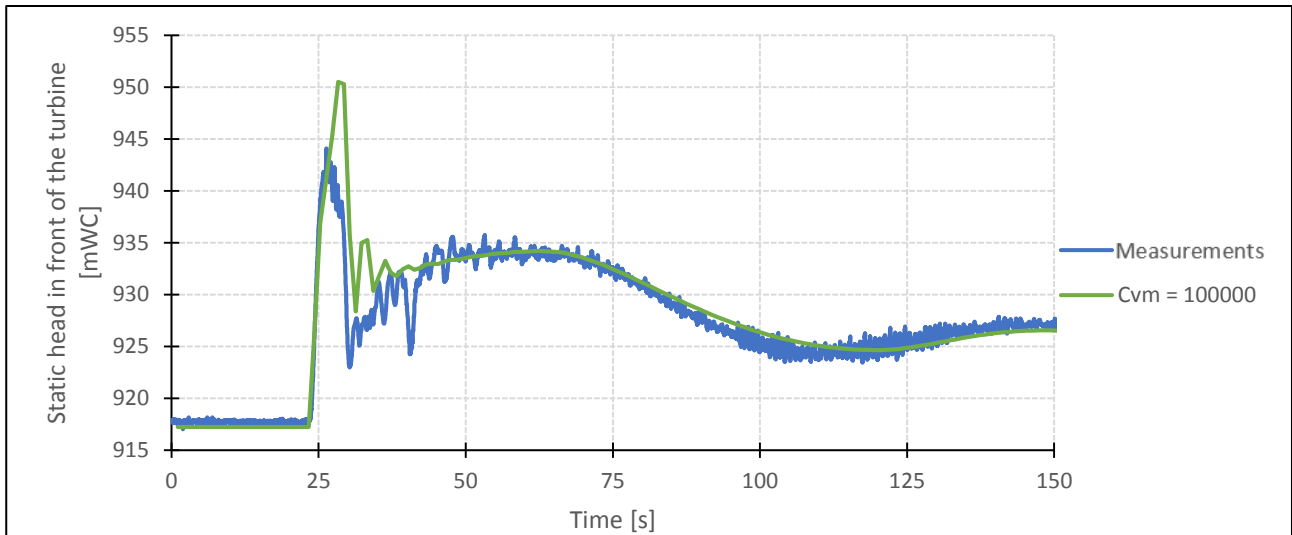


Figure A.8 - Static head in front of the turbine: measurements and model calibrated for the loss coefficient C_{vm} for the brook intake

A2.1.2 Calibration of the parameters of the upstream surge tank

- A

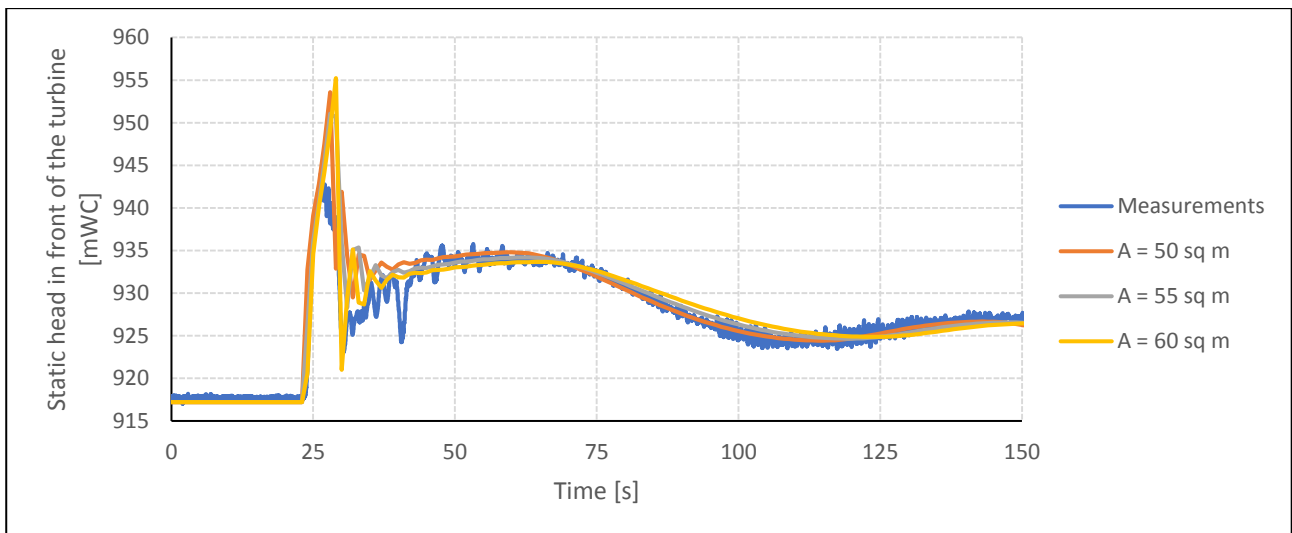


Figure A.9 - Static head in front of the turbine: measurements and simulations for different areas of the vertical shaft of the upstream surge tank

$A = 55 \text{ m}^2$ guarantees the best possible fit, as shown in Figure A.10 below.

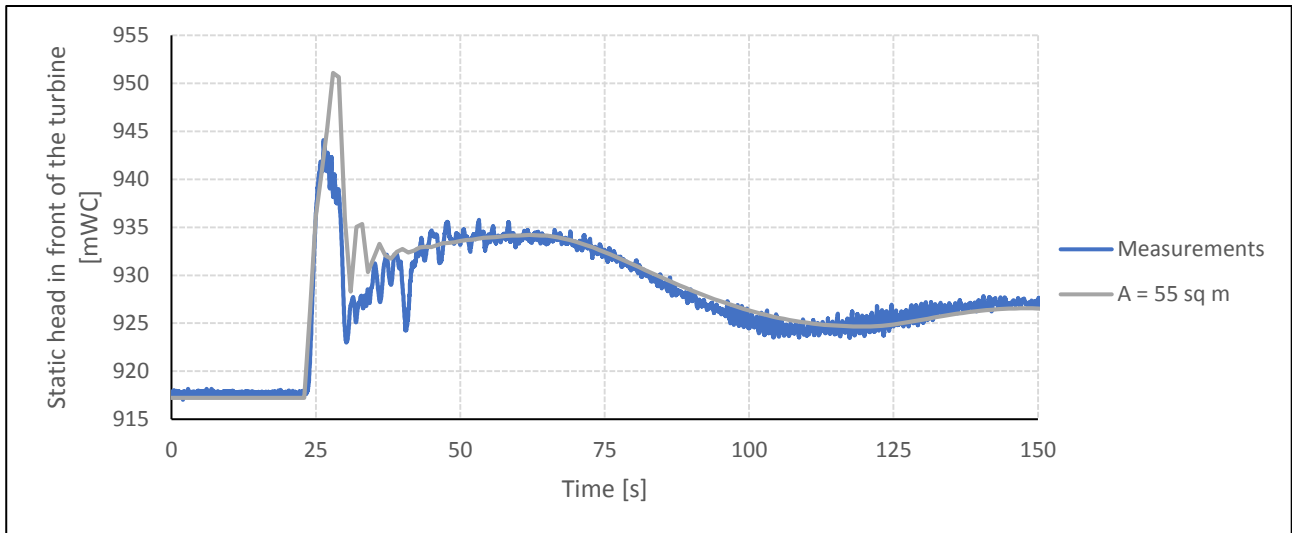


Figure A.10 - Static head in front of the turbine: measurements and model calibrated for the area of the vertical shaft of the upstream surge tank

- Cvp and Cvm

In this case, the value of Cvm does not influence particularly the result, reason why it is simply chosen equal to the value of Cvp.

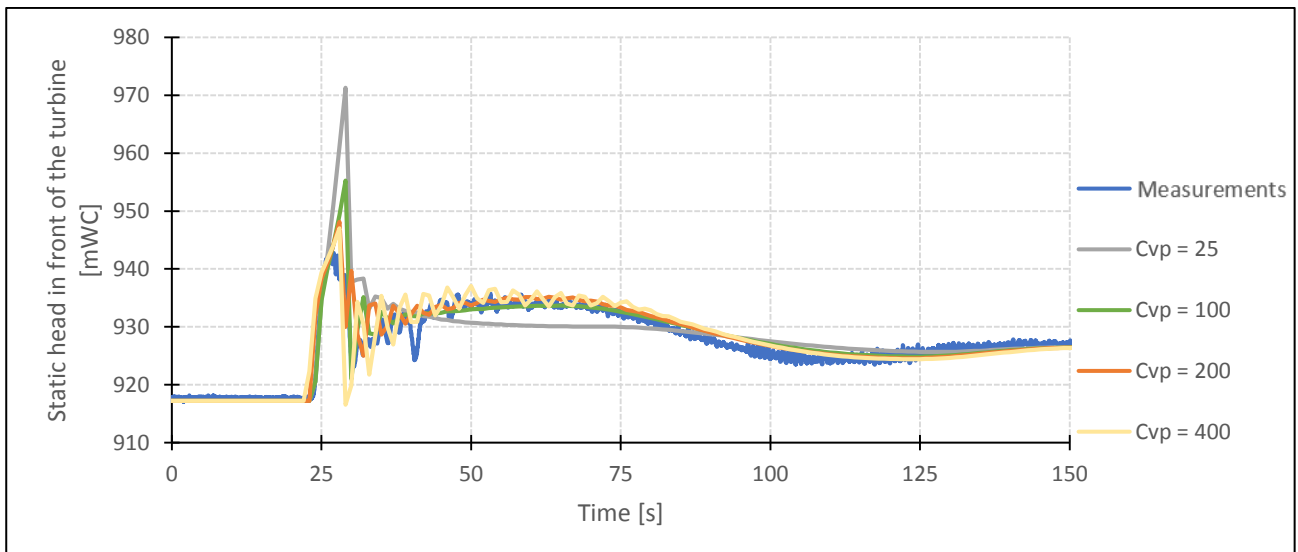


Figure A.11 - Static head in front of the turbine: measurements and simulations for different loss coefficients Cvp for the upstream surge tank

The best possible fit is guaranteed by $C_{vp} = 100$, as a shown in the Figure A.12 below.

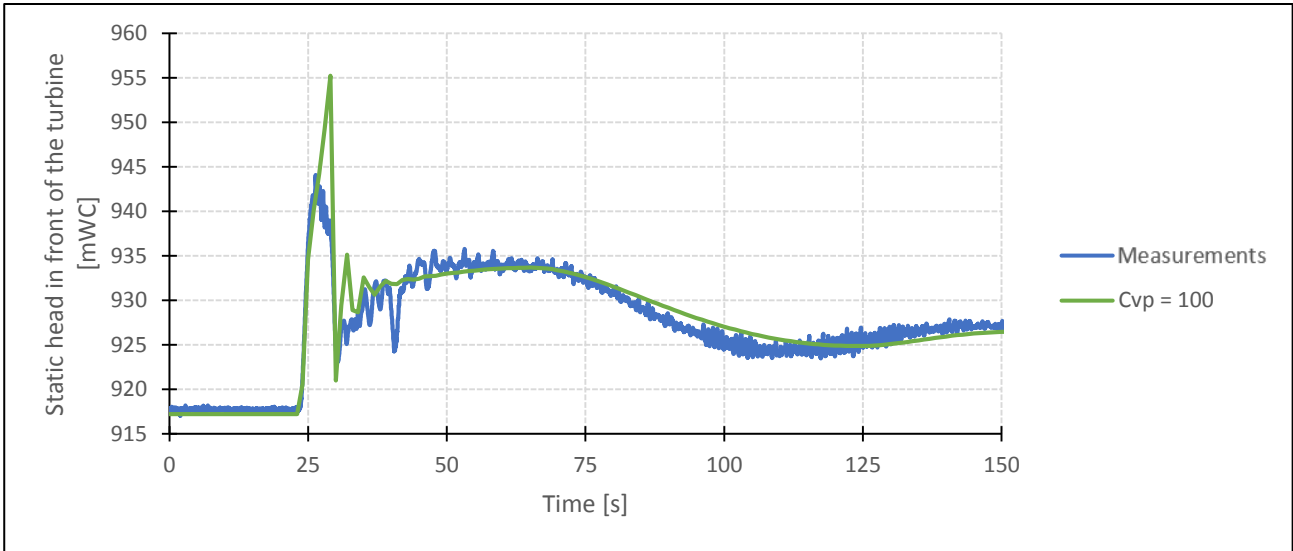


Figure A.12 - Static head in front of the turbine: measurements and model calibrated for the loss coefficient C_{vp} for the upstream surge tank

A2.2 Downstream the turbine

Figure A.13 shows the static head downstream the turbine during the shutdown based on the measurements, adjusted as explained in paragraph 4.3.2.

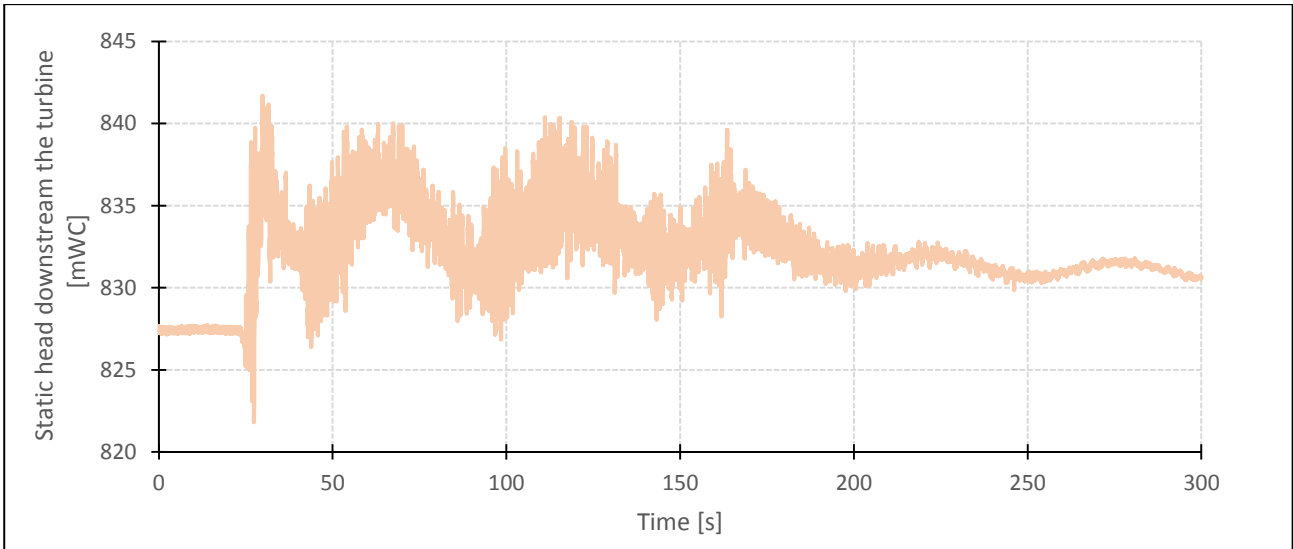


Figure A.13 - Adjusted hydraulic head downstream the turbine

A2.2.1 Calibration of the parameters of the downstream surge tank

- D

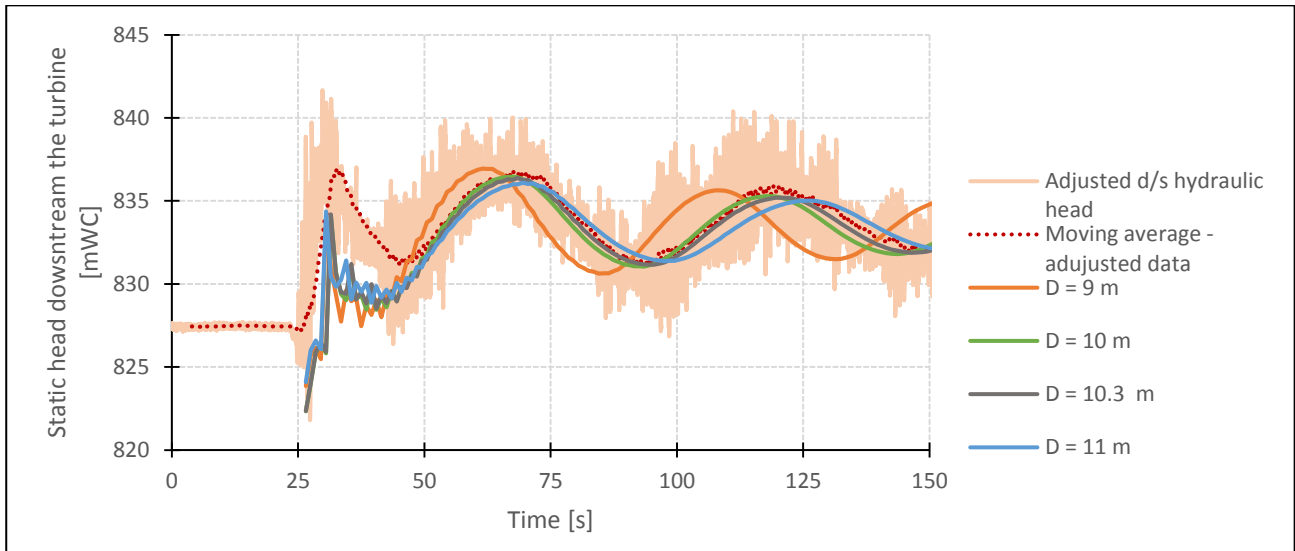


Figure A.14 - Static head downstream the turbine: measurements and simulations for different diameters of the downstream surge tank

As shown in Figure A.15 below, the best possible fit is obtained for $D = 10.3$ m.

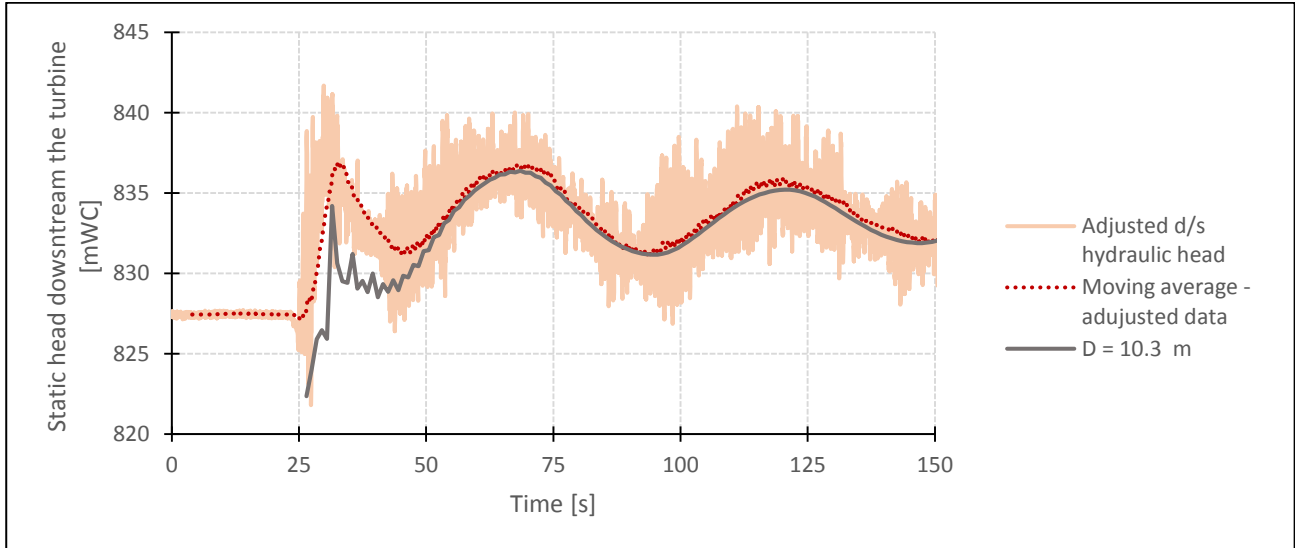


Figure A.15 - Static head downstream the turbine: measurements and model calibrated for the diameter of the downstream surge tank

▪ C_vp and C_vm

The calibration of these two coefficients is performed admitting that they have the same value.

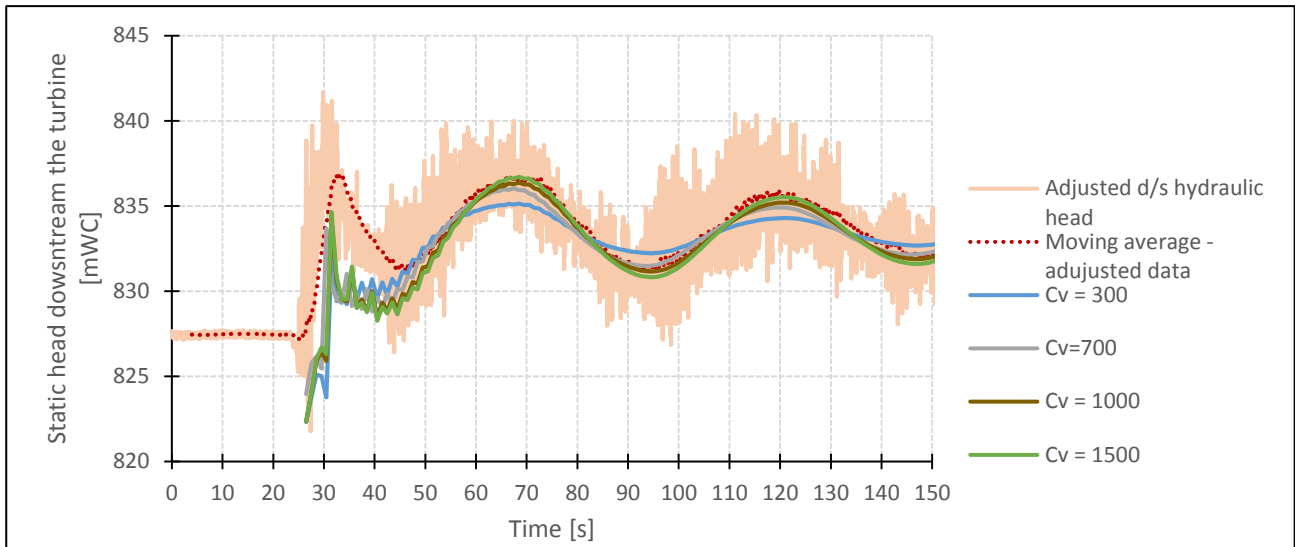


Figure A.16 - Static head in downstream the turbine: measurements and simulations for different loss coefficients C_{vp} and C_{vm} for the downstream, surge tank

The best possible fit is obtained with $C_{vp} = C_{vm} = 1000$, as shown in the Figure A.17 below.

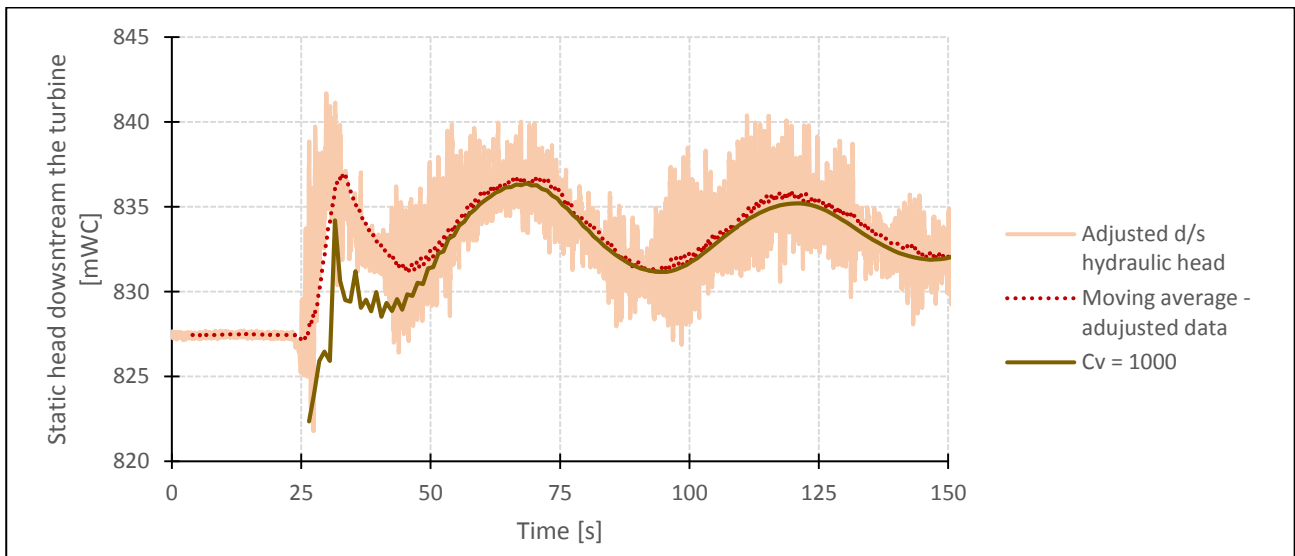


Figure A.17 - Static head downstream the turbine: measurements and model calibrated for the loss coefficients C_{vp} and C_{vm} for the downstream surge tank

Annex 3: Comparison between Thoma area and actual size of the upstream surge tank

This section shows the comparison between the response from the model where, for the upstream surge tank, Thoma area is implemented and the one where the actual design (the one from the drawings) is implemented.

- scenario a, the existing design with no discharge in the brook intake

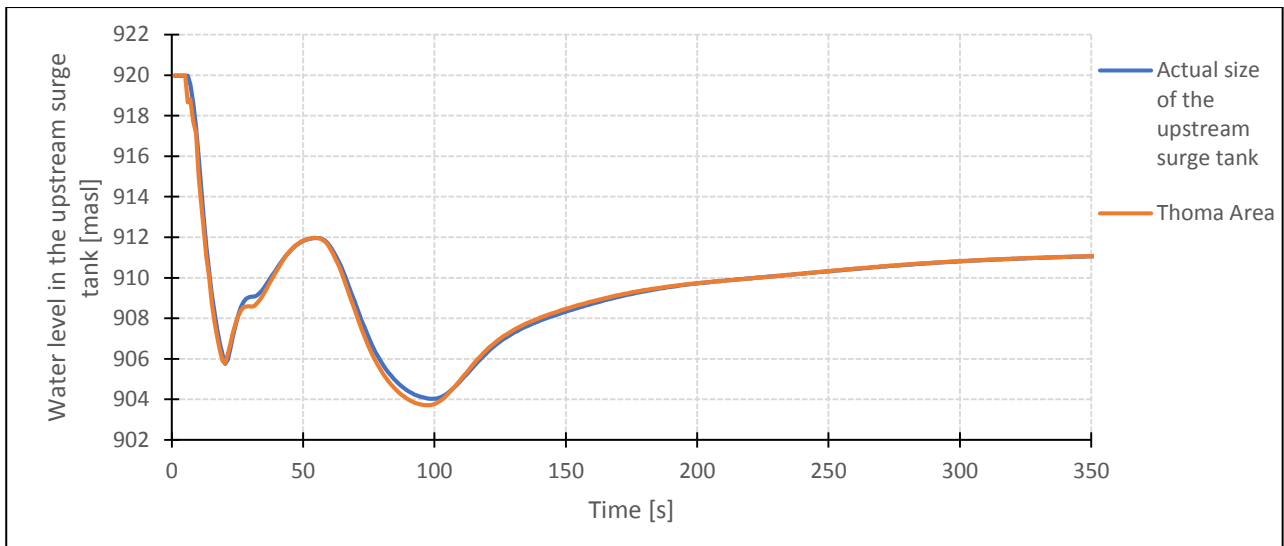


Figure A.18 - scenario a: water level variation in the upstream surge tank, comparison between Thoma area and actual size of the upstream surge tank

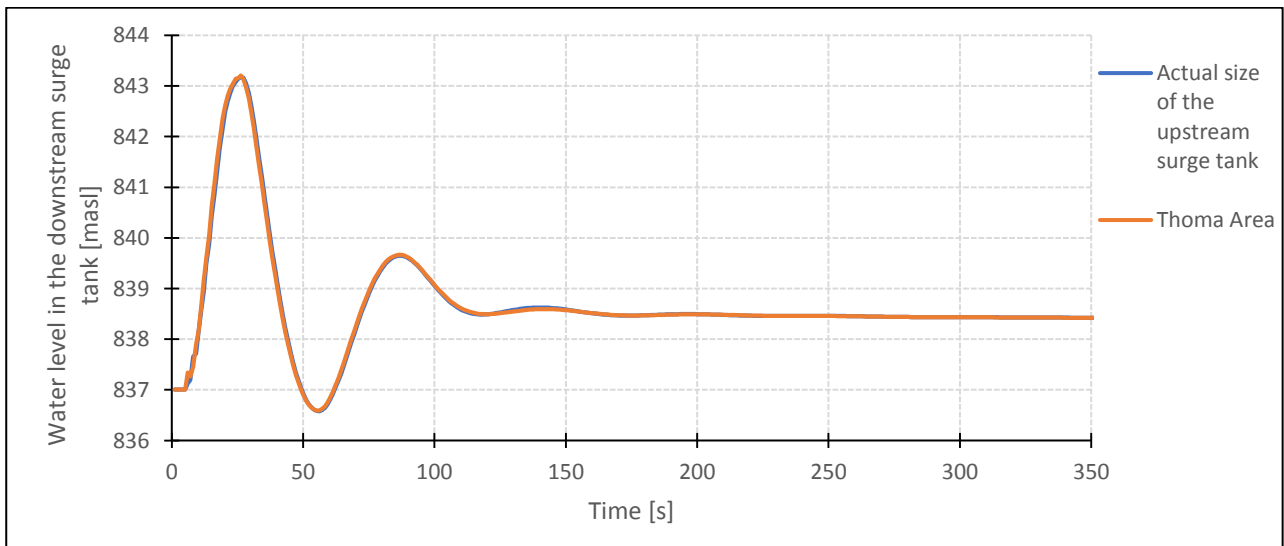


Figure A.19 - scenario a: water level variation in the downstream surge tank, comparison between Thoma area and actual size of the upstream surge tank

- scenario b, the existing design with maximum possible discharge in the brook intake

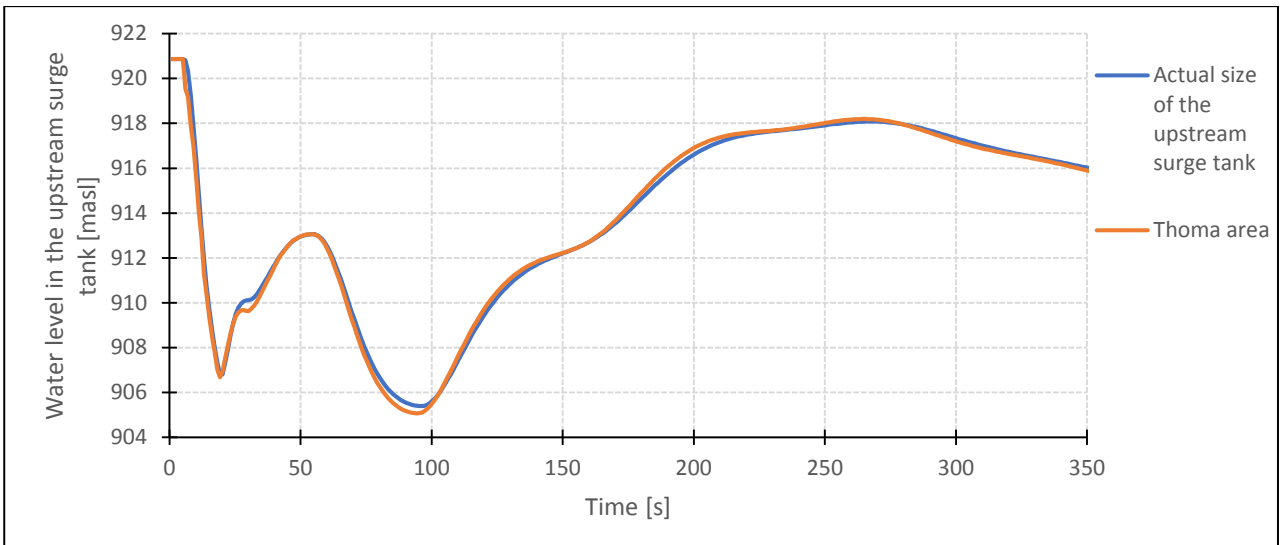


Figure A.20 - scenario b: water level variation in the upstream surge tank, comparison between Thoma area and actual size of the upstream surge tank

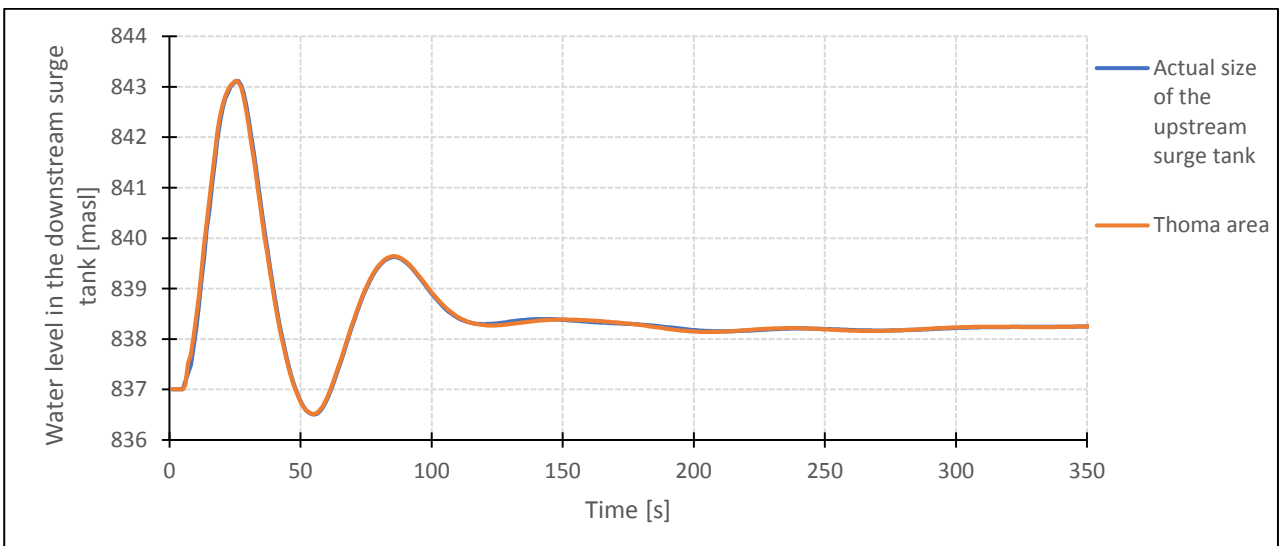


Figure A.21 - scenario b: water level variation in the downstream surge tank, comparison between Thoma area and actual size of the upstream surge tank

- scenario c, design without any brook intakes

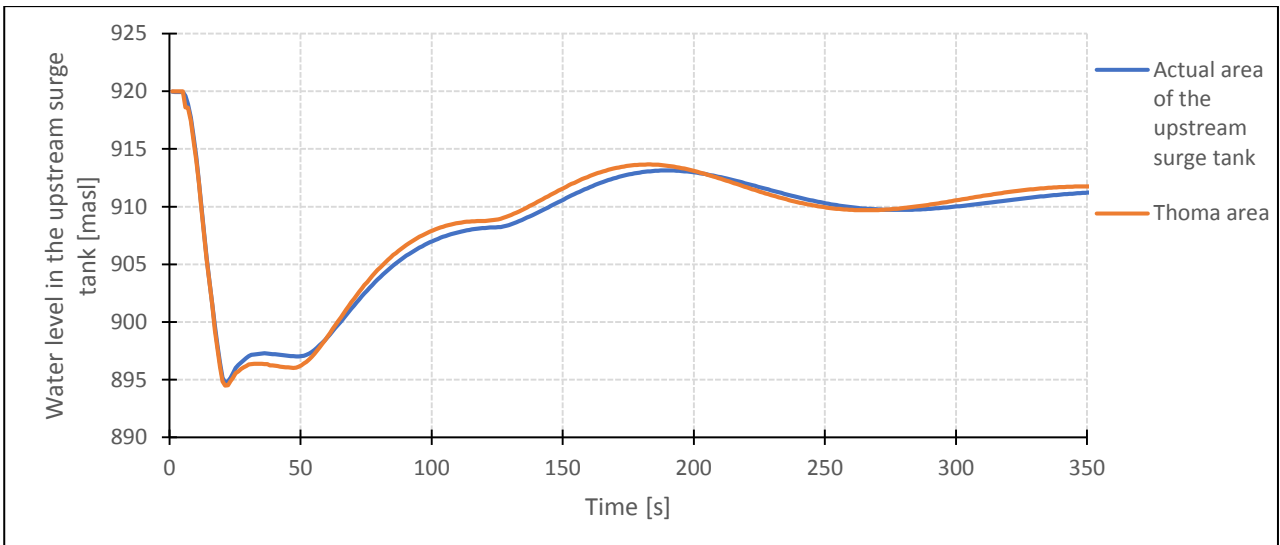


Figure A.22 - scenario c: water level variation in the upstream surge tank, comparison between Thoma area and actual size of the upstream surge tank

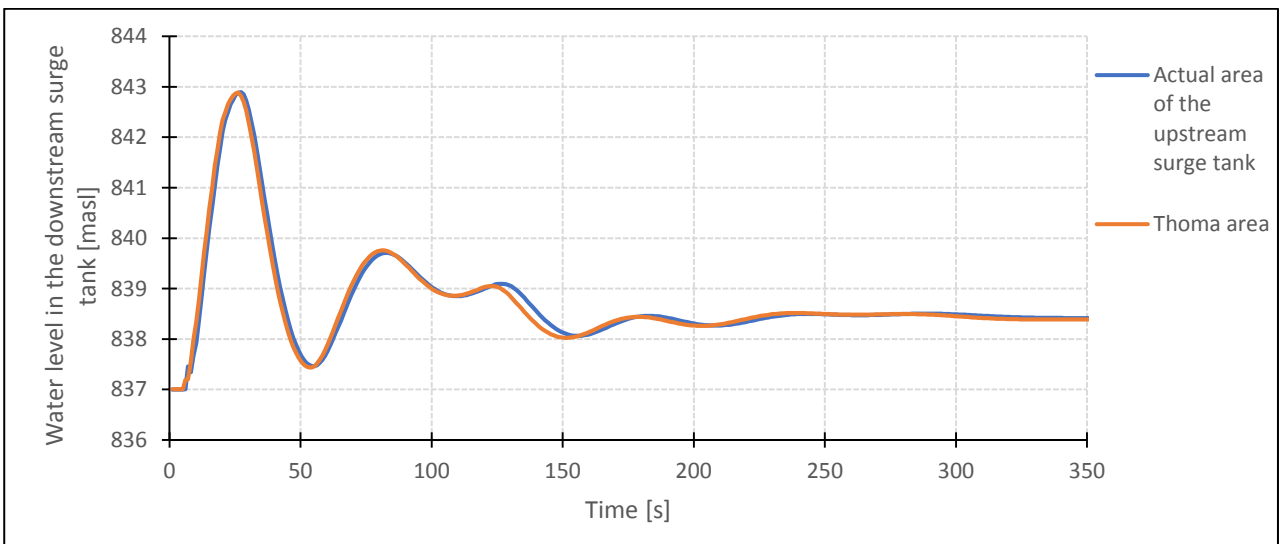


Figure A.23 - scenario c: water level variation in the downstream surge tank, comparison between Thoma area and actual size of the upstream surge tank

- scenario d, design without the downstream surge tank

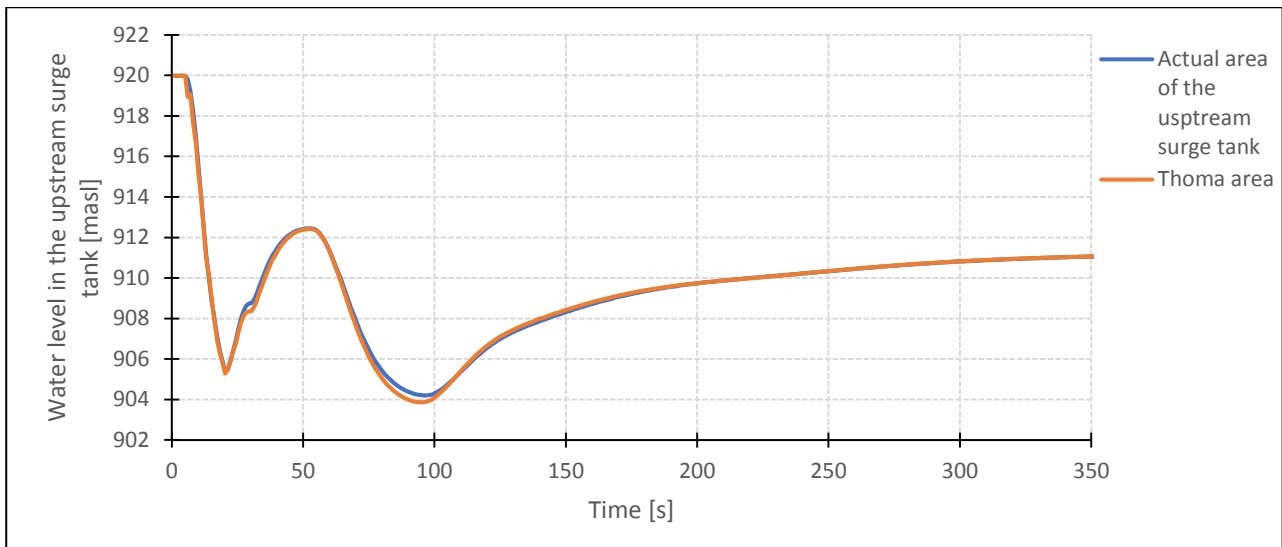


Figure A.24 - scenario d: water level variation in the upstream surge tank, comparison between Thoma area and actual size of the upstream surge tank

Bibliography

- Arredi, F., (1947), *Lo studio della stabilità dei sistemi adduttori-generatori degli impianti idroelettrici col criterio di Leonhard*, Atti del Convegno di Idraulica, Padova.
- Benson, R.P., (1989, December), *Design of unlined and lined pressure tunnels*, 4(2):155-170, Tunnelling and Underground Space Technology, Elsevier.
- Boillat, J.L. and De Souza, P., (2004), *Modélisation des systèmes hydrauliques à écoulements transitoires en charge*, Communication 16, LCH, Lausanne.
- Chaudhry, M. H., (1987), *Applied Hydraulic Transients*, Van Nostrand Reinhold, New York.
- Citrini, D. and Nosedà, G., (1975), *Idraulica*, Casa Editrice Ambrosiana, Milano.
- Defina, A., (2010), *Moto vario nelle condotte*, Università di Padova, Padova.
- Edin, F.S., (2015), *Innovative Surge Systems for Small Hydro*, MSc thesis, NTNU, Trondheim.
- Evangelisti, G., (1941, October), *Alcune osservazioni sul colpo d'ariete e sulla regolazione delle turbine idrauliche*, L'Energia Elettrica, Fasc. X, Vol. XVIII, Società editrice riviste industrie elettriche, Milano.
- Evangelisti, G., (1946, September-October), *Sulla stabilità di regolazione delle installazioni idroelettriche*, L'Energia Elettrica, Fasc. IX-X, Vol. XXIII, Società editrice riviste industrie elettriche, Milano.
- Evangelisti, G., (1947), *Problemi tecnici e sperimentali intorno alle vasche di oscillazione*, Atti del Convegno di Idraulica, Padova.
- Evangelisti, G., (1949), *Adduzioni in pressione e stabilità di regolazione negli impianti idroelettrici*, Società Italiana per il progresso delle scienze, Roma.
- Evangelisti, G., (1950, May-June), *Pozzi piezometrici e stabilità di regolazione*, L'Energia Elettrica, Fasc. V-VI, Vol. XXVII, Società editrice riviste industrie elettriche, Milano.
- Evangelisti, G., (1951, December), *Pozzi piezometrici e stabilità di regolazione*, L'Energia Elettrica, Fasc. XII, Vol. XXVIII, Società editrice riviste industrie elettriche, Milano.
- Evangelisti, G., (1955, January), *Sopra la stabilità dei sistemi complessi di gallerie in pressione e pozzi piezometrici*, L'Energia Elettrica, Fasc. I, Vol. XXXII, Società editrice riviste industrie elettriche, Milano.
- Featherstone, R. E., Narulli, C. and Marriott, M., (2009), *Civil Engineering Hydraulics*, Wiley-Blackwell, Chichester.
- Frank, J. and Schüller, J., (1938), *Schwingungen in den Leitungs-und Ableitungskanalen von Wasserkraftanlage*, Springer, Berlin.
- Ghetti, A., (1947), *Ricerche sperimentali sulla stabilità di regolazione dei gruppi idroelettrici, con derivazione in pressione e pozzo piezometrico*, Atti del Convegno di Idraulica, Padova.
- Ghetti, A., (1947), *Sulla stabilità delle oscillazioni negli impianti idroelettrici provvisti di un sistema complesso di condotte e pozzi piezometrici*, Atti del Convegno di Idraulica, Padova.
- Gomsrud, D., (2015), *Design of a Surge Tank Throttle for Tonstad Hydropower Plant*, MSc thesis, NTNU, Trondheim.

- Guttormsen, O., (2006), *Vassdragsteknikk II – Kompendieforlaget*, NTNU, Trondheim.
- Harris, J.M. and Roach, B., (2017), *Environmental and natural resource economics: a contemporary approach – Fourth edition*, Routledge, Abingdon-on-Thames.
- Jaeger, C., (1977), *Fluid Transients in Hydro-Electric Engineering Practice*, Blackie, Glasgow.
- Leroquais, A., (2018), *Upgrading of Roskrepp hydropower plant to a pumped storage plant: Necessary reconstruction of the surge tank*, MSc thesis, NTNU, Trondheim.
- Mambretti, S., (2004), *Fenomeni di moto vario nelle correnti in pressione*, Aracne Editrice, Roma.
- Marchi, E. and Rubatta, A., (1981), *Meccanica dei fluidi*, UTET, Torino.
- Nabi, G., Kashif, M. and Tariq, M., (2011), *Hydraulic Transient Analysis of Surge Tanks : Case Study of Satpara and Golen Gol Hydropower Projects in Pakistan*, Pak. J. Engg. & Appl, Islamabad.
- Nielsen, T., (2015), *Dynamic Dimensioning of Hydro Power Plants*, Vannkraftlaboratiet, NTNU, Trondheim.
- Pickford, J., (1969), *Analysis of surge*, Macmillan, Bath.
- Scimemi, E., (1947), *Sulla validità della regola di Thoma nelle vasche di oscillazione degli impianti idroloeltrici*, Atti del Convegno di Idraulica, Padova.
- Seymour, J. and Horsley, T., (2005), *The Seven Types of Power Problems*, American Power Conversion (APC), West Kingston.
- Sira-Kvina Kraftselskap, (2018), *Roskrepp Kraftverk*, [ONLINE] Available at: <https://www.sirakvina.no/roskrepp-kraftverk/roskrepp-kraftverk-article257-921.html>, [Accessed 29 April 2018].
- Solvik Ø. and Storler A.Ø., (1980), *Roskrepp kraftverk – falltapsmålinger*, Sira-Kvina Kraftselskap, Tonstad.
- Svingen, B., (2016), *Manual LVTrans*, SINTEF Energy Research, Trondheim.
- Statkraft, (2018), *Roskrepp*, [ONLINE] Available at: <https://www.statkraft.com/energy-sources/Power-plants/Norway/Roskrepp/>, [Accessed 29 April 2018].
- Thoma, D., (1910), *Zur Theorie des Wasserschlosses bei selbsttätig geregelten Turbinenanlagen (The theory of surge tanks for turbine installations equipped with governors)*, translated by Jan C. Van Tienhoven (1955), F.B. Campbell, Vicksburg.
- Vereide, K., (2016), *Hydraulics and Thermodynamics of Closed Surge Tanks for Hydropower Plants*, Ph.D. thesis, NTNU, Trondheim.
- Wylie, E. B. and Streeter, V. L., (1993), *Fluid Transients in Systems*, Prentice Hall, Englewood Cliffs.